IntechOpen

Ligand

Edited by Chandraleka Saravanan and Bhaskar Biswas

LIGAND

Edited by **Chandraleka Saravanan**
and **Bhaskar Biswas**

Ligand
http://dx.doi.org/10.5772/intechopen.68405
Edited by Chandraleka Saravanan and Bhaskar Biswas

Contributors

Bogdan-Cezar Iacob, Ede Bodoki, Andreea Elena Bodoki, Luminita Oprean, Yuichi Negishi, Nurfadly Zain, Burcin Duan Sahbaz, Necla Birgul Iyison, Virginia Montiel-Palma, Julio Zamora-Moreno

Notice

First published in London, United Kingdom, 2018 by IntechOpen
eBook (PDF) Published by IntechOpen, 2019
IntechOpen is the global imprint of INTECHOPEN LIMITED, registered in England and Wales, registration number: 11086078, The Shard, 25th floor, 32 London Bridge Street
London, SE19SG – United Kingdom
Printed in Croatia

British Library Cataloguing-in-Publication Data
A catalogue record for this book is available from the British Library

Additional hard and PDF copies can be obtained from orders@intechopen.com

Ligand
Edited by Chandraleka Saravanan and Bhaskar Biswas

p. cm.

Print ISBN 978-1-78923-182-3

Online ISBN 978-1-78923-183-0

eBook (PDF) ISBN 978-1-83881-319-2

Meet the editors

Dr. Chandraleka Saravanan is working as an Assistant Professor at the Department of Chemistry, Urumu Dhanalakshmi College, Tiruchirappalli, Tamil Nadu, India. She has experience in the field of coordination chemistry and bioinorganic chemistry. Her current research focuses on metal complex synthesis, structural characterization and their utility in pharmacological and biological applications. She has published 20 research papers and 1 book: *Transition Metal Complexes*: *Biological Activity*. She guided eight MPhil candidates and participated in summer school on materials science. She has presented 16 research papers in national and international conferences/seminars. She is an editorial board member of national and international journals and an examiner committee member of MSc, MPhil, and PhD in Chemistry.

Dr. Bhaskar Biswas is currently working as an Assistant Professor of Chemistry at the Surendranath College, Kolkata, India. He is actively engaged in teaching as well as in research. He is an inorganic chemist with a vast experience in synthetic coordination chemistry. He also actively engrossed in the investigation of catalytic activities of different metal complexes, supramolecular aspects of coordination molecules and biological modeling of metelloenzymes and metalloproteins. He has published more than 50 research articles in national and international reputes. At present, Dr. Biswas is the supervisor of four research scholars on various aspects of inorganic chemistry and one research scholar (Sri Dhananjay Dey) who already received his doctoral degree under the supervision of Dr. Biswas.

Contents

Preface

Ligands are a special class of species, having a significant character to control the electronic properties of metal ions through some kind of chemical attachment. They have a great ability to enhance the reactivity and/or selectivity in controlling the physico-chemical properties of chemical entities.

This book consists of five chapters. Chapter 1 aims to outline the beneficial role of various functional ligands in pairing of metal ions in the molecular imprinting process and to provide an up-to-date overview of various applications in chemical sensing, separation processes (stationary phases and selective sorbents), drug delivery and catalysis. Chapter 2 covers the incorporation of both Si and P functionalities in a ligand backbone (silylphosphines), along with their applicability in reactivity in catalysis. The topic of discussion in Chapter 3 focuses on preparative route for gold clusters consisting of chalcogenate (thiolate, selenolate or tellurolate) ligands. A description of their geometric/electronic structures including physical and chemical properties is also depicted here. In Chapter 4, the concept of neuropeptide, including its intracellular maturation process and characteristics of some typical neuropeptide families with common properties of their cognate GPCRs, is dealt with. Chapter 5 highlights the significant contribution to soluble Fas ligand, a Type II membrane protein belonging to TNF family in the pathogenesis against dengue infection. The importance of Fas ligand and its mechanistic aspects in preventing dengue disease is also depicted here.

So, the book *Ligand* describes the diversity and versatility of ligands covering structural features, donor-acceptor properties and secondary functions like molecular recognition. Moreover, this book also provides a comprehensive account on the applicability: catalysis, sensors, supramolecular assembly, photochemical property, bioinorganic chemistry, and so on.

Dr. Chandraleka Saravanan
Department of Chemistry
Urumu Dhanalakshmi College
Tamil Nadu, India

Dr. Bhaskar Biswas
Department of Chemistry
Surendranath College
West Bengal, India

Section 1

Chemical Bonding in Ligand Chemistry

Chapter 1

Metal–Ligand Interactions in Molecular Imprinting

Bogdan-Cezar Iacob, Andreea Elena Bodoki,
Luminița Oprean and Ede Bodoki

Additional information is available at the end of the chapter

http://dx.doi.org/10.5772/intechopen.73407

Abstract

Molecular imprinting enables the design of highly crosslinked polymeric materials that are able to mimic natural recognition processes. Molecularly imprinted polymers exhibit binding sites with tailored selectivity toward target structures ranging from inorganic ions to biomacromolecules and even viruses or living cells. The choice of the appropriate functional monomer, crosslinker, and the nature and specificity of template–monomer interactions are critical for a successful imprinting process. The use of a metal ion mediating the interaction between the monomer and template (acting as ligands) has proven to offer a higher fidelity of imprint, which modulates the molecularly imprinted polymers (MIPs) selectivity or to endow additional features to the polymer, such as stimuli-responsiveness, catalytic activity, etc. Furthermore, limitations in using nonpolar and aprotic solvents are overcome, allowing the use of more polar solvents and even aqueous solutions as imprinting media, opening new prospects toward the imprinting of biomacromolecules (proteins, DNA, RNA, antibodies, biological receptors, etc.). This chapter aims to outline the beneficial pairing of metal ions as coordination centers and various functional ligands in the molecular imprinting process, as well as to provide an up to date overview of the various applications in chemical sensing, separation processes (stationary phases and selective sorbents), drug delivery, and catalysis.

Keywords: molecular imprinting, metal pivot imprinting, ion imprinting, drug delivery systems, catalysis, metal-ligand interactions, sensors, surface imprinting, chiral analysis

1. Introduction

Molecular recognition is indispensable to most of natural occurring phenomena, such as antibody–antigen immune response, ligand-receptor interactions, and enzyme catalysis. The complexity and specificity of these phenomena is the refined product of millions of years of evolution inciting scientists to search ways of mimicking these natural processes. The most

promising and advanced field of biomimetics is molecular imprinting (MI), a technique that gained popularity after the 90s, even though the first reports of imprinting date back to 1931, related to the findings of the Soviet chemist M. V. Polyakov. Compared with their natural counterparts, molecularly imprinted polymers (MIPs) possess, besides a similar selectivity, good chemical and thermal stability, ease of preparation, and low-cost production. By far, their main applications have been reported in the analytical field, and especially in separation techniques, where they have been used as stationary phases for (electro)chromatography and chiral separations and as selective sorbents in solid phase extraction [1]. They have also been applied as promising recognition elements in the development of biosensors, particularly electrochemical [2] and optical [3] ones. In the last few years, MIPs have proven to be versatile engineered materials in the construction of drug delivery systems [4] and as catalysts [5].

The MI process is a relatively simple concept, enabling the synthesis of highly crosslinked polymeric materials of various formats with highly specific binding sites for target structures. The synthesis procedure is relatively easy, versatile, and straightforward, and in general, five components are required: template molecule, functional monomer(s), crosslinking monomer, solvent (porogen), and initiator. The polymers are prepared in the presence of the target molecule itself as template. The first step in MIP-preparation is the self-assembly of template-functional monomer into a complex to immobilize the template molecules throughout the polymerization process. After the addition of the remaining components, the polymerization is initiated and the functional monomer (linked with the template) is incorporated into the rigid 3D structure of the polymer with the functional groups locked toward the template. Upon the subsequent removal (extraction) of the template, cavities are unveiled in the structure of the rigid polymer, which are complementary in size, shape, and functionality to the template. Hence, a molecular memory is created into the polymeric matrix, which has now the ability to selectively and reversibly bind the analyte or its structural analogs. The strength of the interactions between template and monomer determines the efficiency of the imprinting process [6].

Traditionally, MI is classified according to the chemical nature of the interactions that occur during the functional monomer–template complex formation and template rebinding, into two main approaches: the noncovalent and the covalent approach [7, 8]. By far, the most frequently employed approach is the noncovalent one, based on weak, noncovalent interactions in the template-functional monomer complex formation and also in the subsequent recognition step. These interactions, such as hydrogen bonding, electrostatic interactions and van der Waals forces, are similar with those occurring in biological recognition systems. Because of the weak nature of these bonds, the formed complexes are unstable and a large excess of functional monomer, as compared to the template, is required during the polymerization step in order to favor the formation of the template-monomer assemblies. However, this excess generates a high number of heterogeneous binding sites as a result of random incorporation of the monomer's functional groups outside the imprinted cavities. Moreover, because the complex formation is governed by an equilibrium, a special attention must be paid to the employed porogenic solvent. Usually, nonpolar, aprotic solvents, such as chloroform and toluene promote the template-functional monomer association, whereas polar solvents like methanol and water tend to disrupt the noncovalent interactions in the prepolymerization

complex. The covalent approach or the preorganized approach employs reversible covalent bonds between the functional monomer and template, such as reversible esterification or condensation reactions (boronate ester, ketal/acetal, and Schiff's base formation) both prior to the polymerization, and also in the subsequent rebinding step of the template. This strategy leads to the generation of a higher yield of specific and more homogeneous binding sites along with reduced nonspecific adsorption. However, the applicability of the covalent imprinting approach is limited because of the small number of compounds bearing required functionalities (alcohols (diols), aldehydes, ketones, amines, and carboxylic acids). Removal of the template is generally more difficult, and the chemical cleavage must be achieved under mild conditions. A third, semi-covalent approach, (also called hybrid approach) [9], developed by Whitcombe et al. [10] combines the advantages of the previous two methods. While reversible covalent bonds are employed during the polymerization step, the re-binding is entirely non-covalent in nature.

Unfortunately, most authors neglect in their classification a different strategy, metal ion coordination, even though its first report dates back to 1985 [11]. It has been employed as an alternative to enhance template and functional monomer association in water by introducing a metal ion as mediator [12]. The use of metal ions allows the formation of a ternary complex between the functional monomer, metal ion, and template. The heteroatoms of monomer and template bind to the metal ion (generally first row transition metals) by donating electrons to the unfilled orbitals of the outer coordination sphere of the latter [13]. Coordination of metal ions to natural (e.g. structural elements of DNA, peptides, alkaloids, etc.) or synthetic ligands bearing a large variety of donor atoms has proven to be well suited for the preparation of polymers with outstanding molecular recognition properties, put into good use in a wide variety of applications fields.

Initially, the design and development of MIPs, regardless of the employed imprinting approach, aimed for the rebinding of the template with the highest selectivity. Nevertheless, instead of using the metal ion as mere mediator in the formation of the imprinted polymer, the selective rebinding of a target metal ion is often of interest. Thus, based on the principle of MI, the concept of ion imprinting has also been introduced, in which case the metal ion assumes the role of template.

2. Metal pivot imprinting (metal ion as mediator)

In this approach, metal ions act as a bridge between the functional monomer and the template. Compared to noncovalent interactions, coordinative bonds are stronger, leading to a better stability in aqueous media. The stronger the interactions within the ternary complex, the more specific the recognition sites. Thus, the functional monomer and the template are maintained in close and fixed positions throughout the polymerization step [14]. Monomers are regularly positioned around the template via coordinate bonds, the relative motion of species is restrained, thus leading to improved imprinting factors and lower number of nonspecific binding sites. A key role in the imprinting process is represented by the nature of the

metal ion, which needs to simultaneously meet several requirements, that is, no inhibition of the polymerization process, well-defined coordination sphere, and optimal affinity toward the template and monomer.

2.1. Metal ion

Generally, only a small number of transitional metal ions are employed as pivots in MI, such as: Co(II), Co(III), Cu(II), Ni(II), Zn(II), Cd(II), Fe(II), and Fe(III). Due to their high ability in forming coordination compounds with the majority of ligands of interest cobalt [15–26] and copper [27–33] ions are most often chosen by default. Nevertheless, in the absence of rational guidelines for matching the optimal metal pivot ion with the ligand of interest, a systematic pairing process would be required for each individual set of components.

Wu and Li [27] reported Cu(II) being complexed in the pre-polymerization step by 2 molecules of monomer (4-vinylpyridine (4-VPy)), one of template (picolinamide) and two acetates. They also have shown that the anion in the copper salt participates in the recognition process and in the complex formation [27]. Even though Cu(II) forms the most stable coordination compounds with ligands bearing N-donor atoms, the best imprinting efficiency is achieved in the case of Co(II), as evidenced in multiple studies that compared the imprinting performances of multiple metal ions [15, 18, 21]. In an attempt to separate the enantiomers of mandelic acid, the R(+) enantiomer and 4-VPy were used as template and functional monomer, respectively, alongside different metal ions as pivot (Co(II), Ni(II), Cu(II), and Zn(II)) to create imprinted monoliths [15]. The best resolutions were obtained using Co(II) and Ni(II) as mediators (R_S = 1.87 and R_S = 1.41, respectively), while in the case of Cu(II) and Zn(II) no separation was observed. The smallest template retention recorded in the case of Zn(II) monolith implies that no ternary complex (template:metal ion:monomer) is formed due to zinc's weak coordination capacity. In the case of Cu(II), even though it produces the most stable hexa-coordinated complexes, because of Jahn–Teller distortion, these coordination compounds are known to be susceptible to tetragonal distortion (elongation/ compression) [34]. In another study, the Co(II) mediated imprinted monolith showed the best retention (k = 2.75) and imprinting factors (I.F. = 3.1) for the gallic acid (template), in comparison with Ni(II) mediated polymer (k = 2.49) or different other ion-mediated MIP monoliths that were tested [18]. The Co(II)-mediated MIPs emerge also in other two studies [21, 22] in which ketoprofen and ketoprofen with naproxen, respectively were used as templates. In the first study, [21] the ability of molecular recognition of the ion-mediated imprinted polymers decreases in the order: Co(II) > Ni(II) > Zn(II). The binding affinity of Ni(II) to the N containing ligands (especially aminoacids containing compounds) was employed in creating imprinted polyacrylamides as artificial receptors for different peptides (cholecystokinin C-terminal pentapeptide (CCK-5) [35] and His-Alac [36]). The functional monomer (nitrilotriacetic acid) occupies four positions in the octahedral coordination sphere of Ni(II), leaving the remaining two for selective interactions with the template. Both Fe(II) and Fe(III) were successfully used in developing MIP adsorbents for tetracyclines enriching [37, 38]. It was found that Fe(II) could form a ternary complex with tetracycline (template) and methacrylic acid (MAA) (functional monomer), made of one molecule of template, one Fe(II) and four MAAs. The same mole ratio 2:1:2, methacryloyl-l-cysteine methyl ester (functional

monomer):Fe(III):template (uric acid) was found in the coordination compound used for the surface plasmon resonance (SPR) detection of uric acid [39]. Fe(III)-MIP was developed as a drug carrier that showed larger drug loading capacity and a higher amount of drug release at its equilibrium state compared with the Fe-free MIP. Moreover, the Fe-MIP drug release rate was more controlled than that of the MIP and the non-imprinted polymer (NIP), especially at the early stages of release [40].

2.2. Template as ligand

Metal–template binding should be stable under polymerization conditions yet labile enough to allow removal of substrates-templates. With few exceptions, [41] the design of MIPs for the selective recognition of amino acids and peptides has been limited to the traditional imprinting strategy, which employs polyacrylates with MAA as the functional monomer in organic solvents. Bulkier templates, such as macromolecules (especially proteins) are not compatible with the organic media because of their low solubility and tendency toward denaturation, thus using water as solvent is essential. However, polar solvents will interfere in template-monomer hydrogen bonding, therefore metal-coordination interactions represent an effective alternative in imprinting biological-relevant compounds. The affinity of N-terminal histidine for Ni(II) allowed the creation of MIP receptors for peptides with exposed histidine residues [36]. It was shown that the metal ion works not just as a link between the monomer and template, it also influences the steric environment around the metal ion during polymerization step. The superior performance of metal-ion mediated imprinting compared with the metal-free approach, was demonstrated for CCK-5 [35]. MIPs produced in the presence Ni(II) showed a more than double average rebinding value and an I.F. of 1.9 with respect to the traditionally imprinted polymer. A Co(II)-mediated imprinted polymer for the bovine serum albumin (BSA) recognition (I.F. = 14.9), was synthesized and compared with the BSA ion-free MIP [17]. The Co(II)-mediated MIP presented an 8-fold increase in the I.F. and a reduced cross-selectivity by a factor of 2.5 compared with the BSA-MIP. Using Cu(II) chelation strategy, the cytochrome *c* was successfully imprinted into a supermacroporous cryogel, which was employed for template separation from a mixture of proteins (cytochrome c, lysozyme, and BSA).

Protein imprinting is still a challenging task mainly because of their huge molecular size and conformational flexibility and complexity, which makes template removal and the subsequent protein rebinding onto imprinted sites very difficult. One alternative to the protein bulk imprinting is the metal-ion mediated surface imprinting in which the specific recognition sites are located at the surface of MIP. Porcine serum albumin was imprinted on the surface of silica microparticles via a metal chelating strategy in phosphate buffer [32]. The thickness of the imprinted polymer layer was about 20 nm, allowing fast binding kinetics (~1 min), the binding of protein template reaching more than 90% of the maximum capacity. Satisfactory selectivity was obtained using three competitive proteins: cytochrome c, ribonuclease B and myoglobin. Another metal-ion imprinted thin polymeric film was synthesized on the surface of cellulose nanofibers for the selective recognition and purification of hemoglobin from hemolysate [33]. The obtained MIP was able to rebind 8 times more template protein

compared to the corresponding NIP. z-Histidine was also imprinted in polar organic solvent (methanol) via the mediation of Co(II) ions [20]. However, it was found a small difference in the rebinding capacities between the polymers prepared in the presence of z-His/Co(II) and Co(II) when they were exposed to the $Co(C_2H_3O_2)_2$(z-Histidine)] coordination compound.

Metal chelating approach was employed for the chiral discrimination of different amino acids, like phenylalanine, tyrosine, alanine, valine, leucine, isoleucine [29], and Boc-L-Phe-OH [25] and other compounds (mandelic acid [15]). The amino acid's side group's size plays a crucial role in obtaining a good enantioselectivity. The MIPs prepared with aliphatic amino acids showed no or little enantioselectivity. Amino acids containing aromatic or heterocyclic groups yielded MIPs with good chiral discriminative properties. According to the three-point interaction model, these bulky groups are responsible for the third necessary interaction with the polymer matrix, sterically hindering the opposite enantiomer.

Regarding the smaller and simpler (no multiple functional groups) molecules, non-covalent imprinting is more difficult because of the smaller number of possible interactions between the template and functional monomer, especially in aqueous media. It is the case of formate, acetate and propionate anions, which showed no imprinting effect using 4-VPy as functional monomer. However, if these anions are part of a ternary complex with picolinamide as ligand and Cu(II) ion as mediator (during the polymerization process as well as during the rebinding step), their indirect analysis is possible [28].

Metal ion mediated approach may be an alternative for compounds with strong intramolecular hydrogen bonds that can interfere in the formation of template-monomer intermolecular hydrogen bonds, thus inhibiting the MI effect. For example, picolinamide cannot be imprinted through the noncovalent approach, but if it is included in a ternary Cu(II) complex with 4-VPy (both as ligand and monomer), the imprinted polymer showed a high molecular recognition ability [27]. Metal ion-mediated imprinting was also used to prepare different MIPs for the specific recognition of multiple drugs with high metal chelating capability: tetracyclines [37, 38], quinolones [37], ketoprofen [21], furosemide [40], and naproxen [26]. Two pharmaceutical compounds, naproxen, and ketoprofen were simultaneously imprinted using metal chelating strategy without loss of selectivity and it was found to give better results versus traditional MIPs [22]. A SPR sensor for a biological-relevant molecule (uric acid) was developed and applied for the metabolite's detection in urine [39].

Because of the stronger coordination binding compared with noncovalent imprinting, metal ion mediated imprinted polymers can be successfully used as selective sorbents for the concentration and the clean-up of different pollutants and toxic compounds (methylmercury from human hair and soil [42], organohalide pesticide 4-(2,4-dichlorophenoxy)butyric acid (2,4-DB) [16], thiabendazole fungicide in citrus and soil samples [31]).

MIPs were also used as extraction media of active compounds from complicated natural products, using metal coordination interactions. Quercetin was shown to form coordination compounds with Zn(II) through 3-hydroxyl-4-ketone electron donor functionality from its structure [43]. Epigallocatechin gallate was separated from natural plant extracts employing gallic acid as a dummy template in order to reduce the MIPs manufacturing costs [18].

The combination of using ionic liquid ([Bmim]BF_4) and metal pivoting was employed in imprinting a polar compound, methyl gallate, exhibiting superior recognition abilities than the ion-free polymer [24]. It is assumed that the ionic liquid improves the imprinting process by limiting the polymer swelling and shrinkage [44].

2.3. Functional monomer

A successful metal ion-imprinting process is achieved if the formation of the template-metal ion-functional monomer ternary complex involves strong coordination interactions. Therefore, the choice of the functional monomer is very important. It must interact with the metal ion and template in a particular geometry offering the anchor point for the coordination compound on the polymer backbone.

One approach is to synthesize the metal ion-functional monomer complex before the addition of template, complex that will be incorporated into the polymer matrix and will be preserved after template removal [16, 17, 29, 35, 36]. Thus, in the rebinding step, the MIP should be exposed only to the free-form of the template. Examples of such coordination compounds: nitrilotriacetic acid–nickel (Ni–NTA) complex [35, 36], Co-porphyrin (Co(III)tetrakis(o-aminophenyl) porphyrin [16], Co(II)-(E)-2-((2 hydrazide-(4-vinylbenzyl) hydrazono)methyl)phenol, Fe(III) chloroprotoporphyrin, vinylferrocene, Zn(II) protoporphyrin [17], and Cu(II)–N-(4-vinylbenzyl)iminodiacetic acid [29].

However, in the metal-mediated imprinting, the most widely used functional monomer is by far 4-VPy, because of its ability to form strong coordination bonds with a large spectrum of divalent metals. Different metal ion-4-VPy molar ratios have been used, ranging from 1:1 [43], 1:2 [19, 20, 27, 28], 1:4 [22] up to 1:6 [15, 18, 23]. It appears that with the increasing molar ratio of functional monomer, the IFs are also increasing up to a ratio of 1:6. An excess of functional monomer is needed in order to stabilize the ternary complex and to achieve good fidelity of the binding sites.

Surprisingly, when 4-VPy was investigated as functional monomer versus acrylamide, and MAA, the best performances were exhibited by acrylamide-imprinted polymer, even though among the three monomers, acrylamide generates the lowest binding energy.

However, acidic acrylates (itaconic acid [37], MAA [25, 32, 38], and acrylic acid (AA) [40]) were successfully employed in metal-ion imprinting using Fe(II) and Fe(III) as central ion.

3. Ion imprinting (metal ion as template)

Commonly used monomers in MI often possess the ability to universally bond a multitude of metal ions, with variable selectivity. Thus, the use of monomers and/or ligands with structural features that enable metal ion chelation has opened new perspectives in the management and analysis of metal ions. First introduced by Nishide et al. [45], the concept of metal ion imprinting has been increasingly developed during the last two decades on the principle of MI.

The series of reviews published throughout the years offer general guidelines and concepts on the development of ion imprinted polymers (IIPs) (synthesis, characterization, types of imprinting, and assessment of analytical performance) and various applications (selective detection, sample enrichment, recovery, and decontamination of metal ions) in the biomedical and environmental fields [46–50]. Herein, several aspects on different materials, natural and synthetic, used in the design of IIPs and the particular features that allow these materials to selectively bind distinct metal ions will be pointed out.

The choice of the chelating agent, the complexation mode, the particular geometry of the coordination compound, the charge, and the size of the imprinted metal ions are key factors in determining the selectivity of the resultant imprinted polymer [34, 51, 52].

The inclusion of the metal binding entity in the polymerization matrix can be achieved through four distinct approaches: (a) crosslinking of linear chain polymers carrying metal-binding groups, (b) chemical immobilization, (c) surface imprinting, and (d) trapping of ligand in the polymeric matrix [47].

3.1. Crosslinking of linear chain polymers carrying metal-binding groups

This approach is currently used mainly with natural linear polymers, such as chitosan (CTS) and cellulose. CTS units, copolymers of glucosamine and N-glucosamine are widely used as functional monomers due to the material's abundance, lack of toxicity, biocompatibility, and biodegradability that add to its particular structure with numerous amino and hydroxyl functional groups which enable structural modifications and crosslinking [53].

The uptake of metal occurs mainly by chelation and is most likely to occur inter- or intra-CTS chains via one to four amino groups, with the nitrogen atoms in the amino and N-acetyl amino groups acting as electron donors. Upon deprotonation, hydroxyl groups may also be involved in metal ion coordination [54]. The poor selectivity, low stability in acidic solutions, and weak mechanical strength of nonimprinted raw CTS renders it inappropriate as selective metal ion sequestrant; these drawbacks, however, may be addressed by crosslinking and functionalization [53–55].

Nevertheless, crosslinking may decrease the metal uptake efficiency as, often, the functional groups of CTS involved in metal binding are also involved in the crosslinking reaction. The reactive amine and hydroxyl groups most likely to be involved in metal chelation are protected by ion imprinting prior to crosslinking [56, 57]. The commonly used crosslinkers include, but are not limited to, aldehydes (formaldehyde, glutaraldehyde, and glyoxal), heterocyclic compounds [epichlorohydrin(ECH)], and ethers [crown ethers, ethylene glycol diglycidyl ether (EGDE)]. Various modes of functionalization intended to modulate selectivity of CTS toward different metal ions have been reported: carbomethylation and thiourea/glutaraldehyde grafting for Ag(I) [58], carboxylation via ketoglutaric acid for Cu(II) [59], derivatization with aminobenzaldehyde for Ni(II), Cu(II) and Pd(II), [60, 61] dithiocarbamate for Sr(II), [62] tetraethylenpentamine for Pb(II) [63].

A different approach was employed by Hande et al. [64] for the design of a Pb(II) imprinted interpenetrating polymer by simultaneous polymerization of MAA and CTS in the presence of Pb(II) ions as template.

3.2. Surface imprinting

Chemical immobilization, trapping, and crosslinking of linear chain polymers, prepared mainly by traditional polymerization methods (bulk, precipitation, and suspension), present several drawbacks (i.e. relatively low rebinding capacity, slow mass transfer, and incomplete removal of template) that arise mostly from the restricted accessibility of the binding site, enclosed in the rigid polymeric mixture [48, 65]. Surface imprinting addresses these issues by generating binding cavities at the surface of the imprinted polymer. A thin imprinted layer is immobilized on the surface of fibers or small sized particles of organic or inorganic nature [48].

Selective sorption of Cu(II) was achieved by copolymerization of ethylene glycol dimethacrylate (EDMA) and $Cu(MAA)_2$ on the surface of a polystyrene core [66]. Li et al. grafted glycidyl methacrylate on polypropylene fibers [67]. A polypropylene membrane was used as support for a Pb(II) imprinted composite material in a process that implied grafting polymerization of AA on the polypropylene membrane and subsequent covalent immobilization of CTS [68].

Surface-imprinting modification of magnetic particles such as TiO_2 and Fe_2O_3 is particularly appealing since the post processing of solid-phase extraction is reduced to a simple magnetic separation. Chen et al. [57] developed thiourea-modified magnetic ion imprinted CTS/TiO_2 for highly effective Cd(II) adsorption and simultaneous 2,4-dichlorophenol degradation via TiO_2 photocatalysis. Fe_2O_3 magnetic particles were immobilized on carbon disulfide modified CTS-Fe(III), for the effective and simultaneous removal of Cd(II) and tetracycline from water samples. The synergistic effect of tetracycline and Cd(II) adsorption was found to be due to the formation, at pH = 8, of a tetracycline-Cd(II) complex bridging the adsorbent and adsorbate [56].

Modified silica gel particles are extensively used as support for the imprinted layer because of their mechanical and chemical stability, low cost, and ease of preparation and functionalization through the silanol groups. A facile approach with good results in terms of selectivity (selectivity coefficients above 50) was reported by Zhang et al. [69] and involved the use of two commonly employed functional monomers, 4-VPy and MAA to obtain ternary Pb(II) complexes, immobilized by polymerization with EDMA and subsequently grafted on hollow mesoporous silica by co-condensation between Si-OH and EDMA. Pb(II) imprinted silica sorbents were designed using a tetradentate chelating silylating agent derived from 3-[2-(2-aminoethylamino)ethylamino]propyltrimethoxysilane and 2-pyridinecarboxaldehyde [70] or a N,N-bidentate group in the structure of the functional monomer 4-(di(1H–pyrazol-1-yl)methyl) phenol [71]. Iminodiacetic functionalized silane ((3-glycidyloxypropyl)trimethoxysilane) [72] and the bifunctional ligand monomer [3-(γ-aminoethylamino)-propyltrimethoxysilane] [72, 73] were used for the imprinting with Ni(II) and Cd(II) ions and the imprinted sites were embedded in mesoporous silica.

3.3. Chemical immobilization

The chemical immobilization technique employs bifunctional ligands that possess both polymerizable functional group (i.e. a vinyl group for free radical polymerization or a silane

coupling agent for sol–gel processes), and electron donor groups for the chelation of metal ions [48, 74].

Currently, the technique is a one-step process that implies mixing together the metal ion, the bifunctional monomer and the crosslinker prior to co-polymerization. Isolation of the binary complex prior to polymerization is a more complicated approach but it offers the advantage of the control of the amount and of the structure of the coordination compound embedded into the polymer's structure [34, 48].

Common monomers such as 4-VPy, 1-vinylimidazole, AA or acrylamide may serve for chemical immobilization, but they show low binding capacities and low selectivity. MAA was used simultaneously with 1-vinylimidazole [75] or 4-VPy [76, 77] to prepare Cd(II), Cu(II), and Zn(II) imprinted polymer particles, respectively. Considering however that the use of simple, commercially available monomers results in materials with generally low binding capacity and selectivity, new tailored bifunctional ligands, bearing both chelating functionalities and polymerizable groups, have been proposed.

Particular features that differ from those of their open-chain analogs such as controlled size and the "macrocyclic effect" that translates into high selectivity and stability, make crown ethers interesting candidates as ligands in ion-imprinting. Benzo-15-crown-5-acrylamide, 4-vinylbenzo-18-crown-6, and 2-(allyoxy)methyl-12-crown-4 have been successfully employed for the imprinting of K(I), [78] Pb(II) [79] and Li(I) ions [80, 81].

Calix[4]resorcinorene, a resorcinol-based macrocyclic compound with a bowl-shape molecular cavity formed by four resorcinol units, was used by Yusof et al. [82] to synthesize diallylaminomethyl-calix[4]-resorcinarene, as host for imprinting Pb(II) ions.

Amino acids or amino acid derivatives bearing vinylated groups, (e.g. N-methacryloyl-(L)-histidine), [83, 84] vinylated SALEN, [85] [N-(4-vinybenzyl)imino]diacetic acid, [34] are other examples of bifunctional ligands that have been reported for the chelation of various metal ions and subsequent copolymerization with a suitable crosslinking agent.

Based on the ability of Hg(II) to form stable coordination compounds with thymine (T), T-Hg(II)-T interactions, Xu et al. [74] synthesized 3-isocyanatopropyltriethoxysilane, bearing thymine (T) bases as recognition elements for the imprinting of Hg(II).

Using 5-(bisulfate N,N-diallyl-N-methyl ammonium)methyl salicylaldoxime, Zhang et al. [86] anchored chelating salicylaldoxime units onto the polymer networks through quaternary ammonium cations serving as spacers.

Chemical immobilization shows the advantage of ligands not being leached out during the elution of the template. The magnitude of the imprinting effect is however rather low; this adds up to the difficulty of the vinylation procedure [47].

3.4. Trapping of the ligand in the polymeric matrix

In case of trapping, ligands do not require the insertion of polymerizable functions, but instead they are used as such and are entrapped inside the network during the polymer's formation,

without being chemically bound to the polymeric network. The stability of the binding sites depends upon the correct immobilization of the ligand in the polymeric matrix and the presence and the integrity of the ligand during and after the template removal [47, 48].

The first trapping procedure was reported by Rao et al. in 2003. The imprinted polymer was synthesized by co-polymerization of a coordination compound between Dy(III), 5,7-dichloroquinoline-8-ol and 4-VPy, in the presence of divinylbenzene (DVB) as crosslinker [87].

The entrapped species may be a metal ion:ligand binary complex, as in the case of Zn(II):8-hydroxyquinoline (1,2) and Al:8-hydroxyquinoline (1,3) coordination compounds embedded in the polymeric matrix formed by MAA and DVB [88]. In most cases, however, a ternary metal complex is formed, the metal ion being coordinated by both the ligand ensuring selectivity and the functional monomer (e.g. 4-VPy, MAA) bearing, it too, electron donating heteroatoms, and therefore coordination ability. The ternary complex can be prepared in situ, just before the polymerization step or synthesized, isolated and characterized before being introduced in the polymerization. Comparative studies on the efficiency of polymers prepared with such ternary complexes vs. binary species where the coordination environment is ensured by the presence of the ligands alone, revealed the importance of the presence of bifunctional species acting as complementary complexing agents. Alizadeh used 4-VPy as functional monomer and quinaldic acid as complexing agent to imprint Cd(II) and employed experimental design to study various binary and ternary mixtures [89]. IPs prepared from binary complexes were found to be less efficient than those prepared with ternary complexes.

Crown ethers and derivatives with cavities of appropriate size were trapped in the polymer network by using suitable functional monomers and crosslinking agents and the polymer imprinted with alkali metals ions. Dicyclohexyl-18-crown-6, [90] dibenzo-21-crown-7, [91] dibenzo-24-crown-8 ether [92] and the aza-thioether crown containing a 1,10-phennathroline subunit (5-azamethyl-2,8-dithia [9],(2,9)-1,10-phenanthrolinophane), [93] were used by Shamsipur and coll. to imprint K(I), Rb(I), Cs(I) and Ag(I) ions, respectively, in the presence of MAA as functional monomer and EDMA as crosslinker.

Other ligands used for ion-imprinting via trapping include isatine for Cu(II), [94] diphenylcarbazide (for Cd(II)), [95] 1,10-phenanthroline for Ag(I) [93] or neocuproine for Cd(II), [96] 8-hydroxyquinoline for Ni(II), [97] etc.

As compared to chemical immobilization, the trapping approach is easier to implement. The stability of the binding sites created via the trapping approach, however, depends upon the correct immobilization of the ligand in the polymeric matrix and the presence and the integrity of the ligand during and after the removal of template [48].

4. MIPs in drug delivery

Polymers have played an integral role in the advancement of drug delivery systems (DDS) through the last three decades, improving safety, efficacy, and patient compliance during

long-term medication therapy by providing sustained release of both hydrophilic and hydrophobic therapeutic agents [98]. MIPs used as excipients of solid pharmaceutical dosage forms have been tested for tuning drug release profiles and eventually protect their load from enzymatic degradation while being freight through the body, nevertheless the inherent feature of these polymers, their selectivity, has not been put to a proper use. Therefore, efforts have been made to integrate MIPs in therapeutic systems for intelligent drug release or as targeting drug vectors [99].

These tailor-made IPs would be therapeutically advantageous for several reasons as they can act as molecular trap (sequestrant) systems, [100] as reservoir for prolonged release of a particular drug, they can enable an increased loading capacity of the therapeutic formulation, facilitate environmentally or physiologically responsive intelligent release of the therapeutic agent [101] and if required, they can confer an enantioselective load or release [102, 103]. Using conventional drug formulations, repeated administration would help in building up the required therapeutic levels of the drug in various biological compartments (blood, tissues, urine, etc.); however, in case of bioactive molecules with a narrow therapeutic index (i.e. digoxin, cyclosporine, sirolimus, theophylline, warfarin, lithium, phenytoin, and flecainide) or with very short plasmatic half-life (i.e. 5-fluorouracil (5-FU), acetylcholine, GABA, catecholamines, adenosine, and NO) repeated administration could lead to elevated risks or severity of toxic side effects.

Several comprehensive reviews have been published concerning the use of MIPs in general as DDS for controlled/sustained drug release or as intelligent drug delivery (DD) platforms (responsive release systems) either for oral, ocular, transdermal, or implant-associated local delivery routes of the therapeutic agent [99–101, 104–108].

Targeted DD relies on the MIP's ability to specifically recognize certain bioreceptors, such as a cell surface epitopes, which could further convey to cellular internalization of the drug loaded carrier and subsequent release of the active pharmaceutical compound. In the initial and most simple approaches the payload of biologically active molecule was non-covalently bound (hydrogen bonding, hydrophobic interactions, charge transfer, or van der Waals forces) to the imprinted polymer network [109]. Nevertheless, the overall controllability and reliability of DDS based on noncovalent binding might not be ideal in a living organism. Therefore, as an alternative, metal ion-mediated coordinate bonds between the functional monomer and the targeted drug molecule (template) has been investigated offering higher specificity and strength, as well as spatial directionality in comparison with noncovalent bonding. Additionally, metal coordination bonds are more compatible with the polar environment of living tissues and they can be easily manipulated through changes of the local hydrogen ion concentration, a feature extremely helpful in the development of pH-responsive delivery systems. Furthermore, MIPs prepared by noncovalent imprinting methods usually require using organic solvents, which eventually leave toxic traces, incompatible with biomedical applications.

Some of the imprinted polymers employed nowadays in intelligent DD [i.e. poly(2-hydroxyethyl methacrylate, (PHEMA)] were initially employed in the early forms of the non-imprinted DDS [98]. Various aspects about the encountered recognition and drug release mechanisms, optimization of the drug loading capacity, latest trends in various routes of DD, as well as

limitations and future prospects of such molecularly imprinted DDS may be found in different reviews [99, 104, 105, 110].

A wide range of biocompatible semi-synthetic and synthetic polymers have been tested as suitable imprinted frameworks for DD. PHEMA and its derivatives or nanocomposites continues to be one of the most widely used biomaterials due to their low toxicity, excellent and long-term biocompatibility (including hemocompatibility) and high resistance to degradation [111, 112].

Such molecularly imprinted biomaterials served for the fabrication of various drug-delivery systems, such as transdermal membranes, [113] ocular inserts [114, 115], and implants (subcutaneous, intra-peritoneal, etc.) [116].

Polymer biodegradability plays also an important role in the biomedical exploitation, patient compliance and safe use of such DD systems. Because PHEMA is not biodegradable, upon the release of the pharmacologically active load the implants must be removed from the body through minor surgery to avoid the formation of pseudocyst. However, in many cases, such as the localized treatment of spinal cord injuries, the use of hydrolytically degradable hydrogel implants is far more convenient. *In vivo* experiments showed that macroporous 2-ethoxyethyl methacrylate/ N-(2-hydroxypropyl) methacrylamide based hydrolysable hydrogels (adjustable degradation between 2 and 40 days) are promising candidates for implantation into tissue defects of the central nervous system [117].

Although metal ion coordination-based imprinting has shown promise in the creation of advanced recognition and DD systems up until now, literature is rather scarce in such studies. Nevertheless, there are some noteworthy publications in this field, such as the one reporting the sustained release (5 days) of copper salicylate, a metal-based nonsteroidal anti-inflammatory drug, successfully embedded in a metal chelate imprinted polymer using 4-VPy and 2-hydroxyethyl methacrylate (HEMA) as functional monomers and EDMA as crosslinker [118]. Another interesting study is the synthesis of Co(II) mediated imprinted hydrogels containing pendent chain linked template (drug) [119]. A pH responsive drug release could be achieved in the range of pH 3–6.8 due to the presence of an imidazole group within the proximity of the polymer-drug (ester or amide) bond responsible of the catalytic hydrolysis of the hydrogel.

Design of dedicated macromolecular architectures through MI able to recognize certain target molecules as well as capable of intelligent DD and release leads to the introduction of feedback-controlled drug release systems employing stimuli-responsive gel systems. As a result of oscillatory swelling, they are able to modulate release in response to pH, temperature, ionic strength, electric fields, or specific analyte concentration differences [101, 104]. The solvation of the hydrogel's macromolecular network is rather well adjustable by the local environment, this leading to a controlled swelling and release of the payload.

The inherent advantages offered by metal pivot-based MI have been successfully exploited in the imprinting process of hydrogels intended for stimuli-responsive DDS. The formation and cleavage of coordination bonds between different metal ions and various drugs of interest are pH-dependent, so by a rational design they could be specifically engineered for an intended use. As such, metal-mediated imprinting of HEMA-based hydrogel backbone crosslinked with N, N-methylenebisacrylamide (MBA) has been described for the pH-responsive and

controlled release of doxorubicine (within 7 days 60% of the drug released at pH 5.0 vs. 10% at pH 7.2). The anticancer drug was loaded onto the hydrogel as a preassembled Cu(II) ion bridged complex of doxorubicin (1,2 molar ratio) as template and 4-VPy as functional monomer [120]. Although by a slightly different approach, Liang et al. reported the encapsulation in self-assembled biodegradable zein/carboxymethyl chitosan (CMCS) nanoparticles of the same anticancer drug by electrostatic interactions [121]. The nanoparticles were additionally coated by a thin layer of metal-tannic acid layer, where the metal ions (Cu(II), Ca(II)) act as stimuli-responsive crosslinking agents, controlling the release of the guest molecule.

The intracellular conversion rate of a key anticancer agent, 5-FU, to its biologically active metabolites is very fast in the human body, however more than 80% of the administered pro-drug is inactivated by the liver (6 min plasmatic half-life) [122]. As a solution, various controlled localized DD approaches have been investigated [123, 124]. Nevertheless, the prospects of metal ion-mediated MI technology for the controlled delivery 5-FU has also been exploited by the formation of a metal-chelate complex of N-methacryloyl-L-histidine (MAH) functional comonomer and 5-FU via Cu(II) ion coordination in the prepolymerization step [125]. A free radical polymerization, crosslinking and a cryogenic processing lead to the formation of 5-FU imprinted PHEMA-N-methacryloyl-(L)-histidine methyl ester) cryogel discs, an interesting class of implantable biomaterials, particularly suitable for the controlled delivery of an antineoplastic agent directly to the site of tumor. *In vitro* studies have shown that drug release may be simply controlled by the amount of used crosslinker, whereas the delivery rate of 5-FU is further tuneable (faster at pH 4 vs. 7.4), through the influence of the coordination compound's stability, rendering the metal ion-mediated imprinted polymer pH-responsive [125].

Due to the inherent large surface area of porous metal–organic frameworks (MOFs) and to the excellent gas adsorption capacity of the active metal atoms, such structures have been described for the delivery of bioactive gas molecules, such as NO as an antithrombosis and vasodilation agent [126]. The gas can be stably stored by the covalently unsaturated metal atoms (Co or Ni) from their structure, each able to coordinate to one NO molecule (accumulating up to 7 mmol NO/g of MOF), whereas the bioactive gas is delivered through a water-triggered release. Although other porous MOFs were also described as promising DD systems, where the pharmaco-active payload is stored in a 3D network of nanoscaled cages by guest-host interactions, in the respective case the metal ion is not actively involved in the drug's (i.e. 6-FU) binding or release [127].

5. MIPs in catalysis

The use of MIPs in catalysis has been gaining in interest in recent years thanks to their low cost of manufacturing, good biocompatibility, and recognition properties and excellent stability compared to their bio-analogues such as enzymes. The main objective in this field is to produce MIPs capable of showing enzyme-like activities for reactions for which no enzyme exists, or to improve the performance of the existing catalytic systems [128]. Many natural enzymes contain metal ions capable of specifically coordinate different molecules.

A salicylaldiminato Co(III)-based catalyst was used for the preparation of Cibacron-reactive-red-dye-imprinted MIP with tert-butyl acrylate as a functional monomer and DVB as a crosslinker. Methyl aluminoxane activated the transition-metal coordination compound, which catalyzed the polymerization of tert-butyl acrylate, and high-molar-mass polymers with very low molecular weight distributions were generated, even in the presence of the polar dye. The obtained MIP was used for the selective rebinding and preconcentration of the red dye from tap water and textiles [129]. Co(II)- and Ni(II)-imprinted hydrogel catalyst were able to significantly improve the hydrolysis kinetics of $NaBH_4$ and NH_3BH_3 in H_2 production (total hydrolysis in 50 s at 60°C) [130]. Rare earth metal ions (Y(III), Ce(III), Nd(III), and La(III)) as doping ions were immobilized by ion-imprinting in photocatalysts on TiO_2 Halloysite. Using two aniline derivatives as monomers (o-phenylenediamine, m-phenylenediamine), the photocatalytic activity was demonstrated on tetracycline degradation (up to 78.80%) in simulated wastewaters under visible light irradiation [131]. Last but not least, as a more stable alternative to the natural enzyme phosphotriesterase (hydrolysis of organophosphotriester pesticides), a MIP was synthesized using a paraoxon analog as template and Co(II)–imidazole coordination compound mimicking the catalytic center of the enzyme. Polymers containing the Co(II)–imidazole coordination compound showed a 20-fold higher hydrolytic activity in comparison with polymers containing only imidazole or a solution containing only Co(II) ions. Additionally, the MIP synthesized using the paraoxon analog as template showed higher paraoxon hydrolysis activity than the control NIP [132].

Acknowledgements

Work supported by the University of Medicine and Pharmacy "Iuliu Hatieganu" Cluj-Napoca, internal grant no. 4944/11/08.03.2016 and internal grant no. 4945/19/08.03.2016.

Author details

Bogdan-Cezar Iacob[1], Andreea Elena Bodoki[2], Luminița Oprean[2] and Ede Bodoki[1]*

*Address all correspondence to: bodokie@umfcluj.ro

1 Analytical Chemistry Department, "Iuliu Hațieganu" University of Medicine and Pharmacy, Cluj-Napoca, Romania

2 General and Inorganic Chemistry Department, "Iuliu Hațieganu" University of Medicine and Pharmacy, Cluj-Napoca, Romania

References

[1] Iacob B-C, Bodoki E, Oprean R. Chiral electrochemical sensors based on molecularly imprinted polymers with pharmaceutical applications. In: Handbook of Sustainable Polymers. Boca Raton: Pan Stanford; 2015. pp. 587-614. DOI: 10.1201/b19600-18

[2] Iacob B-C, Bodoki E, Florea A, Bodoki AE, Oprean R. Simultaneous enantiospecific recognition of several β-blocker enantiomers using molecularly imprinted polymer-based electrochemical sensor. Analytical Chemistry. 2015;**87**(5):2755-2763. DOI: 10.1021/ac504036m

[3] Feng F, He F, An L, Wang S, Li Y, Zhu D. Fluorescent conjugated polyelectrolytes for biomacromolecule detection. Advanced Material. 2008;**20**(15):2959-2964. DOI: 10.1002/adma.200800624

[4] Gagliardi M, Bertero A, Bifone A. Molecularly imprinted biodegradable nanoparticles. Scientific Reports. 2017;**7**:40046. DOI: 10.1038/srep40046

[5] Zhu M, Wang S, Li S. Titanium catalyst with the molecular imprinting of substrate for selective photocatalysis. Journal of the Chinese Advanced Material Society. 2014;**2**(2):71-81. DOI: 10.1080/22243682.2014.905211

[6] Hashim SNNS, Boysen RI, Schwarz LJ, Danylec B, Hearn MTW. A comparison of covalent and non-covalent imprinting strategies for the synthesis of stigmasterol imprinted polymers. Journal of Chromatography A. 2014;**1359**:35-43. DOI: 10.1016/j.chroma.2014.07.034

[7] Maier NM, Lindner W. Chiral recognition applications of molecularly imprinted polymers: A critical review. Analytical and Bioanalytical Chemistry. 2007;**389**(2):377-397. DOI: 10.1007/s00216-007-1427-4

[8] Haupt K, Mosbach K. Molecularly imprinted polymers and their use in biomimetic sensors. Chemical Reviews. 2000;**100**(7):2495-2504. DOI: 10.1021/cr990099w

[9] Zhang H. Water-compatible molecularly imprinted polymers: Promising synthetic substitutes for biological receptors. Polymer. 2014;**55**(3):699-714. DOI: 10.1016/j.polymer.2013.12.064

[10] Whitcombe MJ, Rodriguez ME, Villar P, Vulfson EN. A new method for the introduction of recognition site functionality into polymers prepared by molecular imprinting: Synthesis and characterization of polymeric receptors for cholesterol. Journal of the American Chemical Society. 1995;**117**(27):7105-7111. DOI: 10.1021/ja00132a010

[11] Fujii Y, Matsutani K, Kikuchi K. Formation of a specific co-ordination cavity for a chiral amino acid by template synthesis of a polymer Schiff base cobalt(III) complex. Journal of the Chemical Society, Chemical Communication. 1985;**7**:415-417. DOI:10.1039/C39850000415

[12] Yavuz H, Say R, Denizli A. Iron removal from human plasma based on molecular recognition using imprinted beads. Material Science and Engineering C. 2005;**25**(4):521-528. DOI: 10.1016/j.msec.2005.04.005

[13] Alexander C, Andersson HS, Andersson LI, Ansell RJ, Kirsch N, Nicholls IA, et al. Molecular imprinting science and technology: A survey of the literature for the years up to and including 2003. Journal of Molecular Recognition. 2006;**19**(2):106-180. DOI: 10.1002/jmr.760

[14] Mallik S, Johnson RD, Arnold FH. Synthetic Bis-metal ion receptors for Bis-imidazole "protein Analogs". Journal of the American Chemical Society. 1994;**116**(20):8902-8911. DOI: 10.1021/ja00099a007

[15] Bai LH, Chen XX, Huang YP, Zhang QW, Liu ZS. Chiral separation of racemic mandelic acids by use of an ionic liquid-mediated imprinted monolith with a metal ion as self-assembly pivot. Analytical and Bioanalytical Chemistry. 2013;**405**(27):8935-8943. DOI: 10.1007/s00216-013-7304

[16] Mazzotta E, Malitesta C. Electrochemical detection of the toxic organohalide 2,4-DB using a co-porphyrin based electrosynthesized molecularly imprinted polymer. Sensors and Actuators B Chemical. 2010;**148**(1):186-194. DOI: 10.1016/j.snb.2010.03.089

[17] El-Sharif HF, Yapati H, Kalluru S, Reddy SM. Highly selective BSA imprinted poly-acrylamide hydrogels facilitated by a metal-coding MIP approach. Acta Biomaterialia. 2015;**28**(Supp. C):121-127. DOI:10.1016/j.actbio.2015.09.012

[18] Li X-Y, Bai L-H, Huang Y-P, Liu Z-S. Isolation of Epigallocatechin Gallate from plant extracts with metallic pivot-assisted dummy imprinting. Analytical Letters. 2016;**49**(13):2031-2042. DOI: 10.1080/00032719.2015.1131708

[19] Matsui J, Nicholls IA, Takeuchi T, Mosbach K, Karube I. Metal ion mediated recognition in molecularly imprinted polymers. Analytica Chimica Acta. 1996;**335**(1):71-77. DOI: 10.1016/S0003-2670(96)00356-X

[20] Chaitidou S, Kotrotsiou O, Kiparissides C. On the synthesis and rebinding properties of [co(C2H3O2)2(z-Histidine)] imprinted polymers prepared by precipitation polymerization. Material Science and Engineering C. 2009;**29**(4):1415-1421. DOI: 10.1016/j.msec.2008.11.011

[21] Zhao L, Ban L, Zhang Q-W, Huang Y-P, Liu Z-S. Preparation and characterization of imprinted monolith with metal ion as pivot. Journal of Chromatography A. 2011; **1218**(50):9071-9079. DOI: 10.1016/j.chroma.2011.10.027

[22] Zhang J, Li F, Wang X-H, Xu D, Huang Y-P, Liu Z-S. Preparation and characterization of dual-template molecularly imprinted monolith with metal ion as pivot. European Polymer Journal. 2016;**80**(Supp. C):134-144. DOI:10.1016/j.eurpolymj.2016.05.009

[23] Zhong D-D, Huang Y-P, Xin X-L, Liu Z-S, Aisa HA. Preparation of metallic pivot-based imprinted monolith for polar template. Journal of Chromatography B. 2013;**934**(Supp. C): 109-116. DOI:10.1016/j.jchromb.2013.07.006

[24] Li S, Tong K, Zhang D, Huang X. Rationally designing active molecularly imprinted polymer toward a highly specific catalyst by using metal as an assembled pivot. Journal of Inorganic and Organometallic Polymers and Materials. 2008;**18**(2):264-271. DOI: 10.1007/s10904-007-9172-x

[25] Zheng MX, Li SJ, Luo X. Rationally designing molecularly imprinted polymer toward a high specific adsorbent by using metal as assembled pivot. Journal of Macromolecular Science, Part A. 2007;**44**(11):1187-1194. DOI: 10.1080/10601320701561122

[26] Li S, Liao C, Li W, Chen Y, Hao X. Rationally designing molecularly imprinted polymer towards predetermined high selectivity by using metal as assembled pivot. Macromolecular Bioscience. 2007;**7**(9-10):1112-1120. DOI: 10.1002/mabi.200700047

[27] Wu L, Li Y. Picolinamide–Cu(Ac)2-imprinted polymer with high potential for recognition of picolinamide–copper acetate complex. Analytica Chimica Acta. 2003;**482**(2):175-181. DOI: 10.1016/S0003-2670(03)00208-3

[28] Wu L, Li Y. Metal ion-mediated molecular-imprinting polymer for indirect recognition of formate, acetate and propionate. Analytica Chimica Acta. 2004;**517**(1):145-151. DOI: 10.1016/j.aca.2004.05.015

[29] Vidyasankar S, Ru M, Arnold FH. Molecularly imprinted ligand-exchange adsorbents for the chiral separation of underivatized amino acids. Journal of Chromatography A. 1997;**775**(1):51-63. DOI: 10.1016/S0021-9673(97)00280-X

[30] Tamahkar E, Bereli N, Say R, Denizli A. Molecularly imprinted supermacroporous cryogels for cytochrome c recognition. Journal of Separation Science. 2011;**34**(23):3433-3440. DOI: 10.1002/jssc.201100623

[31] Lian H, Hu Y, Li G. Novel metal-ion-mediated, complex-imprinted solid-phase microextraction fiber for the selective recognition of thiabendazole in citrus and soil samples. Journal of Separation Science. 2014;**37**(1-2):106-113. DOI: 10.1002/jssc.201301049

[32] Li Q, Yang K, Li S, Liu L, Zhang L, Liang Z, et al. Preparation of surface imprinted core-shell particles via a metal chelating strategy: Specific recognition of porcine serum albumin. Microchimica Acta. 2016;**183**(1):345-352. DOI: 10.1007/s00604-015-1640-3

[33] Bakhshpour M, Tamahkar E, Andaç M, Denizli A. Surface imprinted bacterial cellulose nanofibers for hemoglobin purification. Colloids and Surfaces B. 2017;**158**(Supp. C):453-459. DOI:10.1016/j.colsurfb.2017.07.023

[34] Bhaskarapillai A, Narasimhan SV. A comparative investigation of copper and cobalt imprinted polymers: Evidence for retention of the solution-state metal ion-ligand complex stoichiometry in the imprinted cavities. RSC Advances. 2013;**3**(32):13178-13182. DOI: 10.1039/C3RA23384G

[35] Papaioannou EH, Liakopoulou-Kyriakides M, Papi RM, Kyriakidis DA. Artificial receptor for peptide recognition in protic media: The role of metal ion coordination. Material Science and Engineering B. 2008;**152**(1):28-32. DOI: 10.1016/j.mseb.2008.06.017

[36] Hart BR, Shea KJ. Synthetic peptide receptors: Molecularly imprinted polymers for the recognition of peptides using peptide–metal interactions. Journal of the American Chemical Society. 2001;**123**(9):2072-2073. DOI: 10.1021/ja005661a

[37] Qu S, Wang X, Tong C, Wu J. Metal ion mediated molecularly imprinted polymer for selective capturing antibiotics containing beta-diketone structure. Journal of Chromatography A. 2010;**1217**(52):8205-8211. DOI: 10.1016/j.chroma.2010.10.097

[38] Qu G, Zheng S, Liu Y, Xie W, Wu A, Zhang D. Metal ion mediated synthesis of molecularly imprinted polymers targeting tetracyclines in aqueous samples. Journal of Chromatography B. 2009;**877**(27):3187-3193. DOI: 10.1016/j.jchromb.2009.08.012

[39] Göçenoğlu Sarıkaya A, Osman B, Çam T, Denizli A. Molecularly imprinted surface plasmon resonance (SPR) sensor for uric acid determination. Sensors and Actuators B Chemical. 2017;**251**(Supplement C):763-772. DOI:10.1016/j.snb.2017.05.079

[40] Fareghi AR, Moghadam PN, Khalafy J. Preparation of metal ion-mediated furosemide molecularly imprinted polymer: Synthesis, characterization, and drug release studies. Colloid and Polymer Science. 2017;**295**(6):945-957. DOI: 10.1007/s00396-017-4081-1

[41] Klein JU, Whitcombe MJ, Mulholland F, Vulfson EN. Template-mediated synthesis of a polymeric receptor specific to amino acid sequences. Angewandte Chemie, International Edition. 1999;**38**(13-14):2057-2060. DOI: 10.1002/(SICI)1521-3773(19990712)38:13/14<2057:AID-ANIE2057>3.0.CO;2-G

[42] Liu Y, Zai Y, Chang X, Guo Y, Meng S, Feng F. Highly selective determination of methylmercury with methylmercury-imprinted polymers. Analytica Chimica Acta. 2006;**575**(2):159-165. DOI: 10.1016/j.aca.2006.05.081

[43] Fan P, Wang B. Regulatory effects of Zn(II) on the recognition properties of metal coordination imprinted polymers. Journal of Applied Polymer Science. 2010;**116**(1):258-266. DOI: 10.1002/app.31454

[44] Booker K, Bowyer MC, Holdsworth CI, McCluskey A. Efficient preparation and improved sensitivity of molecularly imprinted polymers using room temperature ionic liquids. Chemical Communications. 2006;**16**:1730-1732. DOI: 10.1039/B517886J

[45] Nishide H, Tsuchida E. Selective adsorption of metal ions on poly(4-vinylpyridine) resins in which the ligand chain is immobilized by crosslinking. Die Makromolekulare Chemie. 1976;**177**(8):2295-2310. DOI: 10.1002/macp.1976.021770807

[46] Prasada Rao T, Daniel S, Mary GJ. Tailored materials for preconcentration or separation of metals by ion-imprinted polymers for solid-phase extraction (IIP-SPE). TrAC Trends in Analytical Chemistry. 2004;**23**(1):28-35. DOI: 10.1016/S0165-9936(04)00106-2

[47] Rao TP, Kala R, Daniel S. Metal ion-imprinted polymers—Novel materials for selective recognition of inorganics. Analytica Chimica Acta. 2006;**578**(2):105-116. DOI: 10.1016/j.aca.2006.06.065

[48] Branger C, Meouche W, Margaillan A. Recent advances on ion-imprinted polymers. Reactive and Functional Polymers. 2013;**73**(6):859-875. DOI: 10.1016/j.reactfunctpolym.2013.03.021

[49] Mafu LD, Msagati TAM, Mamba BB. Ion-imprinted polymers for environmental monitoring of inorganic pollutants: Synthesis, characterization, and applications. Environmental Science and Pollution Research. 2013;**20**(2):790-802. DOI: 10.1007/s11356-012-1215-3

[50] Fu J, Chen L, Li J, Zhang Z. Current status and challenges of ion imprinting. Journal of Materials Chemistry A. 2015;**3**(26):13598-13627. DOI: 10.1039/C5TA02421H

[51] Pustam AN, Alexandratos SD. Engineering selectivity into polymer-supported reagents for transition metal ion complex formation. Reactive and Functional Polymers. 2010;**70**(8):545-554. DOI: 10.1016/j.reactfunctpolym.2010.05.002

[52] Turiel E, Martín-Esteban A. Molecularly imprinted polymers for sample preparation: A review. Analytica Chimica Acta. 2010;**668**(2):87-99. DOI: 10.1016/j.aca.2010.04.019

[53] Xu L, Huang Y-A, Zhu Q-J, Ye C. Chitosan in molecularly-imprinted polymers: Current and future prospects. Internatioanl Journal of Molecular Science. 2015;**16**(8):18328. DOI: 10.3390/ijms160818328

[54] Gerente C, Lee VKC, Cloirec PL, McKay G. Application of chitosan for the removal of metals from wastewaters by adsorption—Mechanisms and models review. Critical Reviews in Environmental Science and Technology. 2007;**37**(1):41-127. DOI: 10.1080/10643380600729089

[55] Chen JH, Liu QL, Zhang XH, Zhang QG. Pervaporation and characterization of chitosan membranes cross-linked by 3-aminopropyltriethoxysilane. Journal of Membrane Science. 2007;**292**(1):125-132. DOI: 10.1016/j.memsci.2007.01.026

[56] Chen A, Shang C, Shao J, Lin Y, Luo S, Zhang J, et al. Carbon disulfide-modified magnetic ion-imprinted chitosan-Fe(III): A novel adsorbent for simultaneous removal of tetracycline and cadmium. Carbohydr Polymer. 2017;**155**(Supp. C):19-27. DOI:10.1016/j.carbpol.2016.08.038

[57] Chen A, Zeng G, Chen G, Hu X, Yan M, Guan S, et al. Novel thiourea-modified magnetic ion-imprinted chitosan/TiO2 composite for simultaneous removal of cadmium and 2,4-dichlorophenol. Chemical Engineering Journal. 2012;**191**(Supp. C):85-94. DOI:10.1016/j.cej.2012.02.071

[58] Zhang M, Zhang Y, Helleur R. Selective adsorption of Ag+ by ion-imprinted O-carboxymethyl chitosan beads grafted with thiourea–glutaraldehyde. Chemical Engineering Journal. 2015;**264**(Supp. C):56-65. DOI:10.1016/j.cej.2014.11.062

[59] Yoshida W, Oshima T, Baba Y, Goto M. Cu(II)-imprinted chitosan derivative containing carboxyl groups for the selective removal of cu(II) from aqueous solution. Journal of Chemical Engineering of Japan. 2016;**49**(7):630-634. DOI: 10.1252/jcej.15we293

[60] Monier M, Abdel-Latif DA, Abou El-Reash YG. Ion-imprinted modified chitosan resin for selective removal of Pd(II) ions. Journal of Colloid Interface Science. 2016;**469**(Supp. C):344-354. DOI:10.1016/j.jcis.2016.01.074

[61] Dhakal RP, Oshima T, Baba Y. Planarity-recognition enhancement of N-(2-pyridylmethyl) chitosan by imprinting planar metal ions. Reactive and Functional Polymers. 2008;**68**(11):1549-1556. DOI: 10.1016/j.reactfunctpolym.2008.08.008

[62] Liu F, Liu Y, Xu Y, Ni L, Meng X, Hu Z, et al. Efficient static and dynamic removal of Sr(II) from aqueous solution using chitosan ion-imprinted polymer functionalized with dithiocarbamate. Journal of Environmental Chemical Engineering. 2015;**3**(2):1061-1071. DOI: 10.1016/j.jece.2015.03.014

[63] Liu B, Chen W, Peng X, Cao Q, Wang Q, Wang D, et al. Biosorption of lead from aqueous solutions by ion-imprinted tetraethylenepentamine modified chitosan beads. International Journal of Biological Macromolecule. 2016;**86**(Supp. C):562-569. DOI:10.1016/j.ijbiomac.2016.01.100

[64] Hande PE, Kamble S, Samui AB, Kulkarni PS. Chitosan-based lead ion-imprinted interpenetrating polymer network by simultaneous polymerization for selective extraction of lead. Industrial and Engineering Chemistry Research. 2016;**55**(12):3668-3678. DOI: 10.1021/acs.iecr.5b04889

[65] Luo X, Luo S, Zhan Y, Shu H, Huang Y, Tu X. Novel cu (II) magnetic ion imprinted materials prepared by surface imprinted technique combined with a sol–gel process. Journal of Hazardous Materials. 2011;**192**(3):949-955. DOI: 10.1016/j.jhazmat.2011.05.042

[66] Dam HA, Kim D. Selective copper(II) sorption behavior of surface-imprinted core−shell-type polymethacrylate microspheres. Industrial and Engineering Chemistry Research. 2009;**48**(12):5679-5685. DOI: 10.1021/ie801321d

[67] Li T, Wu L, Chen S, Li H, Xu X. A simple scheme for grafting an ion-imprinted layer onto the surface of poly(propylene) Fibers. Macromolecular Chemistry and Physics. 2011;**212**(19):2166-2172. DOI: 10.1002/macp.201100195

[68] Zheng XM, Fan RY, Xu ZK. Preparation and properties evaluation of Pb(II) ion-imprinted composite membrane. Acta Polymerica Sinica 2012;**5**:561-570

[69] Zhang Z, Zhang X, Niu D, Li Y, Shi J. Highly efficient and selective removal of trace lead from aqueous solutions by hollow mesoporous silica loaded with molecularly imprinted polymers. Journal of Hazardous Material. 2017;**328**(Supp. C):160-169. DOI:10.1016/j.jhazmat.2017.01.003

[70] Fan H-T, Sun X-T, Zhang Z-G, Li W-X. Selective removal of lead(II) from aqueous solution by an ion-imprinted silica sorbent functionalized with chelating N-donor atoms. Journal of Chemical & Engineering Data. 2014;**59**(6):2106-2114. DOI: 10.1021/je500328t

[71] Cui H-Z, Li Y-L, Liu S, Zhang J-F, Zhou Q, Zhong R, et al. Novel Pb(II) ion-imprinted materials based on bis-pyrazolyl functionalized mesoporous silica for the selective removal of Pb(II) in water samples. Microporous and Mesoporous Material. 2017;**241**:165-177. DOI: 10.1016/j.micromeso.2016.12.036

[72] He R, Wang Z, Tan L, Zhong Y, Li W, Xing D, et al. Design and fabrication of highly ordered ion imprinted SBA-15 and MCM-41 mesoporous organosilicas for efficient removal of Ni2+ from different properties of wastewaters. Microporous Mesoporous Material. 2018;**257**(Supp. C):212-221. DOI:10.1016/j.micromeso.2017.08.007

[73] Li W, He R, Tan L, Xu S, Kang C, Wei C, et al. One-step synthesis of periodic ion imprinted mesoporous silica particles for highly specific removal of Cd2+ from mine wastewater. Journal of Sol-Gel Science and Technology. 2016;**78**(3):632-640. DOI: 10.1007/s10971-016-3987-2

[74] Xu S, Chen L, Li J, Guan Y, Lu H. Novel Hg^{2+}-imprinted polymers based on thymine–Hg^{2+}–thymine interaction for highly selective preconcentration of Hg^{2+} in water samples. Journal of Hazardous Material. 2012;**237-238**(Supp. C):347-354.doi:10.1016/j.jhazmat.2012.08.058

[75] ACd L, Marchioni C, Mendes TV, Wisniewski C, Fadini PS, Luccas PO. Ion imprinted polymer for Preconcentration and determination of ultra-trace cadmium, employing flow injection analysis with thermo spray flame furnace atomic absorption spectrometry. Applied Spectroscopy. 2016;**70**(11):1842-1850. DOI: 10.1177/0003702816658669

[76] Hoai NT, Yoo D-K, Kim D. Batch and column separation characteristics of copper-imprinted porous polymer micro-beads synthesized by a direct imprinting method. Journal of Hazardous Materials. 2010;**173**(1):462-467. DOI: 10.1016/j.jhazmat.2009.08.107

[77] Memon GZ, Sarwar S, Memon F, Samejo MQ, Vasandani AGM. Synthesis and characterization of ion-imprinted polymer for selective adsorption of zinc ions in aqueous media. Asian Journal of Chemistry 2017;**29**:1229-1234. DOI: 10.14233/ajchem.2017.20440

[78] Wu H-G, Ju X-J, Xie R, Liu Y-M, Deng J-G, Niu CH, et al. A novel ion-imprinted hydrogel for recognition of potassium ions with rapid response. Polymers for Advanced Technologies. 2011;**22**(9):1389-1394. DOI: 10.1002/pat.1843

[79] Luo X, Liu L, Deng F, Luo S. Novel ion-imprinted polymer using crown ether as a functional monomer for selective removal of Pb(II) ions in real environmental water samples. Journal of Materials Chemistry A. 2013;**1**(28):8280-8286. DOI: 10.1039/C3TA11098B

[80] Sun D, Zhu Y, Meng M, Qiao Y, Yan Y, Li C. Fabrication of highly selective ion imprinted macroporous membranes with crown ether for targeted separation of lithium ion. Separation and Purification Technology. 2017;**175**:19-26. DOI: 10.1016/j.seppur.2016.11.029

[81] Luo X, Guo B, Luo J, Deng F, Zhang S, Luo S, et al. Recovery of lithium from wastewater using development of li ion-imprinted polymers. ACS Sustainable Chemistry & Engineering. 2015;**3**(3):460-467. DOI: 10.1021/sc500659h

[82] Yusof NNM, Kobayashi T, Kikuchi Y. Ionic imprinting polymers using aiallylaminomethyl-calix[4] resorcinarene host for the recognition of Pb(II) ions. Polymers and Polymer Composites. 2016;**24**(9):687-694

[83] Yilmaz V, Yilmaz H, Arslan Z, Leszczynski J. Novel imprinted polymer for the Preconcentration of cadmium with determination by inductively coupled plasma mass spectrometry. Analytical Letters. 2017;**50**(3):482-499. DOI: 10.1080/00032719.2016.1182544

[84] Tamahkar E, Bakhshpour M, Andac M, Denizli A. Ion imprinted cryogels for selective removal of Ni(II) ions from aqueous solutions. Separation and Purification Technology. 2017;**179**:36-44. DOI: 10.1016/j.seppur.2016.12.048

[85] Walas S, Tobiasz A, Gawin M, Trzewik B, Strojny M, Mrowiec H. Application of a metal ion-imprinted polymer based on salen–cu complex to flow injection preconcentration and FAAS determination of copper. Talanta. 2008;**76**(1):96-101. DOI: 10.1016/j.talanta.2008.02.008

[86] Zhang T, Yue X, Zhang K, Zhao F, Wang Y, Zhang K. Synthesis of Cu(II) ion-imprinted polymers as solid phase adsorbents for deep removal of copper from concentrated zinc sulfate solution. Hydrometallurgy. 2017;**169**(Supp. C):599-606. DOI:10.1016/j.hydromet.2017.04.005

[87] Biju VM, Gladis JM, Rao TP. Ion imprinted polymer particles: Synthesis, characterization and dysprosium ion uptake properties suitable for analytical applications. Analytica Chimica Acta. 2003;**478**(1):43-51. DOI: 10.1016/S0003-2670(02)01416-2

[88] Ara B, Muhammad M, Amin H, Noori BR, Jabeen S, et al. Synthesis of ion imprinted polymers by copolymerization of Zn(II) and al(III)8-hydroxy quinolone complexes with divinylbenzene and methacryclic acid. Polymer - Plastics Technology and Engineering. 2016;**55**(14):1460-1473. DOI: 10.1080/03602559.2015.1132462

[89] Alizadeh T. An imprinted polymer for removal of Cd2+ from water samples: Optimization of adsorption and recovery steps by experimental design. Chinese Journal of Polym Science. 2011;**29**(6):658. DOI: 10.1007/s10118-011-1082-2

[90] Rajabi HR, Shamsipur M, Pourmortazavi SM. Preparation of a novel potassium ion imprinted polymeric nanoparticles based on dicyclohexyl 18C6 for selective determination of K+ ion in different water samples. Materials Science and Engineering: C. 2013;**33**(6):3374-3381. DOI: 10.1016/j.msec.2013.04.022

[91] Hashemi B, Shamsipur M. Synthesis of novel ion-imprinted polymeric nanoparticles based on dibenzo-21-crown-7 for the selective pre-concentration and recognition of rubidium ions. Journal of Separation Science. 2015;**38**(24):4248-4254. DOI: 10.1002/jssc.201500851

[92] Shamsipur M, Rajabi H. Flame Photometric determination of cesium ion after its preconcentration with nanoparticles imprinted with the cesium-dibenzo-24-crown-8 complex. Microchimica Acta 2013;**180**(3/4):243-252. DOI:10.1007/s00604-012-0927-x

[93] Shamsipur M, Hashemi B, Dehdashtian S, Mohammadi M, Gholivand MB, Garau A, et al. Silver ion imprinted polymer nanobeads based on a aza-thioether crown containing a 1,10-phenanthroline subunit for solid phase extraction and for voltammetric and potentiometric silver sensors. Analytica Chimica Acta. 2014;**852**(Supp. C):223-235. DOI:10.1016/j.aca.2014.09.028

[94] Dahaghin Z, Mousavi HZ, Boutorabi L. Application of magnetic ion-imprinted polymer as a new environmentally-friendly nonocomposite for a selective adsorption of the trace level of Cu(II) from aqueous solution and different samples. Journal of Molecular Liquid. 2017;**243**(Supp. C):380-386. DOI:10.1016/j.molliq.2017.08.018

[95] Ashouri N, Mohammadi A, Hajiaghaee R, Shekarchi M, Khoshayand MR. Preparation of a new nanoparticle cd(II)-imprinted polymer and its application for selective separation of cadmium(II) ions from aqueous solutions and determination via inductively coupled plasma optical emission spectrometry. Desalination and Water Treatment. 2016;**57**(30):14280-14289. DOI: 10.1080/19443994.2015.1072742

[96] Behbahani M, Barati M, Bojdi MK, Pourali AR, Bagheri A, Tapeh NAG. A nanosized cadmium(II)-imprinted polymer for use in selective trace determination of cadmium in complex matrices. Microchimica Acta. 2013;**180**(11):1117-1125. DOI: 10.1007/s00604-013-1036-1

[97] Barciela-Alonso MC, Plata-García V, Rouco-López A, Moreda-Piñeiro A, Bermejo-Barrera P. Ionic imprinted polymer based solid phase extraction for cadmium and lead pre-concentration/determination in seafood. Microchemical Journal. 2014;**114**(Supp. C):106-110. DOI:10.1016/j.microc.2013.12.008

[98] Langer R. Polymer-controlled drug delivery systems. Accounts of Chemical Research. 1993;**26**(10):537-542. DOI: 10.1021/ar00034a004

[99] Sellergren B, Allender CJ. Molecularly imprinted polymers: A bridge to advanced drug delivery. Advanced Drug Delivery Reviews. 2005;**57**(12):1733-1741. DOI: 10.1016/j.addr.2005.07.010

[100] Alvarez-Lorenzo C, Concheiro A. Molecularly imprinted polymers for drug delivery. Journal of Chromatography B. 2004;**804**(1):231-245. DOI: 10.1016/j.jchromb.2003.12.032

[101] Kryscio DR, Peppas NA. Mimicking biological delivery through feedback-controlled drug release systems based on molecular imprinting. AICHE Journal. 2009;**55**(6):1311-1324. DOI: 10.1002/aic.11779

[102] Suedee R, Srichana T, Rattananont T. Enantioselective release of controlled delivery granules based on molecularly imprinted polymers. Drug Delivery. 2002;**9**(1):19-30. DOI: 10.1080/107175402753413145

[103] Suedee R, Bodhibukkana C, Tangthong N, Amnuaikit C, Kaewnopparat S, Srichana T. Development of a reservoir-type transdermal enantioselective-controlled delivery system for racemic propranolol using a molecularly imprinted polymer composite membrane. Journal of Controlled Release. 2008;**129**(3):170-178. DOI: 10.1016/j.jconrel.2008.05.001

[104] Langer R, Peppas NA. Advances in biomaterials, drug delivery, and bionanotechnology. AICHE Journal. 2003;**49**(12):2990-3006. DOI: 10.1002/aic.690491202

[105] Hilt JZ, Byrne ME. Configurational biomimesis in drug delivery: Molecular imprinting of biologically significant molecules. Advanced Drug Delivery Reviews. 2004;**56**(11):1599-1620. DOI: 10.1016/j.addr.2004.04.002

[106] Cunliffe D, Kirby A, Alexander C. Molecularly imprinted drug delivery systems. Advanced Drug Delivery Reviews. 2005;**57**(12):1836-1853. DOI: 10.1016/j.addr.2005.07.015

[107] Puoci F, Cirillo G, Curcio M, Parisi OI, Iemma F, Picci N. Molecularly imprinted polymers in drug delivery: State of art and future perspectives. Expert Opinion on Drug Delivery. 2011;**8**(10):1379-1393. DOI: 10.1517/17425247.2011.609166

[108] Chen W, Ma Y, Pan J, Meng Z, Pan G, Sellergren B. Molecularly imprinted polymers with stimuli-responsive affinity: Progress and perspectives. Polymer 2015;**7**(9):1478. DOI:10.3390/polym7091478

[109] Norell MC, Andersson HS, Nicholls IA. Theophylline molecularly imprinted polymer dissociation kinetics: A novel sustained release drug dosage mechanism. Journal of Molecular Recognition. 1998;**11**(1-6):98-102. DOI: 10.1002/(SICI)1099-1352(199812)11:1/6<98::AID-JMR399>3.0.CO;2-Y

[110] Zaidi SA. Latest trends in molecular imprinted polymer based drug delivery systems. RSC Advances. 2016;**6**(91):88807-88819. DOI: 10.1039/C6RA18911C

[111] Montheard J-P, Chatzopoulos M, Chappard D. 2-Hydroxyethyl methacrylate (HEMA): Chemical properties and applications in biomedical fields. Journal of Macromolecular Sciences C. 1992;**32**(1):1-34. DOI: 10.1080/15321799208018377

[112] Achilias D, Siafaka P. Polymerization kinetics of poly(2-Hydroxyethyl methacrylate) hydrogels and Nanocomposite materials. PRO. 2017;**5**(2):21. DOI: 10.3390/pr5020021

[113] Giri A, Bhunia T, Mishra SR, Goswami L, Panda AB, Bandyopadhyay A. A transdermal device from 2-hydroxyethyl methacrylate grafted carboxymethyl guar gum-multiwalled carbon nanotube composites. RSC Advances. 2014;**4**(26):13546-13556. DOI: 10.1039/C3RA47511E

[114] Kumari A, Sharma P, Garg V, Garg G. Ocular inserts - advancement in therapy of eye diseases. Journal of Advanced Pharmaceutical Technology and Research. 2010;**1**(3):291-296. DOI: 10.4103/0110-5558.72419

[115] Lee D, Cho S, Park HS, Kwon I. Ocular Drug Delivery through pHEMA-hydrogel contact lenses co-loaded with lipophilic vitamins. Scientific Reports 2016;**6**:34194. DOI:10.1038/srep34194

[116] Bhrany AD, Irvin CA, Fujitani K, Liu Z, Ratner BD. Evaluation of a sphere-templated polymeric scaffold as a subcutaneous implant. JAMA Facial Plastic Surgery. 2013;**15**(1):29-33. DOI: 10.1001/2013.jamafacial.4

[117] Přádný M, Michálek J, Lesný P, Hejčl A, Vacík J, Šlouf M, et al. Macroporous hydrogels based on 2-hydroxyethyl methacrylate. Part 5: Hydrolytically degradable materials. Journal of Materials Science. Materials in Medicine. 2006;**17**(12):1357-1364. DOI: 10.1007/s10856-006-0611-y

[118] Sumi VS, Kala R, Praveen RS, Prasada Rao T. Imprinted polymers as drug delivery vehicles for metal-based anti-inflammatory drug. International Journal of Pharmaceutics. 2008;**349**(1-2):30-37. DOI: 10.1016/j.ijpharm.2007.07.017

[119] Karmalkar RN, Kulkarni MG, Mashelkar RA. Pendent chain linked delivery systems: II. Facile hydrolysis through molecular imprinting effects. Journal of Controlled Release. 1997;**43**(2):235-243. DOI: 10.1016/S0168-3659(96)01488-5

[120] Zhang Q, Zhang L, Wang P, Du S. Coordinate bonding strategy for molecularly imprinted hydrogels: Toward pH-responsive doxorubicin delivery. Journal of Pharmaceutical Sciences. 2014;**103**(2):643-651. DOI: 10.1002/jps.23838

[121] Liang H, Zhou B, He Y, Pei Y, Li B, Li J. Tailoring stimuli-responsive delivery system driven by metal–ligand coordination bonding. International Journal of Nanomedicine. 2017;**12**:3315-3330. DOI: 10.2147/IJN.S130859

[122] Miura K, Kinouchi M, Ishida K, Fujibuchi W, Naitoh T, Ogawa H, et al. 5-FU metabolism in cancer and orally-administrable 5-FU drugs. Cancer. 2010;**2**(3):1717

[123] Blanco MD, García O, Olmo R, Teijón J, Katime I. Release of 5-fluorouracil from poly(acrylamide-co-monopropyl itaconate) hydrogels. Journal of Chromatography B Biomedical Sciences and Applications. 1996;**680**(1):243-253. DOI: 10.1016/0378-4347(95)00401-7

[124] Fournier E, Passirani C, Colin N, Breton P, Sagodira S, Benoit J-P. Development of novel 5-FU-loaded poly(methylidene malonate 2.1.2)based microspheres for the treatment of brain cancers. European Journal of Pharmaceutics and Biopharmaceutics. 2004;**57**(2):189-197. DOI: 10.1016/s0939-6411(03)00146-2

[125] Çetin K, Denizli A. 5-Fluorouracil delivery from metal-ion mediated molecularly imprinted cryogel discs. Colloids Surface B Biointerfaces. 2015;**126**(Supp. C):401-406. DOI:10.1016/j.colsurfb.2014.12.038

[126] McKinlay AC, Xiao B, Wragg DS, Wheatley PS, Megson IL, Morris RE. Exceptional behavior over the whole adsorption−storage−delivery cycle for NO in porous metal organic frameworks. Journal of the American Chemical Society. 2008;**130**(31):10440-10444. DOI: 10.1021/ja801997r

[127] Sun C-Y, Qin C, Wang C-G, Su Z-M, Wang S, Wang X-L, et al. Chiral Nanoporous metal-organic frameworks with high porosity as materials for drug delivery. Advanced Materials. 2011;**23**(47):5629-5632. DOI: 10.1002/adma.201102538

[128] Zhang H, Piacham T, Drew M, Patek M, Mosbach K, Ye L. Molecularly imprinted nanoreactors for regioselective Huisgen 1,3-dipolar cycloaddition reaction. Journal of the American Chemical Society. 2006;**128**(13):4178-4179. DOI: 10.1021/ja057781u

[129] Abu-Surrah AS, Al-Degs YS. A molecularly imprinted polymer via a salicylaldiminato-based cobalt(III) complex: A highly selective solid-phase extractant for anionic reactive dyes. Journal of Applied Polymer Science. 2010;**117**(4):2316-2323. DOI: 10.1002/app.32072

[130] Seven F, Sahiner N. Metal ion-imprinted hydrogel with magnetic properties and enhanced catalytic performances in hydrolysis of NaBH4 and NH3BH3. International Journal of Hydrogen Energy. 2013;**38**(35):15275-15284. DOI: 10.1016/j.ijhydene.2013.09.076

[131] Yu X, Lu Z, Si N, Zhou W, Chen T, Gao X, et al. Preparation of rare earth metal ion/TiO2Hal-conducting polymers by ions imprinting technique and its photodegradation property on tetracycline. Applied Clay Science. 2014;**99**(Supp. C):125-130. DOI:10.1016/j.clay.2014.06.021

[132] Yamazaki T, Yilmaz E, Mosbach K, Sode K. Towards the use of molecularly imprinted polymers containing imidazoles and bivalent metal complexes for the detection and degradation of organophosphotriester pesticides. Analytica Chimica Acta. 2001;**435**(1):209-214. DOI: 10.1016/S0003-2670(01)00933-3

Chapter 2

Versatile Silylphosphine Ligands for Transition Metal Complexation

Julio Zamora-Moreno and Virginia Montiel-Palma

Additional information is available at the end of the chapter

http://dx.doi.org/10.5772/intechopen.73502

Abstract

In this chapter, a review throughout the literature on the chemistry of multidentate silylphosphines is presented. The incorporation of P and Si functionalities in cooperation in a single ligand backbone is exceptionally versatile, and examples of this rich chemistry stemming from the works of many research groups around the world are herein provided. The ligand systems can be flexible or rigid and incorporate varying numbers of P, Si and even other atoms. Exceptional ligand-metal systems are discussed in terms of their structure, reactivity and, in some cases, catalytic activity.

Keywords: silicon, phosphorous, silylphosphines, transition metals, multidentate ligands

1. Introduction

In modern Coordination and Organometallic Chemistry, ligand design is recognised as crucial for the development of efficient and selective complexes for important transformations including medicinal chemistry, material science and catalysis. Polydentate-rigid or semi-rigid ligands constrain the geometry at the metal centre providing inherently well-defined coordination geometries for potential incoming substrates. Indeed, a good number of these metal-ligand systems are capable of performing selectively difficult activations and many research groups around the world have directed their endeavours to the study of their chemical properties.

The incorporation of dual functionalities in a single ligand backbone has also been shown to modify the properties of the compounds making them especially prone to undergo selective

transformations resulting from differing reactivity of the coordinating atoms in the ligand. A wide variety of combinations of donor atoms have been employed to date, including for example, soft and hard donor atoms in what is known as hemilabile ligands.

In this chapter, the chemistry related to silylphosphine ligands which include in their structure both a basic P as well as a Si is reviewed. Si derivatives are exceptionally good sigma donors and exert a considerably high *trans*-influence/effect, thus their coordination generates electron rich metal centres in turn capable of activating otherwise inert substrates. Phosphines have long been preferred ligands due to their ability to tune their steric and electronic properties depending on the substituents on P. The incorporation of P and Si in a ligand framework also allows for the employment of NMR spectroscopic tools deriving from ^{31}P and ^{29}Si nuclei.

2. Silylphosphine ligands: definition, general structure and bonding

Silylphosphines can be described as bi- or polydentate ligands bearing at least one basic phosphorous (III) atom, usually a phosphine PR_3 or phosphite $P(OR)_3$, and at least one silicon-substituted

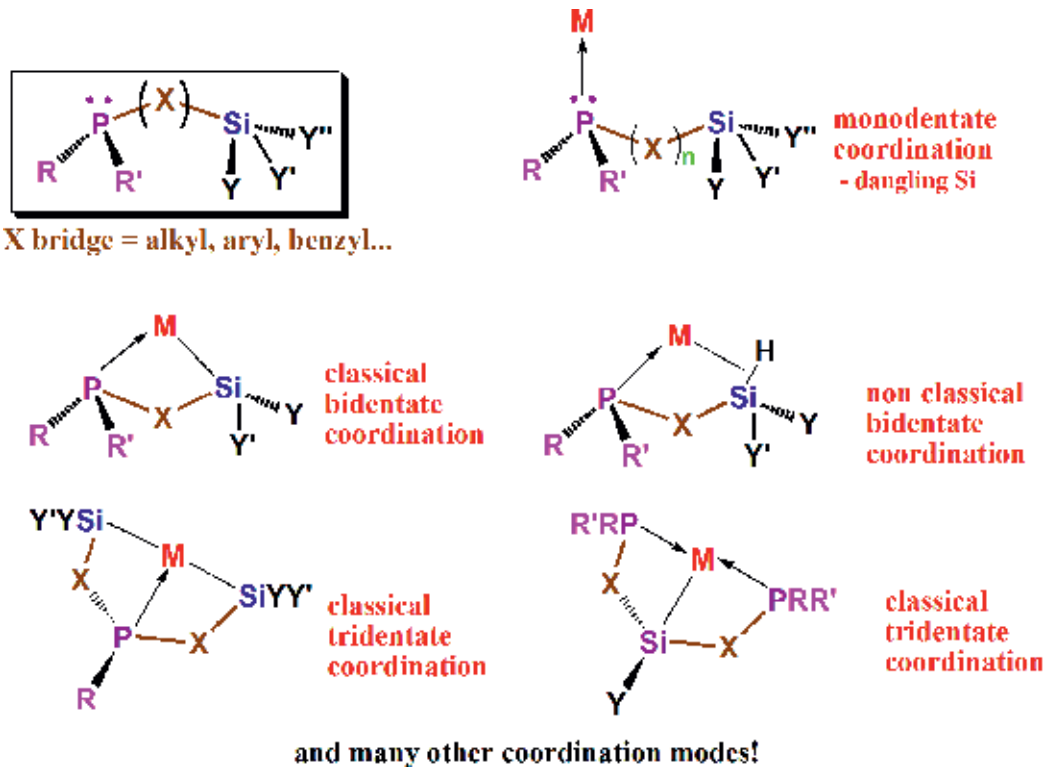

Scheme 1. General structure of silylphosphine ligands and examples of main coordination modes.

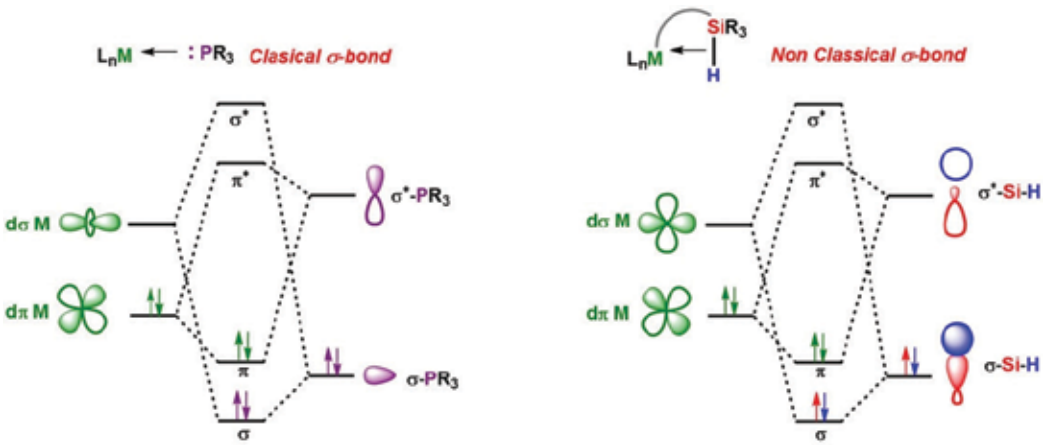

Figure 1. Molecular orbital diagrams of the phosphine and non-classical Si—H sigma moieties.

moiety. The P (III) group is able to form a coordination bond to the transition metal, while the silyl moiety is potentially prone to bind by means of loss of H_2, alkane or arene molecules. Between the P and Si atoms, there are generally a number of carbon atoms in the form of an alkyl or aryl bridges (**Scheme 1**). Else a direct P—Si bond can be established. Silylphosphines are potentially bi-, tri- or polydentate ligands, the coordination number depending on the number of P or Si moieties present in the ligand backbone.

Therefore, the molecular orbitals can be described as those of the phosphine and silicon donor moieties. For example, for the non-classical bidentate coordination mode, the frontier orbitals are shown schematically in **Figure 1**. A bidentate *P*, *Si* ligand can readily coordinate to the metal centre both through the phosphorous atom via the donation of the electron lone pair on P to an empty d-orbital on the metal and through the σ-Si—H electron pair donated to a suitable empty d-orbital on the metal generating a 3c-2e non-classical bond. In both bonds, the stabilisation is given by the retro-donation of electron density of a filled d-orbital to an anti-bonding orbital. In the full oxidative addition process of the Si—H bond to the metal, due to the strong retro-donation of the d-orbital → σ*(Si—H), the final product results in the formation of two 2c-2e bonds: M—H, M—Si. As expected, depending on the substituents on both the P and Si atoms, the molecular orbital diagrams and the energy of the HOMO and LUMO will vary. In general, it could be said according to **Figure 1**, the HOMO generally possess a higher ligand character, while the LUMO is more metal centred.

3. Silylphosphine ligands throughout the chemical literature: a review

Stobart and co-workers pioneered the systematic study of transition metals bound to silylphosphine ligands. As early as in 1983, they reported the synthesis and full characteri-

sation of an extensive family of silanes modified with a phosphorous fragment connected to the silicon atom by a polymethylene chain, of general formula $(XYZ)Si(CH_2)_nPR_2$ (where X, Y, Z = Me, Ph, Cl or H; n = 1–3; R = Me or Ph;) (**Figure 2**, compounds **1–33**) [1]. The reactivity of Vaska's complex *trans*-$[Ir(PPh_3)_2(CO)(Cl)]$ towards $Ph_2P(CH_2)_2SiRR'H$ (compounds: **12**, **14**, **16**, **18**, **20**) was also investigated. The reaction results in the formation of air stable six-coordinated Ir(III) compounds, resulting from coordination of the ligands through the P atom and of the oxidative addition of the Si—H bond (compounds: **34–38**) (**Figure 3**). Furthermore, the reactions of $Ph_2P(CH_2)_2SiMe_2H$ towards the dimers $[M(\mu\text{-}Cl)(COD)]_2$ (M = Rh, Ir; COD = 1, 5-cyclooctadiene), also afford the M(III) complexes $[MCl\{Ph_2P(CH_2)_2SiMe_2\}_2]$ (M = Rh **39**; Ir **40**) which are quiral with the two phosphorous atoms in *trans* disposition while the two Si dispose in a *cis* fashion (**Figure 3**) [2]. The fact that the reactivity of complexes **39** and **40** was remarkably constrained due to the *trans*-labilising effect of the silyl groups, was exploited in their use as catalysts for transformations of organic substrates [3]. Several works reported in the literature have argued on the high extent of *trans*-influence silyl groups exercise on a transition metal centre. There are various reasons for this behaviour including an excellent sigma orbital overlap as well as a favourable electronic release of the Si [4, 5]. This is in agreement with only a few compounds exhibiting a *trans* coordination of the Si atoms in many cases as kinetic products in equilibria with their *cis* isomers [6, 7] even when employing chelating silylphosphines (*vide supra*) [8–11] (Section 8).

It was found that the ligands with two or three phosphorous atoms and a Si-H bond (compounds **41**-**52**, **Figure 4**) coordinate via oxidative addition to the metal centre (i.e. rhodium, iridium, ruthenium and platinum) and impose steric constraints on the coordination sphere in turn restraining substrate entry to sites which could suffer the strongly labilising *trans* effect of the silyl group, increasing the complexes' capabilities as catalysts [12] (**Figure 4**).

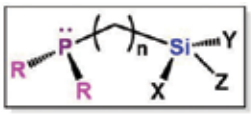

R = Ph
1. n = 1; X = Y = Z = Me
2. n = 1; X = Y = Me, Z = Cl
3. n = 1; X = Y = Me, Z = H
4. n = 1; X = Me, Y = Ph, Z = Cl
5. n = 1; X = Me, Y = Ph, Z = H
6. n = 1; X = Y = Ph, Z = Cl
7. n = 1; X = Y = Ph, Z = H
8. n = 1; X = Y = Z = Ph
9. n = 1; X = Ph, Y = Z = Cl
10. n = 1; X = Ph, Y = Z = H
11. n = 2; X = Y = Me, Z = Cl
12. n = 2; X = Y = Me, Z = H
13. n = 2; X = Me, Y = Ph, Z = Cl
14. n = 2; X = Me, Y = Ph, Z = H
15. n = 2; X = Y = Ph, Z = Cl
16. n = 2; X = Y = Ph, Z = H
17. n = 2; X = Me, Y = Z = Cl
18. n = 2; X = Me, Y = Z = H
19. n = 2; X = Ph, Y = Z = Cl
20. n = 2; X = Ph, Y = Z = H
21. n = 2; X = Y =Z = Cl
22. n = 2; X = Y =Z = H
23. n = 3; X = Y = Z = Me
24. n = 3; X = Y = Me, Z = Cl
25. n = 3; X = Y = Me, Z = H
26. n = 3; X = Y = Z = Cl
27. n = 3; X = Y = Z = H

R = Me
28. n = 2; X = Y = Me, Z = Cl
29. n = 2; X = Me, Y = Ph, Z = Cl
30. n = 2; X = Me, Y = Z = Cl
31. n = 2; X = Y = Me, Z = H
32. n = 2; X = Me, Y = Ph, Z = H
33. n = 2; X = Me, Y = Z = H

Figure 2. The silylphosphine ligands bearing alkyl bridges reported in Ref. [1].

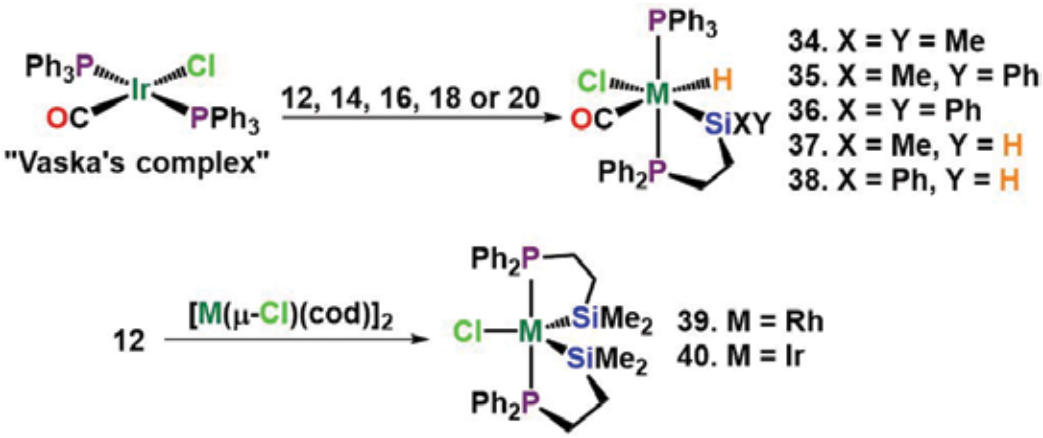

Figure 3. The reactivity of group 9 metals as reported in Ref. [2].

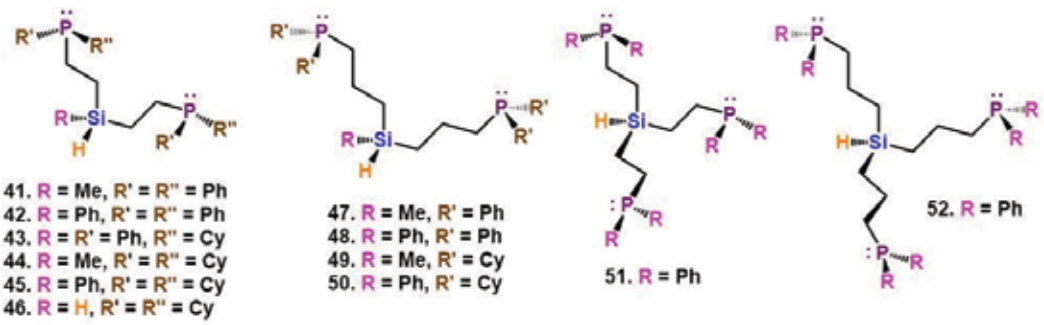

Figure 4. Design of poly(phosphino)-silane ligands reported in Ref. [12].

4. Silylphosphines complexation in tetra-coordinated systems

4.1. Square-planar geometry

Turculet and co-workers have further made significant contributions in the field of silylphosphine chemistry. They introduced a *PSiP*-type ligand [(*o*-C_6H_4-PCy_2)$_2$$SiMe_2$] (**53**) and explored its reactivity with transition metal precursors. The complexes [MCl{(*o*-C_6H_4-PCy_2)$_2$SiMe}] (M = Ni or Pd) (**64**, **65**) were treated with alkyl lithium or Grignard reagents. In the case of **65** treatment with stoichiometric amounts of MeLi led to the formation of [Pd(Me){(*o*-C_6H_4-PCy_2)$_2$SiMe}] (**61**) which regenerates complex **65**, upon reaction with Ph_2SiClH while renders [Pd{(*o*-C_6H_4-PCy_2)$_2$SiMe}($SiHPh_2$)] (**66**) from reaction with Ph_2SiH_2. The direct reaction of **53** and [$Pd_2(dba)_3$] provides complex [Pd{(*o*-C_6H_4-PCy_2)$SiMe_2$}(*o*-C_6H_4-PCy_2)] (**63**) derived from Si-C(sp^2) bond activation. Treatment of complex **64** with MeMgBr led to [Ni(Me){(*o*-C_6H_4-PCy_2)$_2$SiMe}] (**60**) and complex [Ni{(*o*-C_6H_4-PCy_2)$SiMe_2$}(*o*-C_6H_4-PCy_2)] (**62**) resulting from

ligand rearrangement. Complexes **62** (Ni) and **63** (Pd) constitute rare examples of reversible Si-C(sp^2) and Si-C(sp^3) bond cleavage (**Figure 5**) [13, 14].

Moreover, the reactivity of **54** towards $[PtCl_2(SEt_2)_2]$ leads to the generation of [PtCl{(*o*-C_6H_4-$PPh_2)_2$SiMe}] (**67**) where the ligand coordination results in adoption of a distorted square planar geometry around Pt with a persistent Cl atom bonded *trans* to the silyl group (**Figure 5**) [9].

Iwasawa and collaborators reported an interesting system for the catalytic hydrocarboxylation of allenes using the Pd(II) hydride complex [PdH{(*o*-C_6H_4-$PPh_2)_2$SiMe}] (**68**) as the active catalyst. Their methodology also served for the synthesis of β,γ-unsaturated carboxylic acids. In general, complex [Pd(OTf){(*o*-C_6H_4-$PPh_2)_2$SiMe}] (**69**) in catalytic ratios 1.0 mol% or 2.5 mol % was used in soft conditions of CO_2 pressure (1 atm) with 150 mol% of $AlEt_3$ or $ZnEt_2$ for carboxylation of 1,1-disubstituted, monosubstituted or disubstituted allenes to the respective carboxylic acid or ester [15]. In addition, the chemical properties of complex **69** were described as well. To mention some, **69** undergoes transmetalation with $AlEt_3$ followed by β-hydride elimination to generate the proposed complex **68**. Complex **69** reacted with an excess of B_2pin_2 at room temperature leading to HBpin and the monoborylpalladium complex [Pd(Bpin){(*o*-C_6H_4-$PPh_2)_2$SiMe}] (**70**) which promotes the product of borylation of styrene as well as other alkenes (**Figure 5**) [16–18].

Milstein and co-workers described the design and synthesis of the first pincer-type silanol-Pt(II) compound by using a *PSiP* ligand. The ligand {(*o*-C_6H_4-P*i*$Pr_2)_2SiH_2$} (**58**) was obtained in moderate yields from the *o*-bromophosphine. It readily reacts with $[(Me_2S)_2Pt(Me)Cl]$ at room temperature to give the bicyclic complex [PtCl{(*o*-C_6H_4-P*i*$Pr_2)_2$SiH}] (**72**), which then undergoes autoxidation yielding the silanol complex [PtCl{(*o*-C_6H_4-P*i*$Pr_2)_2$Si(OH)}] (**73**) in moderate yields (65%) (**Figure 5**) [19].

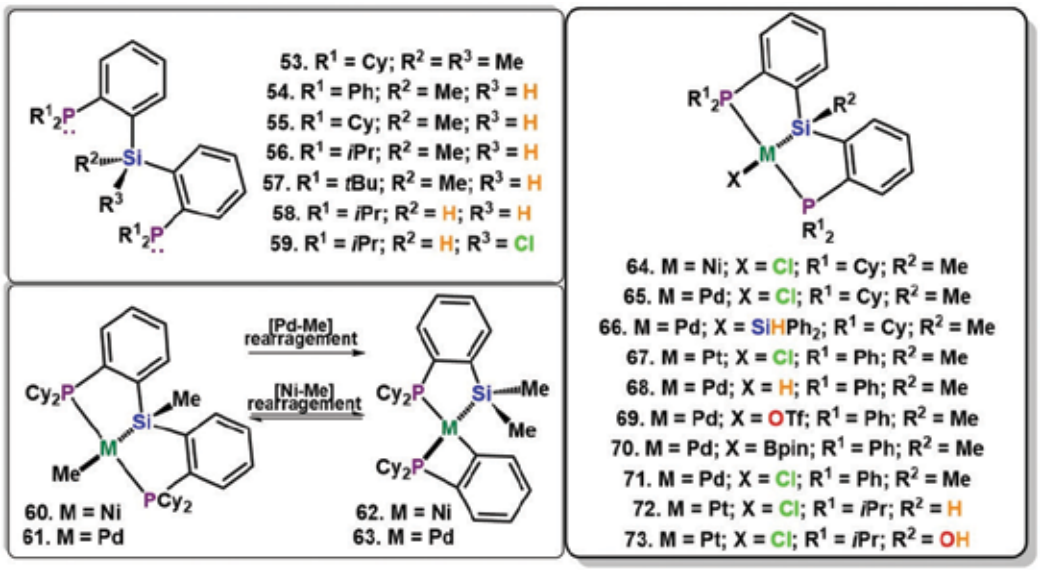

Figure 5. [PSiP] ligands and their square planar group 10 metal complexes [13-19, 26, 59].

Interestingly, changes on the identity of the substituents on the P atoms in the *PSiP* ligand backbone bring about a great strategy for the coordination of ligand **55** towards group 9 metals, in particularly rendering an Ir system able to activate intermolecular arene C—H bonds. Indeed, the reaction of **55** and $[MCl(coe)_2]_2$ (M = Rh, Ir; coe = 1-cyclooctadiene) or $[RhCl(PPh_3)_3]$ produced the monomeric complexes $[MH(Cl)\{(o\text{-}C_6H_4\text{-}PCy_2)_2SiMe\}]$ (M = Rh, **74**; Ir, **75**), which react with organolithium compound $[Me_3SiCH_2Li]$ forming neutral three-coordinate intermediate species able to subsequently coordinate neutral ligands, thus generating $[M(L)\{(o\text{-}C_6H_4\text{-}PCy_2)_2SiMe\}]$ (M = Rh, L = H_2NPh (**76**); M = Rh, L = NH_3 (**77**); M = Ir, L = C_2H_4 (**78**); M = Ir, L = PMe_3 (**79**); M = Rh, L = PMe_3 (**80**)) (**Figure 7**) [20].

4.2. Tetrahedral and trigonal pyramidal geometries

Ligand **54** (see **Figure 5**) reacted with $[Pd(PPh_3)_4]$ or $[CpPd(C_3H_5)]$ yielding complex $[Pd\{\eta^2\text{-}(o\text{-}C_6H_4\text{-}PPh_2)_2SiHMe\}(PPh_3)]$ (**82**) instead of the hypothesised hydride complex **68** which was proposed as the intermediate in the reduction of compound $[PdCl\{(o\text{-}C_6H_4\text{-}PPh_2)_2SiMe\}]$ (**71**, see **Figure 5**) with $LiHBEt_3$ in presence of PPh_3 to afford also **82** [21]. Likewise, the reaction of ligand **54** with $[Ni(PPh_3)_4]$ led to the formation of the Ni(0) complex $[Ni\{\eta^2\text{-}(o\text{-}C_6H_4\text{-}PPh_2)_2SiHMe\}(PPh_3)]$ (**81**). The Si—H, Ni—H and Ni—Si distances are 1.62(3), 1.44(2) and 2.2782(4) Å respectively, suggesting that the Si—H bond was preserved. This non-classical complexation mode is kept in solution because the observed NMR parameters such as coupling constants J_{SiH} = 89 Hz at 300 K and 77 Hz at 193 K are large ($^2J_{SiH} \leq 20$ Hz for a complete Si—H bond cleavage) and in line with the conservation of the η^2-Ni(0) structure seen in solid state (**Figure 6**). On the other hand, the mixture of **54** with $[Pt(PPh_3)_4]$ is discussed in Section 5.2 [22].

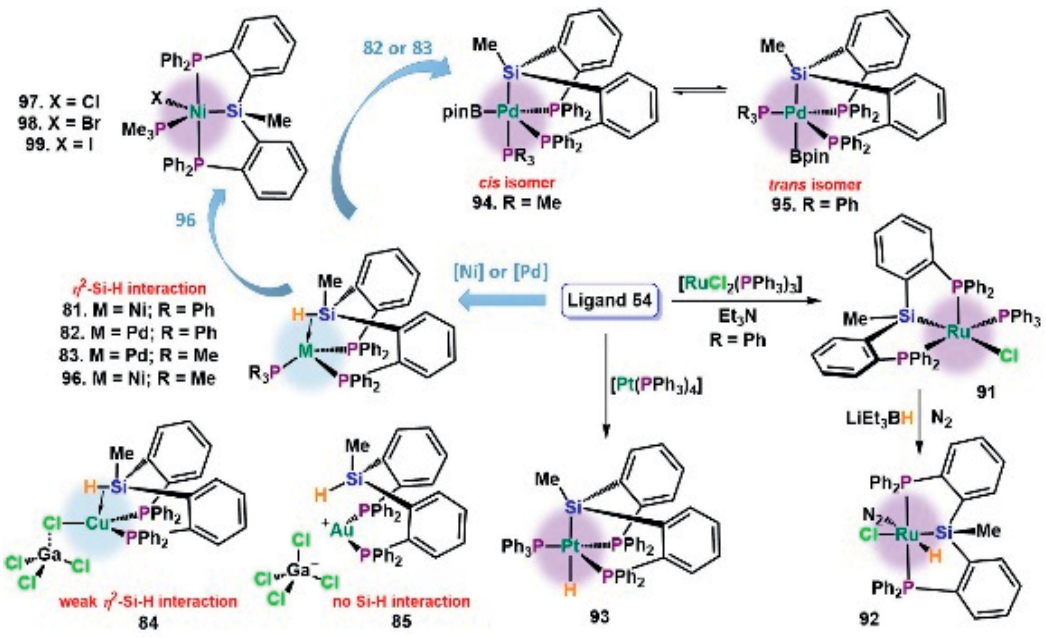

Figure 6. Reactivity of **54**. Tetra-coordination is highlighted in blue and penta-coordinated in purple [21-23, 26-29].

Bourissou and co-workers reported the reactivity of the *PSiP* ligand **54** towards CuCl and AuCl(SMe$_2$), which was subsequently followed by a stoichiometric addition of GaCl$_3$ (complexes **84**, **85**). The addition of the gallium halide was envisioned to increase the electrophilicity of the central metal and thus to escalate the strength of non-classical σ-SiH bond interaction at the metal. In complex **84**, the coordination of the ligand occurs through the two phosphorous atoms and a weak sigma interaction Si—H···Cu. The spectroscopic evidence as well as computational analyses (geometry optimisations and NBO analyses) are in agreement with weak donation σ-SiH → Cu in combination with a negligible Cu → σ*SiH back-donation in **84**. Meanwhile in the cationic gold complex **85**, the coordination of **54** took place only through the two phosphorous atoms as any non-classical Si—H bond interaction to the metal was strongly disfavoured as it was found to be by computational means 15.9 kcal/mol (**Figure 6**) [23].

Extraordinarily, **86** (described in more detail in Section 5.2) demonstrated to be a suitable precursor for the synthesis of stable 14-electron [Ru(X){(*o*-C$_6$H$_4$-Cy$_2$)$_2$SiMe}] (X = O^{t}Bu (**87**), N(SiMe$_3$)$_2$ (**88**); NHPh (**89**); NH(2,6-Me$_2$C$_6$H$_3$) (**90**)) complexes, donning unusual trigonal pyramidal coordination geometries explained once again by the presence of the strongly σ-donating silyl group in the apical site with the contribution of steric effects of the phosphino substituents in the equatorial plane (**Figure 7**) [24].

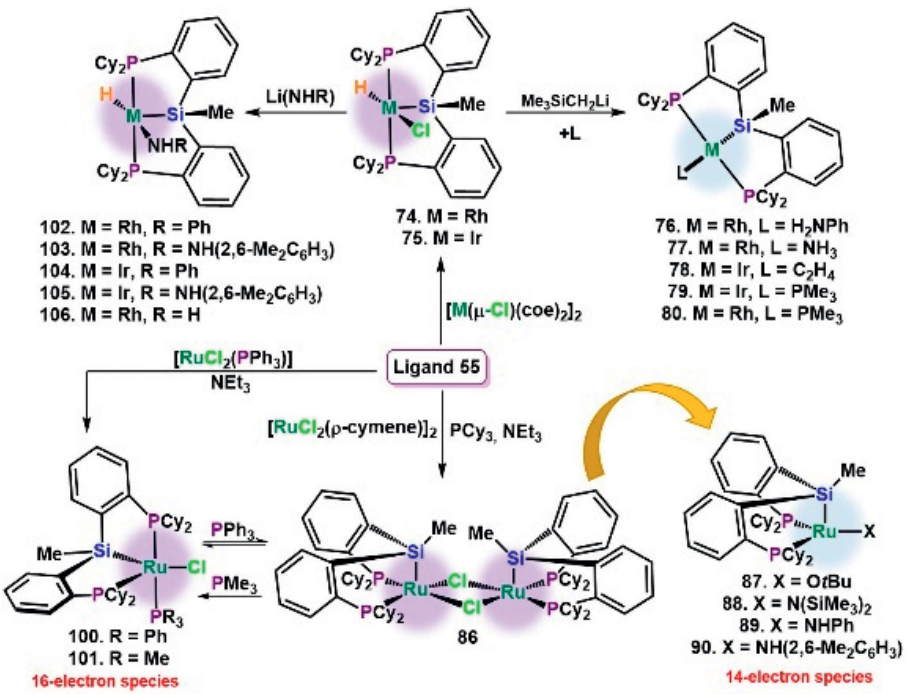

Figure 7. Reactivity of ligand **55**. Tetra-coordination is highlighted in blue and penta-coordination in purple [20, 24-25, 36].

5. Silylphosphines complexation in penta-coordinated systems

5.1. Square pyramidal geometry

The reactivity of **55** with $[RuCl_2(p\text{-cymene})]_2$ was carried out in the presence of PCy_3 and Et_3N rendering a binuclear complex that preserves bridging chloride ligands $[Ru(\mu\text{-Cl})\{(o\text{-}C_6H_4\text{-}PCy_2)_2SiMe\}]_2$ (**86**), which was exhaustively characterised spectroscopically (**Figure 7**). The ligand coordinates each Ru atom through two P, one Si and two Cl atoms in a distorted square pyramidal geometry, in which the silyl group occupies the apical coordination site. This Ru(II)-ligand system brings about stability and selectivity in catalytic transformations including the transfer hydrogenation of ketones. In this case, Li *et al* observed high conversion of the corresponding secondary alcohols for numerous dialkyl, diaryl, and alkyl/aryl ketones, employing 0.2 mol% of **86** with 5 mol% of KO^tBu at 80°C [25].

The activation of Si-H bonds in ligands of general formula $(o\text{-}C_6H_4\text{-}PR_2)_2SiHMe$ (R = Ph or Cy; **54** and **55**) was also observed in monomeric Ru systems. Compound **54** reacted with $[RuCl_2(PPh_3)_3]$ in the presence of triethylamine as a base affording complex $[RuCl\{(o\text{-}C_6H_4\text{-}PPh_2)_2SiMe\}(PPh_3)]$ (**91**). The X-ray diffraction study confirms the coordination of the ligand through the two phosphorous and the silicon atom adopting a facial arrangement with the silyl group occupying the basal position of a distorted square pyramidal geometry around Ru. The Cl atom disposes *trans* to the silyl group, and the remaining site was occupied by a PPh_3. Complex **91** reacted with $LiEt_3BH$ to form octahedral-Ru hydride complex **92** in moderate yield (**Figures 6**) [26].

5.2. Trigonal bipyramidal geometry

The mixture of **54** with $[Pt(PPh_3)_4]$ at room temperature led to the generation of five-coordinated Pt(II) complex $[PtH\{(o\text{-}C_6H_4\text{-}PPh_2)_2SiMe\}(PPh_3)]$ (**93**). In contrast with the derivatives of Ni(0) **81** and Pd(0) **82** (**Figure 6**), where the Si—H bond is only slightly activated, the Pt(II)-hydride complex **93** derives from the complete oxidative addition of the Si—H bond. The crystalline structure displays a trigonal bipyramidal geometry with the silyl group in the apical position in the metal centre. The opposed apical site was taken by the hydride ligand which in the ^1H NMR spectrum revealed a quartet at δ −7.92 ppm ($^2J_{PH}$ = 18.9 Hz) with ^{195}Pt satellites exhibiting a measured coupling constant $^{195}Pt\text{-}^1H$ of 650 Hz, which is considerably small compared with some *cis*-H-Pt(II)-Si species previously reported ($^1J_{PtH}$ = 890–1010 Hz); supporting the proposal that the hydride is located *trans* to Si atom (**Figure 6**) [22].

A study of the reaction of complex **82** and its related analogue $[Pd\{\eta^2\text{-}(o\text{-}C_6H_4\text{-}PPh_2)_2SiHMe\}(PMe_3)]$ (**83**) towards B_2pin_2 was made, since it could provide a means of accessing Pd(II) hydrides via oxidative addition of the Si—H bond. Two isomers: *cis* and *trans* were proposed. Depending on the phosphine choice, the isolation of one isomer was possible through a reversible σ-bond metathesis pathway. In the case of the PMe_3 ligated complex, the kinetic product *cis*-$[Pd(Bpin)\{(o\text{-}C_6H_4\text{-}PPh_2)_2SiMe\}(PMe_3)]$ (**94**) showed a slow reverse reaction and was obtained predominantly. In contrast, for the PPh_3 derivative, the equilibrium favoured the thermodynamic isomer *trans*-$[Pd(Bpin)\{(o\text{-}C_6H_4\text{-}PPh_2)_2SiMe\}(PPh_3)]$ (**95**) as a major product (**Figure 6**) [27, 28]. In relation

to unusual bonding modes, Sun and collaborators reported the systematic reactivity of the tridentate ligand **54** towards the low-valent nickel compound [Ni(PMe_3)$_4$] which induced the formation of Ni(0) complexes [Ni{η^2-(*o*-C_6H_4-PPh_2)$_2$MeSi-H}(PMe_3)] (**96**, **Figure 6**). Complex **96** did not undergo the oxidative addition process of a Si—H bond even in the presence of independent silanes (Et_3SiH, Ph_2MeSiH). However, the reactivity with chlorosilanes Me_3SiCl or $MeHSiCl_2$ led to the formation of Ni(II) complex [NiCl{(*o*-C_6H_4-PPh_2)$_2$MeSi}] (**97**). The halogenated products [NiX{(*o*-C_6H_4-PPh_2)$_2$SiMe}(PMe_3)] (X = Br (**98**); I (**99**)) were easily obtained from reaction with EtBr or MeI of complex **96** (**Figure 6**) [29].

The versatility of ligand **55** was also probed in the coordination towards Ru. With the aim of preparing highly valuable 16-electron complexes, complex **86** was reacted with monodentate phosphines. The reaction with PPh_3 results in small conversion to the five-coordinated compound [Ru(Cl){(*o*-C_6H_4-PCy_2)$_2$SiMe}(PPh_3)] (**100**) in equilibrium with **86**. Interestingly, this latter compounds are also formed from the reaction of ligand **55** and [$RuCl_2(PPh_3)_3$] in the presence of NEt_3 albeit in low yields. However, the production of the isolable penta-coordinate complex [Ru(Cl){(*o*-C_6H_4-PCy_2)$_2$SiMe}(PMe_3)] (**101**) was possible in quantitative yields when employing **86** in solution and the smaller, more σ-electron-donating PMe_3 (**Figure 7**) [30].

In complexes **74** and **75** (**Figure 7**), the ligand coordinates in a tridentate fashion through the phosphorous atoms which dispose in *trans* and the Si which sits in the equatorial plane of a trigonal bipyramidal geometry. The remaining sites were taken by the hydride derived from the ligand and a Cl atom. Remarkably, besides the intermolecular C—H activation ability imposed by the coordination of ligand **55** to Ir, complex **75** also exhibits facile N—H bond activation of ammonia and anilines while its Rh analogues undergo mainly adduct formation. Likewise, the starting complexes **74** and **75** react with lithium anilides [Li(NHR)] generating isolable anilido hydride complexes [MH(NHR){(*o*-C_6H_4-PCy_2)$_2$SiMe}] (M = Rh, R = Ph (**102**); M = Rh, R = {2, 6-$Me_2C_6H_3$} (**103**); M = Ir, R = Ph (**104**); M = Ir, R = {2, 6-$Me_2C_6H_3$} (**105**); M = Ir, R = H (**106**)) upon mixing. The new compounds were described as being very resistant to N—H bond reductive elimination even in the presence of alkyl or aryl substrates (**Figure 7**) [20].

The ligand (*o*-C_6H_4-PPh_2)$_3$Si-H (**107**) reacts with [Ni(PPh_3)$_4$] to yield the complex [Ni{η_2-(*o*-C_6H_4-PPh_2)$_2$Si-H(*o*-C_6H_4-PPh_2)}(PMe_3)] (**109**) bearing non-classical σ-Si—H bonds. On the other hand, complex **109** undergoes thermal oxidative addition at the Ni centre and loss of PMe_3 to allow the coordination of the previously uncoordinated phosphorous, thus rendering a compound of formula [NiH{(*o*-C_6H_4-PPh_2)$_3$Si)}] (**110**). In a subsequent step, HCl was added to afford the formation of [NiCl{(*o*-C_6H_4-PPh_2)$_3$Si)}] (**111**), which was also obtained when compound **109** was combined with one equivalent of $MeHSiCl_2$. Compounds [NiX{(*o*-C_6H_4-PPh_2)$_3$Si}] (X = Br, **112**; I, **113**) were obtained from the reaction of **110** with either EtBr or MeI (**Figure 8**).

Peters and co-workers have also reported the synthesis and reactivity of silanes functionalised with phosphines and/or sulphur derivatives. In particular, the ligand **107** reacts with [Fe_2Mes_4] leading to the formation of [Fe{(*o*-C_6H_4-PPh_2)$_3$Si}Mes] (**114**), which was characterised structurally by single crystal X-ray diffraction. The analysis discloses a distorted octahedral geometry around the Fe atom in which the ligand has taken four out of the six coordination positions, a mesityl group occupies one more and the sixth site (*trans* to silyl group) is occupied by an agostic interaction (C—H···Fe) from a methyl group in *ortho* position of the mesityl bonded to

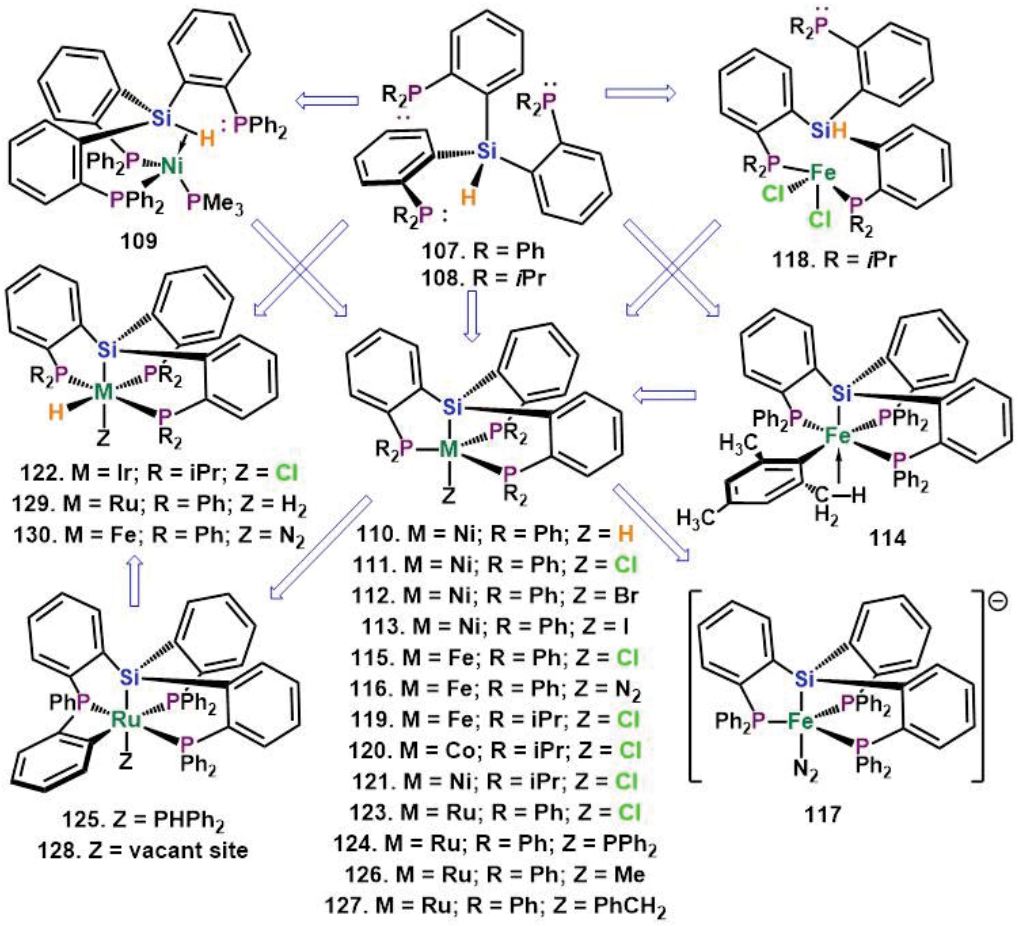

Figure 8. The chemistry of P_3Si systems [31-34].

the metal. The reaction of this agostic complex with HCl leads to the formation of complex [FeCl{(*o*-C_6H_4-PPh_2)$_3$Si}] (**115**). Subsequent reduction with Na/Hg amalgam under a N_2 atmosphere led to the Fe(I) complex [Fe(N_2){(*o*-C_6H_4-PPh_2)$_3$Si}] (**116**), which was again subjected to reduction with an additional equivalent of Na/Hg in the presence of [12]crown-4 to render dark purple ionic pair [Na([12]crown-4)$_2$]$^+$[Fe(N_2){(*o*-C_6H_4-PPh_2)$_3$Si}]$^-$ (**117**) in which Fe is in a zero oxidation state and the dinitrogen ligand is less labile than in **116** because of stronger π backdonation from the more reduced metal [32]. Once again the nature of the substituents on the P atom is determinant. Indeed, ligand (*o*-C_6H_4-P^{i}Pr$_2$)$_3$SiH (**108**) reacts with $FeCl_2$ at room temperature producing a species with one uncoordinated phosphorous atom and the Si—H bond intact [$FeCl_2${(*o*-C_6H_4-P*i*Pr$_2$)$_2$SiH(*o*-C_6H_4-P*i*Pr$_2$)}] (**118**); however, if the reaction was made in the presence of MeMgCl at −78°C, the desired complex [FeCl{(*o*-C_6H_4-P*i*Pr$_2$)$_3$Si}] (**119**) was isolated. The reactivity of **108** with metallic precursors $CoCl_2$, $NiCl_2$ and [Ir(μ-Cl)(COD)]$_2$ was found to yield the tripodal species [CoCl{(*o*-C_6H_4-P*i*Pr$_2$)$_3$Si}] (**120**), [NiCl{(*o*-C_6H_4-P*i*Pr$_2$)$_3$Si}] (**121**) and [IrHCl{(*o*-C_6H_4-P*i*Pr$_2$)$_3$Si}] (**122**), respectively (**Figure 8**) [33].

Another example of the importance of the *trans*-influence of the silyl groups on the metal coordination sphere is given by the chemical properties of [RuCl{(*o*-C_6H_4-PPh_2)$_3$Si}] (**123**). The exchange reaction with $LiPPh_2$ (also with $LiPiPr_2$) led to expected phosphide complex [Ru(PPh_2){(*o*-C_6H_4-PPh_2)$_3$Si}] (**124**), which decays at room temperature to the cyclometalated [Ru($PHPh_2$){Si(*o*-C_6H_4-PPh_2)$_2$(*o*-C_6H_4)P(*o*-C_6H_4)Ph}] (**125**). The reaction of **123** with stoichiometric amounts of MeLi or $PhCH_2MgCl$ leads to [Ru(Z){(*o*-C_6H_4-PPh_2)$_3$Si}] (Z = Me (**126**); $PhCH_2$ (**127**)). Successive loss of methane or toluene renders the formation of the unsaturated square pyramidal species [Ru{Si(*o*-C_6H_4-PPh_2)$_2$(*o*-C_6H_4)P(*o*-C_6H_4)Ph}] (**128**), which in turns affords under H_2 or N_2 atmospheres compounds [Ru(H_2)H{(*o*-C_6H_4-PPh_2)$_3$Si}] (**129**) and [Ru(N_2)H{(*o*-C_6H_4-PPh_2)$_3$Si}] (**130**) in subsequent reactions steps (**Figure 8**) [34].

6. Silylphosphines complexation in hexa-coordinated systems: octahedral geometry

Shimada and collaborators reported on the reactivity of ligands (*o*-C_6H_4-PR_2)$_2$SiHMe (R = Cy (**55**), *i*Pr (**56**), *t*Bu (**57**); **Figure 5**) towards [Ir(μ-Cl)(COD)]$_2$. The complexes [IrClH{(*o*-C_6H_4-PR_2)$_2$SiMe}] (R = Cy, **75**, *i*Pr, **131**, *t*Bu, **132**) (**Figure 7** and **9**) reacted with reducing agent $Me_4N{\cdot}BH_4$ under argon to produce the tetrahydride complexes [IrH_4){(*o*-C_6H_4-PR_2)$_2$SiMe}] (R = Cy (**133**), ^{i}Pr (**134**), ^{t}Bu(**135**)) or under dinitrogen gas to produce rare stable Ir(III) dihydride-dinitrogen complexes of formula [$IrH_2(N_2)$){(*o*-C_6H_4-PR_2)$_2$SiMe}] (R = Cy (**136**), *i*Pr (**137**)). For the last two complexes, NMR spectroscopy reveals the presence of the *fac*/*mer* isomers; the meridional and facial disposition of the *PSiP* ligand was supported by single crystal X-ray diffraction (**Figure 9**) [35].

The complex [FeH{(*o*-C_6H_4-PPh_2)$_2$SiMe}(PMe_3)$_2$] (**138**) was synthesised from [Fe(PMe_3)$_4$], its ν(Fe—H) stretching band was found at 1870 cm^{-1} in the IR spectrum, while a triplet of doublets (td),

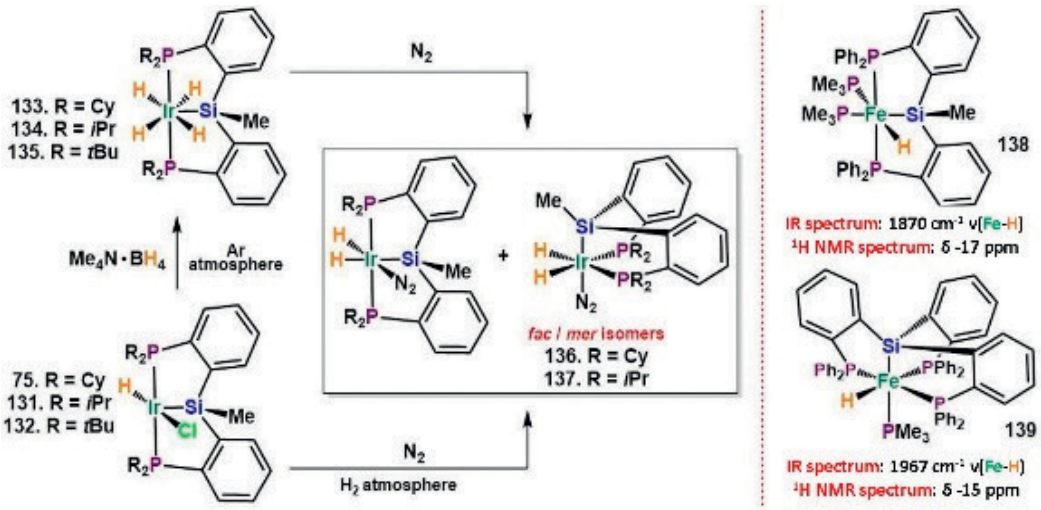

Figure 9. (Left) Chemistry of *PSiP* complexes of group 9. (Right) Related Fe octahedral complexes [35].

signal was found at δ −17.09 (J_{PH} = 71.4, 18.1 Hz) in the ^{1}H NMR spectrum. By comparison, complex [FeH{(*o*-C_6H_4-PPh_2)$_3$Si}(PMe_3)] (**139**) was characterised by a ν(Fe—H) band at 1967 cm^{-1} and a signal in ^{1}H NMR spectrum at δ −15.00 of a triplet of doublets of doublets (tdd) multiplicity with J_{PH} = 79.4, 78.8 and 10.8 Hz (**Figure 9**) [31].

7. Hybrid silylphosphines complexation

PSiN-ligated complexes have also been attractive synthetic targets due to the hemilability property the presence of soft P, Si and hard N atoms could impose. The synthetic strategy for the preparation of *PSiN*-type ligands involved the synthesis of {(*o*-C_6H_4)-NMe_2}SiHMeCl and its reactivity towards organolithium {(*o*-C_6H_4Li)-P*t*Bu_2}. In this manner, the mixed-donor ligand {(*o*-C_6H_4)-P*t*Bu_2}{(*o*-C_6H_4)-NMe_2}SiHMe (**140**) was synthesised. This new-fangled ligand reacted with group 10 precursors $PdBr_2$ or [$PtCl_2$(cod)] to give the complexes [M(X){(*o*-C_6H_4)-P^tBu_2}{(*o*-C_6H_4)-NMe_2-SiMe}] (M = Pd, X = Br (**144**); M = Pt, X = Cl (**145**)), respectively. Treatment of the latter complexes with OTf- led to the formation of compounds [M(OTf){(*o*-C_6H_4)-P*t*Bu_2}{(*o*-C_6H_4)-NMe_2-SiMe}] (M = Pd (**146**); Pt (**147**)) showing in the X-ray diffraction molecular structure a distance Pd-O of 2.3518(11) Å in **146**, which once again highlights the strong *trans*-influence of the silyl donor. The selective reversible de-coordination of the amine arm in **144** and **145** was observed upon the use of PMe_3 which yields compounds [M(X){(*o*-C_6H_4)-P*t*Bu_2-SiMe-(*o*-C_6H_4)-NMe_2}(PMe_3)] (M = Pd, X = Br (**148**); M = Pt, X = Cl (**149**)). The coordination of the *PSiN* ligand towards group 9 (Rh, Ir) and 8 (Ru) has also been studied. The complex [Ru{(*o*-C_6H_4)-P*t*Bu_2}{(*o*-C_6H_4)-CHNMe-SiMe}(η^3-cyclooctene)] (**150**) was achieved upon thermal reaction of the *PSiN* ligand with one equivalent of [Ru(2-methylallyl)$_2$(cod)]. The complex resulted from the coordination of the P and Si atoms of the ligand as well as a C—H bond activation of the methyl group (NMe) with a hydrogenated cyclooctene, remaining on the coordination sphere of the metal. Overall, a square planar geometry around Ru centre is structurally proposed (**Figure 10**) [36].

Another example of an elegant catalytic application of systems derived of *PSiN* pincer-like ligands is that comprising the ligands of general formula {(*o*-C_6H_4)-PR_2}{(*o*-C_6H_4)-NMe_2}SiHMe

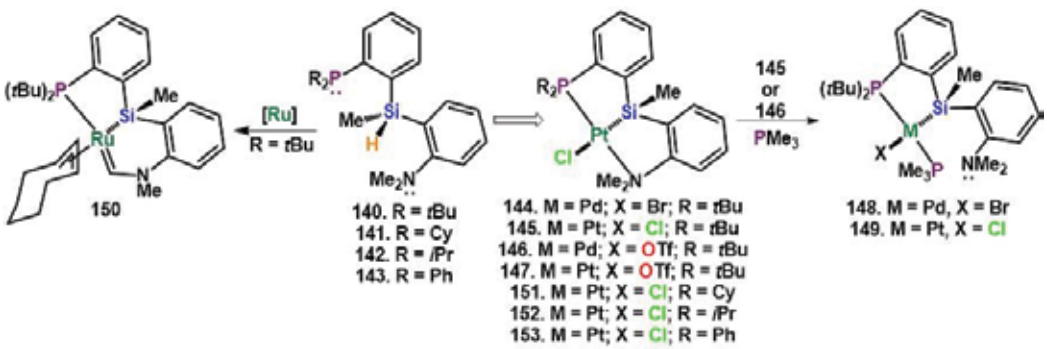

Figure 10. The chemistry of mixed *PSiN* ligands [36-37].

(R = *t*Bu (**140**); Cy (**141**); *i*Pr (**142**); Ph (**143**)) [36]. The complexes [PtCl{(*o*-C_6H_4)-PR_2(*o*-C_6H_4)-NMe_2-SiMe}] (R = *t*Bu (**145**); Cy (**151**); *i*Pr (**152**); Ph (**153**)) were synthesised by the reaction with [$PtCl_2\eta^2$-(C_2H_4)]$_2$ in the presence of Et_3N. In particular, the *PSiN*-platinum complex **151** successfully catalysed C—H borylation not only of highly electron deficient perfluoroarenes but also of the monofluorinated arenes, chloroarenes and benzoate (**Figure 10**) [37].

Regarding [M(*P_3Si*)] tripodal systems, an extended series of organometallic species of general formulae [M(X){(*o*-C_6H_4-PR_2)$_3$Si}] or [M(L){(*o*-C_6H_4-PR_2)$_3$Si}] (R = Ph, *i*Pr; X = Me, Cl; L = H_2, N_2, CO, NH_3, N_3R', PMe_3) has been disclosed with a variety of metals including, Fe [38–44], Co [45, 46], Ni [47], Ru [48], Os [48], Rh [45] and Ir [45], with outstanding and specific properties. Perhaps among the most novel systems, one can find the chemistry of novel hybrids (thioether/phosphine)-silane ligands (*o*-C_6H_4-P*i*Pr$_2$)$_{3-n}$(*o*-C_6H_4-SAd)$_n$SiH (n = 2 (**154**); 1 (**155**)) synthesised from silyl-phosphines such as (*o*-C_6H_4-P*i*Pr$_2$)$_2$SiHCl, **59** (**Figure 5**, section 4.1), upon lithiation of Br(*o*-C_6H_4)E (E = P*i*Pr$_2$ or SAd) with varying stoichiometric amounts of Li(*o*-C_6H_4)E. The reactivity of these hybrids with $FeCl_2$ afforded a new class of iron complexes featuring a S—Fe—N_2 linkage (**Figure 11**) [49]. The bulky hexa-dentate ligand {(*o*-C_6H_4-P*i*Pr$_2$)$_2$HSi-O-SiH(*o*-C_6H_4-P*i*Pr$_2$)$_2$} (**156**) was synthesised by the controlled hydrolysis of **59** (**Figure 11**). The reactivity of **59** was also reported towards $FeBr_2$ and NiX_2·DME (X = Cl or Br). The complex [$Fe_2(N_2)$(μ-H)$_2${((*o*-C_6H_4-P*i*Pr$_2$)$_2$Si)$_2$O}] (**157**) was formed in an equilibrium mixture with [$Fe_2(N_2)_2$(μ-H)$_2${((*o*-C_6H_4-P*i*Pr$_2$)$_2$Si)$_2$O}] (**158**), which were observed at low temperature in the IR spectrum (two ν(N—N) bands at 2097 and 2060 cm^{-1}) in accordance with the determined thermodynamic parameters including a large negative entropy (−30(2) cal/mol K), consistent with the coordination of a gas molecule and a rather small enthalpy of binding (−9.0(4) kcal/mol) in line with the observation of both species at low temperature (**Figure 11**) [50]. This research is particularly relevant for the understanding of nitrogenase mimicking systems. From the reactivity of a binucleating variant of a *PSiP* ligand with NiX_2.DME (X = Cl, Br) in the presence of triethylamine, dinuclear zerovalent nickel complexes bearing both η^2-(Si—H) and η^2-H_2 moieties were observed by the group of Peters. Theoretical studies suggest that the Ni centre facilitates H atom exchange between the η^2-(Si—H) and η^2-H_2 ligands via interconversion with a higher valent Ni(II) isomer (compounds **159–161**) (**Figure 11**). This exchange has been exploited in the selective catalytic deuteration of exogenous silanes [51].

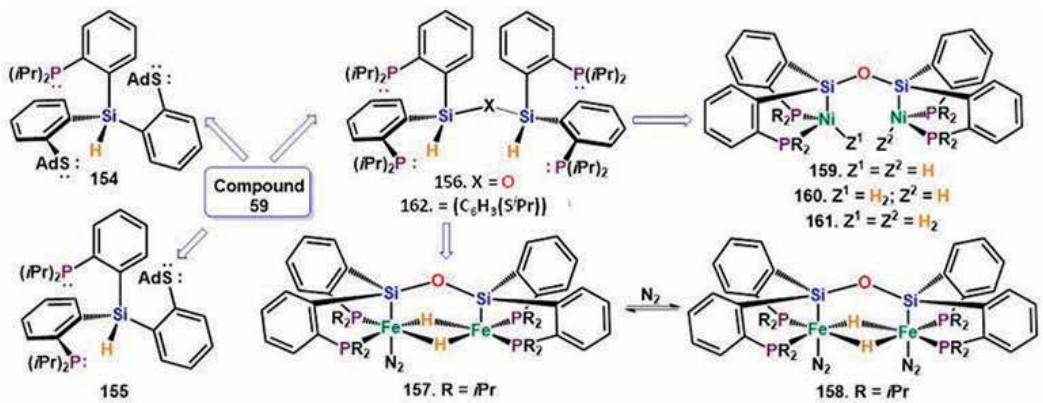

Figure 11. Chemistry of compound **59** and related reactions [49-52].

Interestingly, the synthesis of the bulkier ligand (o-C_6H_4-PiPr$_2$)$_2$HSi-(C_6H_3)SiPr-SiH(o-C_6H_4-PiPr$_2$)$_2$ (**162**) was reported very recently. The lithiation of (2,6-dibromophenyl)-isopropyl thioether with *n*BuLi in one pot followed by the stoichiometric addition of **59** affords the formation of (3-bromo-2-(isopropylthio)phenyl)(bis(2-diisopropylphenylphosphino)silane, which received the same treatment that (2,6-dibromophenyl)-isopropyl, to form the desired compound **162** (**Figure 11**) [52].

8. Bulky silylphosphines complexation

An example of rare kinetic stabilisation of *trans* bis(silyl) isomers was provided by the contributions of Kang, Ko and coworkers on the reaction of the bulky carborane silyl-phosphines {(R_2P)$C_2B_{10}H_{10}$(SiMe$_2$H)} (R = Me (**163**), OEt (**164**), Ph (**165**)) towards [Pt(η^2-C_2H_4)(PPh$_3$)$_3$] or [Pt(COD)$_2$], which afforded extremely uncommon *trans*-bis(P,Si-chelates) [Pt{(R_2P)$C_2B_{10}H_{10}$(SiMe$_2$)}$_2$] (R = Me (**166**); OEt (**167**)) formed by "chelate-assisted" oxidative addition. However, in the presence of dimethyl acetylenedicarboxylate, the complexes endure thermally rearrangements to the thermodynamically favoured *cis* isomers **166'** and **167'**. Besides, the reaction of [Pt(η^2-C_2H_4)(PPh$_3$)$_3$] towards **165** occurs via oxidative addition resulting in the mono(chelate)

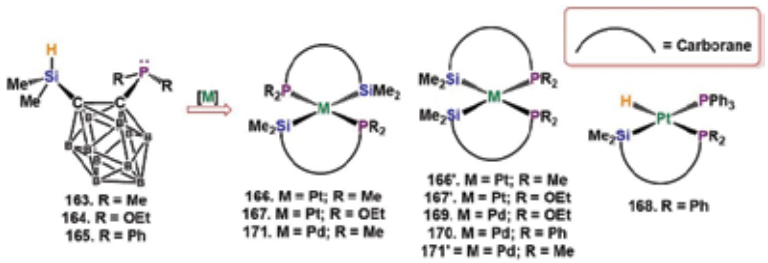

Figure 12. Bulky carborane silyl-phosphine ligands [53].

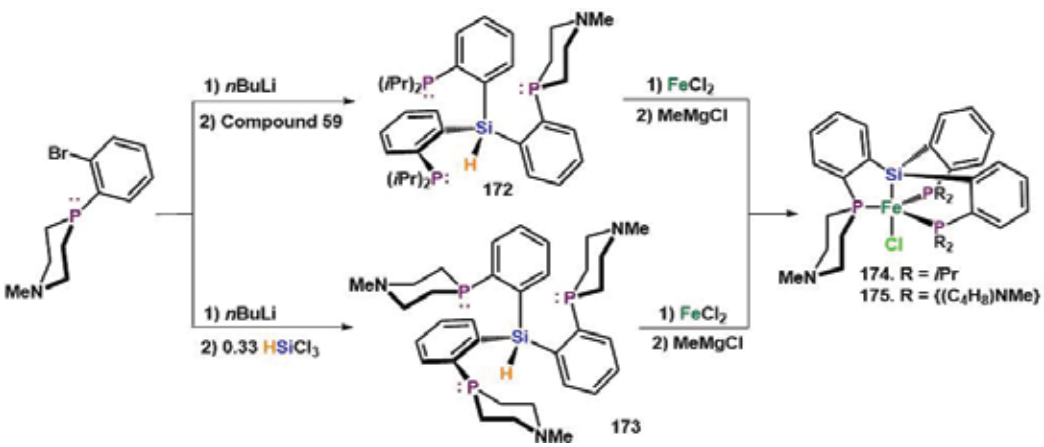

Figure 13. Syntheses of bulky cage trigonal bipyramidal iron complexes [54].

[PtH{(Ph_2P)$C_2B_{10}H_{10}$($SiMe_2$)}(PPh_3)] (**168**). These authors also investigated the reactivity of the same bulky carborane silyl-phosphines with the palladium precursor [$Pd_2(dba)_3$] and observed that depending of the substituents over the phosphorous atoms, the *cis* isomer was exclusively formed [Pd{(R_2P)$C_2B_{10}H_{10}$($SiMe_2$)}$_2$] (R = OEt (**169**); Ph (**170**)) or a mixture of the *trans*/*cis* isomers was detected when R = Me (**171**/**171′**) (**Figure 12**) [53].

Recently, the syntheses of bulky-cage trigonal bipyramidal iron complexes **174** and **175** with remote tertiary amines were reported. The synthesis of ligands **172** and **173** is shown in **Figure 13**. Once again, in this regard, the incorporation of secondary sphere interactions into iron-phosphine scaffolds is relevant to synthetic nitrogen fixation research [54].

9. Non-rigid and semi-rigid silylphosphines

Sola reported tridentate systems exemplified by [IrHCl{[$Ph_2P(CH_2)_3$]$_2$SiMe}] (**176**) [55] derived from the reaction of the ligand *PSiP* {[$Ph_2P(CH_2)_3$]$_2$SiHMe} (**47**, **Figure 3**) with the dimeric compound [Ir(μ-Cl)(cod)]$_2$. In solution, complex **176** displays an equilibrium between the *syn* (**176**) and *anti* (**176′**) isomers in a ratio 93:7 in C_6D_6 and C_7D_8, while in $CDCl_3$ or CD_2Cl_2 solutions, the ratio is *ca.* 83:17. Complex **176** (and **176′**) reacted with NaX (X = Br or I) leading to the corresponding complexes [IrHX{[$Ph_2P(CH_2)_3$]$_2$SiMe}] ((X = Br (**177**); I (**178**)) also in equilibrium with their respective *syn* and *anti*-isomers (**177′**, **178′**) in similar ratios that those of **176** [56]. The mixture of isomers **176**, also reacted with Me(O_3SCF_3) to produce the isomers *syn* **179** and *anti* **179′** with general formula [IrH(O_3SCF_3){[$Ph_2P(CH_2)_3$]$_2$SiMe}]; likewise the reactivity of **176** with AgX or HX (X = PF_6) in the presence of a neutral ligand afforded the mixture of the respective *syn*/*anti* cationic species [IrH(L)$_2$){[$Ph_2P(CH_2)_3$]$_2$SiMe}]$^+$[PF_6]$^-$ (L = NCMe (**180**/**180′**), CO (**181**/**181′**), bipy (**182**/**182′**)) (**Figure 14**) [57].

Our research group studied the reactivity of *PSi* ligand phosphino-(benzyl)-silane Ph_2P\{(*o*-C_6H_4)CH_2SiMe_2H} (**183**) towards the complexes [$RuH_2(\eta^2\text{-}H_2)(PCy_3)_2$] (**184**) and [Ru(cod)(cot)]. Complex **185** resulted from the substitution of two molecules of dihydrogen and two of the ligands PCy_3 in **184** by two ligands **183** bonded to the ruthenium atom through the phosphorous atoms and two σ-bonds of the fragments Si—H. Following loss of H_2, complex **183** slowly transformed to the cyclometalated complex **186** and subsequently into the bis(cyclometalated) **187**. When **183** was added to [Ru(cod)(cot)], the synthetic precursor of **184**, it generated directly complex **187** in very high yield. The increase on the acidity of the methylene groups of ligand

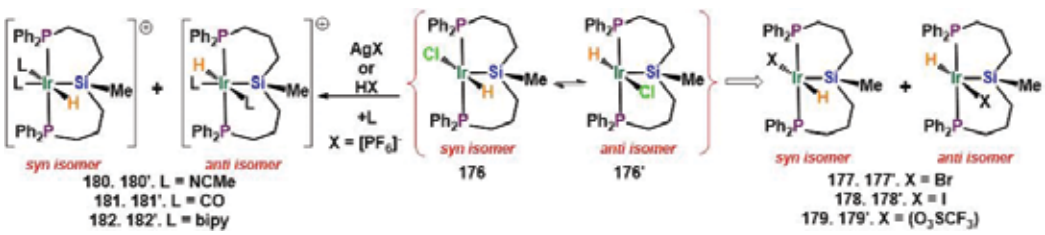

Figure 14. The chemistry of [IrP_2Si] [56, 57].

183 with respect to a non-benzilic phenylphosphine analogue, coupled with the presence of the non-classical Si—H bond interactions, which could undergo a low energy dissociation-coordination process of the Si—H bonds, was claimed to induce the gradual loss of H_2 in **185** to the final stable bis(carbometallated) complex **187**. Thus, it was reasonable to propose that the agostic interactions preceded and favoured the C—H bonds activation process [58]. Ligand *SiPSi* phosphinodibenzyl-silane PhP{(*o*-C_6H_4)CH_2SiMe_2H}$_2$ (**188**) was synthesised from PhP(*o*-tolyl)$_2$, it behaved as a pincer-like ligand capable of adopting different coordination modes at ruthenium through different degrees of Si—H bond activation. The reaction of **188** towards complex **184** yielded exclusively the formation of **189**, in which a Ru(II) centre is coordinated to one ligand **188**, through the P atom and two non-fully activated Si—H bonds preserving one PCy_3 and two hydride ligands of the original Ru complex. The phosphorous atoms arrange in a distorted *cis* with a P-Ru-P angle 113.32(4)° in **189** which should be compared to 107.1(4)° in bis-cyclometallated **187**. This sterically encumbered arrangement of the phosphine ligands around ruthenium has been explained due to the favourable exchange of the two formally terminal and two non-classical sigma hydrides around the metal. Certainly, the measured value of the J_{SiH} together with theoretical calculations and the observed chemical behaviour of **189** in solution agree with the presence of non-classical η^2-Si-H character of the silyl moieties. Thus, the complex **189** was formulated as an 18-electron species stabilised by two unusual intramolecular ε-non-classical interactions. Complex **189** undergoes facile and reversible loss of dihydrogen to afford quantitatively 16-electron complex **190,** which is thought to preserve a single non-classical hydride as well as a terminal one. Moreover, NMR spectroscopic experiments on complex **189** show it to be very fluxional in the temperature range accessible, while hydride exchange in complex **190** takes place at the high-temperature regime but in the slow exchange indicates only one

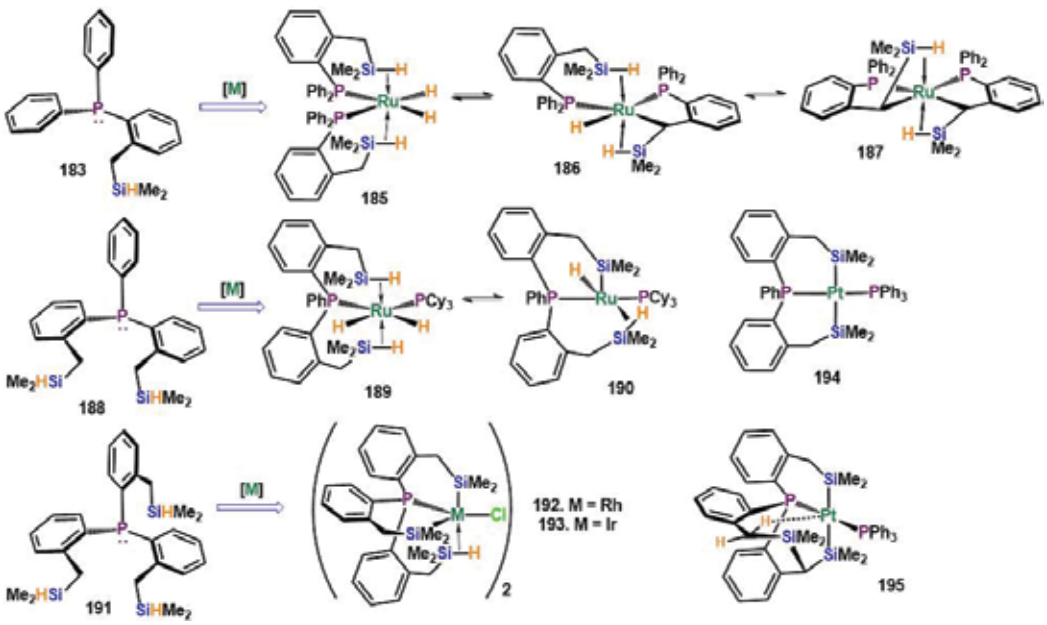

Figure 15. Chemistry of silyl-benzyl phosphines bi-, tri- and tetradentate [58-60].

hydride is bound to the two silicon atoms. In the solid-state X-ray diffraction analysis, a P-Ru-P angle of 154.37(3)° was determined, which is significantly more obtuse than in **189** and in **187**, as expected due to the diminished hydride exchange in **190**. The free energy $\Delta_r G_{298}$ of the reaction **189** to **190** + H_2 is +16.9 kJ/mol; in line with the experimentally observed conversion at 308 K [59]. The reactivity of the ligands **183**, **188** and new PSi_3 ligand P{(*o*-C_6H_4)CH_2SiMe_2H}$_3$ (**191**) was also investigated with compounds [M(μ-Cl)(cod)]$_2$ (M = Rh, Ir) [60] and with [Pt(PPh_3)$_3$] [8]. Compound **191** coordinates to Rh and Ir centres as a tetradentate ligand through the phosphorus and two silyl groups, while a third Si atom engages in an agostic Si─H interaction mode [60]. Complexes **192** and **193** react with adventitious water to generate dimeric siloxane compounds. Additionally, compounds **188** and **191** react with Pt as tridentate ligands leading exclusively to compounds exhibiting a very rare *trans* silyl disposition at square planar Pt (**194**, **195**). These two complexes feature ligand (**188** and **191**) in a close to meridional disposition. Complex **195** results from ligand modification at one of the benzylic positions which undergoes formation of a new C-Si bond. Furthermore, d^8 Pt(II) complex **195** is the first case of a silyl-platinum complex that includes a novel C─H···Pt anagostic interaction (**Figure 15**).

10. Applications of silylphosphines in the chemical industry

From the examples throughout this chapter, one can safely envisage transition metal complexes of silylphosphines as active catalysts in a variety of industrial processes. The industrial application of this type of ligand systems, nevertheless, is still at its cradle with future applications expected to materialise in the mid-term.

In principle, Si and P are capable of displaying nucleophilic behaviour and both also possess the ability to displace leaving groups such as halogens, neutral/monodentate ligands, and so on, while the factors affecting their stereochemistry may also assist the complex in the attainment of specific geometries [61]. Catalysed transfer hydrogenation has been developed mainly based on complexes derived from the platinum-metals group [62], and it is applied in industrial process and organic synthesis [63]. [PSiP-Ru] species also have shown to play an excellent role in the reduction of ketones employing ^{i}PrOH as the hydrogen source. The well-known Kumada's cross-coupling reaction is an actual tool for the low-cost synthesis of styrene derivatives in the industrial scale by using Ni and Pd complexes as catalysts [64]. Some advances revealed the crucial use of phosphorous-containing compounds [65–67] and/or the very bulky donor ligands [68, 69]. Nevertheless, [PSiP-Co] systems have shown efficient conversions in relative mild reaction conditions of an aryl-Grignard reagent reaction with organic halides at 50°C for 24 h [70].

11. Conclusion and perspectives

The incorporation of dual functionalities P and Si in single ligand backbones, silylphosphines, notably modifies the properties of the complexes they form, making them especially reactive and able to undergo selective transformations resulting from differing reactivity of the coordinating atoms in the ligand in conjunction with the chelate effect.

Predictably, the observed reactivity stems from the combination of the most important qualities of the Si ligands, specifically their extremely high σ-donating character and thus their

capability of forming σ-complexes, coupled to those features of the P moieties, which can be greatly modified by the choice of substituents.

Throughout this chapter, it has been shown the study of transition metal systems bonded to silylphosphine ligands has thrived in the last decades, but the findings in the last years highlight the importance of their study. Numerous extraordinary systems displaying unusual bonding modes, structures or physicochemical properties have been reported to date and many more can be envisioned to be informed in the near future given the relatively accessible synthesis of ligands and the seemingly unlimited structural variations.

However, the catalytic and other applications of these compounds have been sparingly explored; yet the potential of many of the reported systems is foreseen. We thus expect this field of chemistry to continue growing rapidly and encourage other research groups to direct their endeavours to this fascinating area of research.

Acknowledgements

We acknowledge financial support from CONACyT-Mexico through project CB 242818 and ANR-CONACyT 274001 and a PhD grant to JZ-M

Conflict of interest

The authors declare no conflict of interest.

Author details

Julio Zamora-Moreno and Virginia Montiel-Palma*

*Address all correspondence to: vmontielp@uaem.mx

Center for Chemical Research, Autonomous University of the State of Morelos, Cuernavaca, Morelos, Mexico

References

[1] Holmes-Smith RD, Osei RD, Stobart SR. Phosphinoalkylsilanes: Synthesis and spectroscopic properties of phosphino(silyl)methanes, 1-phosphino-2-silylethanes, and 1-phosphino-3-silylpropanes. Journal of the Chemical Society, Perkin Transactions. 1983; **I**:861-866

[2] Auburn MJ, Holmes-Smith RD, Stobart SR. (Phosphinoalkyl)silyl complexes: 3. "Chelate-assisted" hydrosilylation: Formation of enantiomeric and diasteroisomeric iridium(III) complexes with chelating (phosphinoethyl)silyl ligands. Journal of the American Chemical Society. 1984;**106**:1314-1318

[3] Auburn MJ, Stobart SR. (Phosphinoalkyl)silyl complexes. 5. Synthesis and reactivity of congeneric chelate-stabilized disilyl complexes of rhodium(III) and iridium (III): Cholorobis[[(diphenylphosphino)ethyl]dimethylsilyl] rhodium and -iridium. Inorganic Chemistry. 1985;**24**(3):318-323

[4] Zhu J, Lin Z, Marder TB. Trans influence of boryl ligands and comparison with C, Si, and Sn ligands. Inorganic Chemistry. 2005;**44**(25):9384-9390

[5] Koller SG, Martín-Romo R, Melero JS, Colquhoun VP, Schildbach D, Strohmann C, et al. Structural consequences of an extreme difference between the trans influence of the donor atoms in a palladacycle. Organometallics. 2014;**33**(24):7329-7332

[6] Kim Y-J, Park J-I, Lee S-C, Osakada K, Tanabe M, Choi J-C, et al. Cis and trans isomers of $Pt(SiHAr_2)_2(PR_3)_2$ (R = Me, Et) in the solid state and in solutions. Organometallics. 1999; **18**(7):1349-1352

[7] Kohtaro O, Makoto T. Platinum and palladium complexes with metal–silicon bonds. New bonding, structures, and chemical properties. Bulletin of the Chemical Society of Japan. 2005;**78**(11):1887-1898

[8] Cuevas-Chávez CA, Zamora-Moreno J, Muñoz-Hernández MA, Bijani C, Sabo-Etienne S, Montiel-Palma V. Stabilization of trans disilyl coordination at square-planar platinum complexes. Organometallics, ASAP article, 2017. DOI: 10.1021/acs.organomet.7b00566

[9] Mitton SJ, McDonald R, Turculet L. Synthesis and characterization of neutral and cationic platinum(II) complexes featuring pincer-like Bis(phosphino)silyl ligands: Si−H and Si−Cl bond activation chemistry. Organometallics. 2009;**28**(17):5122-5136

[10] Shimada S, Tanaka M. Group 10 transition-metal complexes with metal–silicon bonds derived from 1,2-disilylbenzenes and bis(2-silylphenyl)silane. Coordination Chemistry Reviews. 2006;**250**(9):991-1011

[11] Shimada S, Tanaka M, Honda K. Unusual reactivity of 1,2-disilylbenzene toward Pt(0) complexes. Isolation of the first $Pt^{IV}Si_4P_2$ and dinuclear, mixed-valence $Pt^{II}Pt^{IV}Si_4P_4$ complexes. Journal of the American Chemical Society. 1995;**117**(31):8289-8290

[12] Joslin FL, Stobart SR. (Phosphinoalkyl)silanes. 2. Synthesis and spectroscopic properties of poly(phosphinoalkyl)silanes. Inorganic Chemistry. 1993;**32**:2221-2223

[13] Mitton SJ, McDonald R, Turculet L. Nickel and palladium silyl pincer complexes: Unusual structural rearrangements that involve reversible Si-C(sp^3) and Si-C(sp^2) bond activation. Angewandte Chemie (International Edition in English). 2009;**48**(45):8568-8571

[14] Mitton SJ, McDonald R, Turculet L. Facile intramolecular silicon–carbon bond activation at Pt(0) and Pt(II) centers. Polyhedron. 2013;**52**:750-754

[15] Takaya J, Iwasawa N. Hydrocarboxylation of allenes with CO_2 catalized by silyl pincer-type palladium complexes. Journal of the American Chemical Society. 2008;**130**:15254-15255

[16] Takaya J, Kirai N, Iwasawa N. Efficient synthesis of diborylalkenes from alkenes and diboron by a new PSiP-pincer palladium-catalyzed dehydrogenative borylation. Journal of the American Chemical Society. 2011;**133**(33):12980-12983

[17] Kirai N, Iguchi S, Ito T, Takaya J, Iwasawa N. PSiP-pincer type palladium-catalyzed dehydrogenative borylation of alkenes and 1,3-dienes. Bulletin of the Chemical Society of Japan. 2013;**86**(7):784-799

[18] Takaya J, Iwasawa N. Silyl ligand mediated reversible beta-hydrogen elimination and hydrometalation at palladium. Chemistry—A European Journal. 2014;**20**(37):11812-11819

[19] Korshin EE, Leitus G, Shimon LJW, Konstantinovski L, Milstein D. Silanol-based pincer Pt(II) complexes: Synthesis, structure, and unusual reactivity. Inorganic Chemistry. 2008;**47**(16):7177-7189

[20] Morgan E, MacLean DF, McDonald R, Turculet L. Rhodium and iridium amido complexes supported by silyl pincer ligation: Ammonia N-H bond activation by a [PSiP]Ir complex. Journal of the American Chemical Society. 2009;**131**:14234-14236

[21] Takaya J, Iwasawa N. Bis(o-phosphinophenyl)silane as a scaffold for dynamic behavior of H–Si and C–Si bonds with palladium(0). Organometallics. 2009;**28**(23):6636-6638

[22] Takaya J, Iwasawa N. Reaction of bis(o-phosphinophenyl)silane with $M(PPh_3)_4$ (M = Ni, Pd, Pt): Synthesis and structural analysis of η^2-(Si–H) metal(0) and pentacoordinate silyl metal(II) hydride complexes of the Ni triad bearing a PSiP-pincer ligand. Dalton Transactions. 2011;**40**(35):8814-8821

[23] Joost M, Mallet-Ladeira S, Miqueu K, Amgoune A, Bourissou D. σ-SiH complexes of copper: Experimental evidence and computational analysis. Organometallics. 2013; **32**(3):898-902

[24] MacInnis MC, McDonald R, Ferguson MJ, Tobisch S, Turculet L. Four-coordinate, 14-electron Ru(II) complexes: Unusual trigonal pyramidal geometry enforced by bis(phosphino) silyl ligation. Journal of the American Chemical Society. 2011;**133**(34):13622-13633

[25] Li Y-H, Ding X-H, Zhang Y, He W-R, Huang W. Synthesis, characterization, and catalytic behavior of a PSiP pincer-type ruthenium(II) complex. Inorganic Chemistry Communications. 2012;**15**:194-197

[26] MacInnis MC, MacLean DF, Lundgren RJ, McDonald R, Turculet L. Synthesis and reactivity of platinum group metal complexes featuring the new pincer-like bis(phosphino) silyl ligand $[K_3$-$(2\text{-}Ph_2PC_6H_4)_2SiMe]$-([PSiP]): Application in the ruthenium-mediated transfer hydrogenation of ketones. Organometallics. 2007;**26**:6522-6525

[27] Kirai N, Takaya J, Iwasawa N. Two reversible sigma-bond metathesis pathways for boron-palladium bond formation: Selective synthesis of isomeric five-coordinate borylpalladium complexes. Journal of the American Chemical Society. 2013;**135**(7):2493-2496

[28] Takaya J, Kirai N, Iwasawa N. Mechanistic studies on the stereoisomerization between two stereoisomeric, isolable five-coordinate borylpalladium(II) complexes bearing a phenylene-bridged PSiP-pincer type ligand. Organometallics. 2014;**33**(6):1499-1502

[29] Wu S, Li X, Xiong Z, Xu W, Lu Y, Sun H. Synthesis and reactivity of silyl iron, cobalt, and nickel complexes bearing a [PSiP]-pincer ligand via Si–H bond activation. Organometallics. 2013;**32**(11):3227-3237

[30] MacInnis MC, Ruddy AJ, McDonald R, Ferguson MJ, Turculet L. Synthesis and characterization of five-coordinate, 16-electron RuII complexes supported by tridentate bis(phosphino)silyl ligation. Dalton Transactions. 2016;**45**(40):15850-15858

[31] Xu S, Li X, Zhang S, Sun H. Synthesis and characterization of stable tripodal silyl iron and nickel complexes. Inorganica Chimica Acta. 2015;**430**:161-167

[32] Mankad NP, Whited MT, Peters JC. Terminal Fe(I)-N2 and Fe(II)…H-C interactions supported by tris(phosphino)silyl ligands. Angewandte Chemie (International Edition in English). 2007;**46**(30):5768-7571

[33] Whited MT, Mankad NP, Lee Y, Oblad PF, Peters JC. Dinitrogen complexes supported by tris(phosphino)silyl ligands. Inorganic Chemistry. 2009;**48**:2507-2517

[34] Takaoka A, Mendiratta A, Peters JC. E–H bond activation reactions (E = H, C, Si, Ge) at ruthenium: Terminal phosphides, silylenes, and germylenes. Organometallics. 2009; **28**(13):3744-3753

[35] Fang H, Choe YK, Li Y, Shimada S. Synthesis, structure, and reactivity of hydridoiridium complexes bearing a pincer-type PSiP ligand. Chemistry, an Asian Journal. 2011; **6**(9):2512-2521

[36] Ruddy AJ, Mitton SJ, McDonald R, Turculet L. 'Hemilabile' silyl pincer ligation: Platinum group PSiN complexes and triple C-H activation to form a (PSiC)Ru carbene complex. Chemical communications (Cambridge, England). 2012;**48**(8):1159-1161

[37] Takaya J, Ito S, Nomoto H, Saito N, Kirai N, Iwasawa N. Fluorine-controlled C-H borylation of arenes catalyzed by a PSiN-pincer platinum complex. Chemical Communications. 2015;**51**(100):17662-17665

[38] Mankad NP, Müller P, Peters JC. Catalytic N-N coupling of aril azides to yield azoarenes via trigonal bipyramid iron-nitrene intermediates. Journal of the American Chemical Society Communications. 2010;**132**:4083-4085

[39] Lee Y, Mankad NP, Peters JC. Triggering N2 uptake via redox-induced expulsion of coordinated NH3 and N2 silylation at trigonal bipyramidal iron. Nature Chemistry. 2010;**2**(7):558-565

[40] Lee Y, Peters JC. Silylation of iron-bound carbon monoxide affords a terminal Fe carbyne. Journal of the American Chemical Society. 2011;**133**(12):4438-4446

[41] Fong H, Peters JC. Hydricity of an Fe-H species and catalytic CO_2 hydrogenation. Inorganic Chemistry. 2015;**54**(11):5124-5135

[42] Rittle J, Peters JC. Proton-coupled reduction of an iron cyanide complex to methane and ammonia. Angewandte Chemie (International Edition in English). 2016;**55**:1-5

[43] Rittle J, Peters JC. An Fe-N_2 complex that generates hydrazine and ammonia via Fe=NNH_2: Demonstrating a hybrid distal-to-alternating pathway for N_2 reduction. Journal of the American Chemical Society. 2016;**138**(12):4243-4248

[44] Mankad NP, Müller P, Peters JC. Catalytic N–N coupling of aryl azides to yield azoarenes via trigonal bipyramid iron–nitrene intermediates. Journal of the American Chemical Society. 2010;**132**(12):4083-4085

[45] Takaoka A, Peters JC. A homologous series of cobalt, rhodium, and iridium metalloradicals. Inorganic Chemistry. 2012;**51**(1):16-18

[46] Suess DL, Tsay C, Peters JC. Dihydrogen binding to isostructural S = (1/2) and S = 0 cobalt complexes. Journal of the American Chemical Society. 2012;**134**(34):14158-14164

[47] Tsay C, Peters JC. Thermally stable N_2 and H_2 adducts of cationic nickel(II). Chemical Science. 2012;**3**(4):1313-1318

[48] Takaoka A, Gerber LC, Peters JC. Access to well-defined ruthenium(I) and osmium(I) metalloradicals. Angewandte Chemie (International Edition in English). 2010;**49**(24):4088-4091

[49] Takaoka A, Mankad NP, Peters JC. Dinitrogen complexes of sulfur-ligated iron. Journal of the American Chemical Society. 2011;**133**(22):8440-8443

[50] Rittle J, McCrory CCL, Peters JC. A 10^6-fold enhancement in N_2-binding affinity of an $Fe_2(\mu\text{-}H)_2$ core upon reduction to a mixed-valence $Fe^{II}Fe^{I}$ state. Journal of the American Chemical Society. 2014;**136**(39):13853-13862

[51] Connor BA, Rittle J, VanderVelde D, Peters JC. A Ni0(η^2-(Si–H))(η^2-H_2) complex that mediates facile H atom exchange between two σ-ligands. Organometallics. 2016;**35**(5):686-690

[52] Creutz SE, Peters JC. Diiron bridged-thiolate complexes that bind N_2 at the Fe(II)Fe(II), Fe(II)Fe(I), and Fe(I)Fe(I) redox states. Journal of the American Chemical Society. 2015; **137**(23):7310-7313

[53] Lee Y-J, Lee J-D, Kim S-J, Keum S, Ko J, Suh I-H, et al. Synthesis, structure, and DFT calculation of (phosphino-o-carboranyl)silyl group 10 metal complexes: Formation of stable trans-Bis(P,Si-chelate)metal complexes. Organometallics. 2004;**23**(2):203-214

[54] Creutz SE, Peters JC. Exploring secondary-sphere interactions in Fe-N x H y complexes relevant to N_2 fixation. Chemical Science. 2017;**8**(3):2321-2328

[55] Brost RD, Bruce GC, Joslin FL, Stobart SR. Phosphinoalkylsilyl complexes. 12. Stereochemistry of the tridentate Bis(diphenylphosphinopropyl)silyl (biPSi) framework: Complexation that introduces "face discrimination" at Coordinatively unsaturated metal centers. X-ray crystal and molecular structures of Pt[SiMe($CH_2CH_2CH_2PPh_2)_2$]Cl, IrH[SiMe($CH_2CH_2CH_2PPh_2)_2$]Cl, and RuH[SiMe($CH_2CH_2CH_2PPh_2)_2$]$(CO)_2$. Organometallics. 1997;**16**(26):5669-5680

[56] Sola E, Garcia-Camprubi A, Andrés JL, Martin M, Plou P. Iridium compounds with κ-P,P,Si (biPSi) pincer ligands: Favoring reactive structures in unsaturated complexes. Journal of the American Chemical Society. 2010;**132**:1911-1921

[57] Garcia-Camprubi A, Martin M, Sola E. Addition of water across Si-Ir bonds in iridium complexes with kappa-P,P,Si (biPSi) pincer ligands. Inorganic Chemistry. 2010; **49**(22):10649-10657

[58] Montiel-Palma V, Muñoz-Hernandez MA, Ayed T, Barthelat JC, Grellier M, Vendier L, Sabo-Etienne S. Agostic Si-H bond coordination assists C-H bond activation at ruthenium in bis(phosphinobenzylsilane) complexes. Chemical Communications. 2007;**0**(38):3963-3965

[59] Montiel-Palma V, Muñoz-Hernandez MA, Cuevas-Chavez CA, Vendier L, Grellier M, Sabo-Etienne S. Phosphinodi(benzylsilane) PhP{(o-$C_6H_4CH_2$)$SiMe_2H$}$_2$: A versatile"PSi_2H_x" pincer-type ligand at ruthenium. Inorganic Chemistry. 2013;**52**(17):9798-9806

[60] Corona-Gonzalez MV, Zamora-Moreno J, Cuevas-Chavez CA, Rufino-Felipe E, Mothes-Martin E, Coppel Y, Muñoz-Hernandez MA, Vendier L, Flores-Alamo M, Grellier M, Sabo-Etienne S, Montiel-Palma V. A family of rhodium and iridium complexes with semirigid benzylsilyl phosphines: From bidentate to tetradentate coordination modes. Dalton Transactions. 2017;**46**(27):8827-8838

[61] Shimizu H, Nagasaki I, Matsumura K, Sayo N, Saito T. Developments in asymmetric hydrogenation from an industrial perspective. Accounts of Chemical Research. 2007; **40**(12):1385-1393

[62] Colacot T. Nobel Prize in Chemistry. Timely recognition for Rh, Ru and Os-catalysed chiral reactions. Platinum Metals Review. 2001, 2002;**46**(2):82-83

[63] Ikariya T, Murata K, Noyori R. Bifunctional transition metal-based molecular catalysts for asymmetric syntheses. Organic & Biomolecular Chemistry. 2006;**4**(3):393-406

[64] Tamao K, Sumitani K, Kumada M. Selective carbon-carbon bond formation by crosscoupling of Grignard reagents with organic halides. Catalysis by nickel-phosphine complexes. Journal of the American Chemical Society. 1972;**94**(12):4374-4376

[65] Hua X, Masson-Makdissi J, Sullivan RJ, Newman SG. Inherent vs apparent chemoselectivity in the Kumada–Corriu cross-coupling reaction. Organic Letters. 2016; **18**(20):5312-5315

[66] Yoshikai N, Matsuda H, Nakamura E. Hydroxyphosphine ligand for nickel-catalyzed cross-coupling through nickel/magnesium bimetallic cooperation. Journal of the American Chemical Society. 2009;**131**(27):9590-9599

[67] Liu N, Wang Z-X. Kumada coupling of aryl, heteroaryl, and vinyl chlorides catalyzed by amido pincer nickel complexes. The Journal of Organic Chemistry. 2011; **76**(24):10031-10038

[68] Xi Z, Liu B, Chen W. Room-temperature Kumada cross-coupling of unactivated aryl chlorides catalyzed by N-heterocylic carbene-based nickel(II) complexes. The Journal of Organic Chemistry. 2008;**73**(10):3954-3957

[69] Iglesias MJ, Prieto A, Nicasio MC. Kumada–Tamao–Corriu coupling of heteroaromatic chlorides and aryl ethers catalyzed by (IPr)Ni(allyl)Cl. Organic Letters. 2012; **14**(17):4318-4321

[70] Xiong Z, Li X, Zhang S, Shi Y, Sun H. Synthesis and reactivity of N-heterocyclic PSiP pincer iron and cobalt complexes and catalytic application of cobalt hydride in Kumada coupling reactions. Organometallics. 2016;**35**(3):357-363

Chapter 3

Ligand-Protected Gold Clusters

Sakiat Hossain, Lakshmi V. Nair, Junta Inoue,

Yuki Koyama, Wataru Kurashige and Yuichi Negishi

Additional information is available at the end of the chapter

http://dx.doi.org/10.5772/intechopen.73441

Abstract

Small gold clusters with diameters less than or equal to 2 nm (below approximately 200 atoms) possess geometric and electronic structures different from bulk gold. When these gold clusters are protected by ligands, these clusters can be treated as chemical compounds. This review focuses on gold clusters protected by chalcogenate (thiolate, selenolate, or tellurolate) ligands and describes the methods by which these clusters are synthesized as well as their geometric/electronic structures and physical and chemical properties. Recent findings regarding ligand exchange reactions, which may be used to impart functionality to these compounds, are also described.

Keywords: gold clusters, chalcogenate, geometric and electronic structures, physical and chemical properties, ligand exchange reactions

1. Introduction

Small gold clusters with diameters less than or equal to 2 nm (below approximately 200 atoms) possess geometric and electronic structures different from those of bulk gold [1]. The geometric structure often consists of an atomic arrangement, such as an icosahedral structure, that differs from the close-packed structure of bulk gold, as a result of reducing the surface energy. In addition, a discrete electronic structure appears rather than the continuous structure observed in the bulk element. Owing to these characteristics, small gold clusters exhibit fundamental properties and functionalities different from those of bulk gold. In addition, when these gold clusters are protected by ligands, it is possible to treat them as chemical compounds. In early

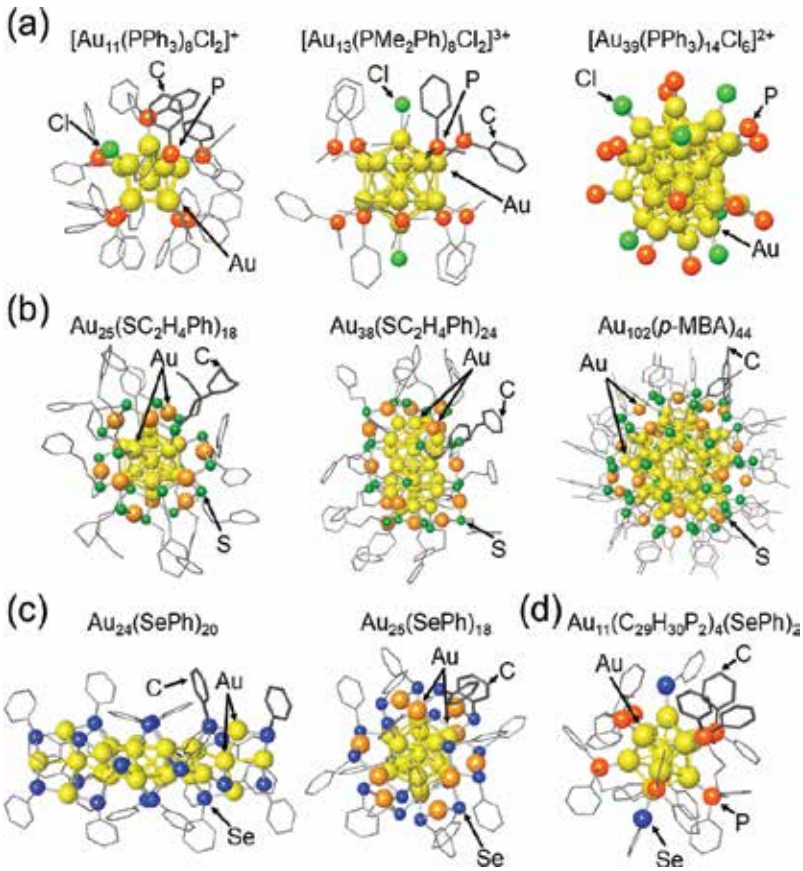

Figure 1. The crystal structures of (a) $Au_n(PR_3)_m$, (b) $Au_n(SR)_m$, (c) $Au_n(SeR)_m$, and (d) $Au_n(PR_3)_m(SeR)_l$. H atoms are omitted for clarity. In $[Au_{39}(PPh_3)_{14}Cl_6]^{2+}$, C atoms are also not shown (these figures were adapted from Refs. [2, 10, 11, 29, 30, 34, 47, 48, 59]).

studies, beginning in the 1960s, phosphine was employed as a protective ligand [2–16]. Representative phosphine (PR_3)-protected gold clusters ($Au_n(PR_3)_m$) include $[Au_{11}(PPh_3)_8Cl_2]^+$, $[Au_{13}(PMe_2Ph)_8Cl_2]^{3+}$, $[Au_{39}(PPh_3)_{14}Cl_6]^{2+}$, and $Au_{55}(PPh_3)_{12}Cl_6$ (**Figure 1(a)**). Unfortunately, these clusters have been found to be unstable in solution, which restricts their practical applications. In contrast, thiolate (SR)-protected gold clusters ($Au_n(SR)_m$), first synthesized by Brust et al. in 1994 (**Figure 1(b)**) [17], are highly stable both in solution and in the solid state, because the SR ligands form strong bonds with gold atoms. These $Au_n(SR)_m$ clusters exhibit various physical and chemical properties not shown by bulk gold, such as photoluminescence and catalytic activity. For these reasons, SR ligands have become the most common choice for use with gold clusters [18–40]. Recently, the synthesis of gold clusters protected by other chalcogenates (selenolate (SeR) or tellurolate (TeR); **Figure 1(c)**) [41–51], by alkynes [52–54], or by two kinds of ligand (**Figure 1(d)**) [55–59] has also been reported. In this chapter, we focus on gold clusters protected by chalcogenates ($Au_n(XR)_m$; XR = SR, SeR, or TeR) and describe the synthetic procedures, geometric/electronic structures, and physical and chemical properties of these compounds. Moreover, the physical and chemical properties of these gold clusters are greatly affected by the type of functional group of the protecting ligand. The ligand exchange

http://dx.doi.org/10.5772/intechopen.73441

reaction is a very powerful means for introducing the different ligands into the pre-synthesized cluster. Although this type of reaction was discovered nearly 20 years ago [60–65], the associated mechanism was not fully understood at that time. Recently, tremendous progress has been made in terms of the precise synthesis and evaluation of metal clusters, and details of these reactions have been elucidated [66, 67]. Recent findings regarding these reactions are therefore also included herein.

2. Synthesis of $Au_n(XR)_m$ clusters

The method used most frequently to synthesize $Au_n(XR)_m$ clusters is based on the chemical reduction of gold ions in the presence of ligands in solution (**Figure 2**). In this approach, a gold salt and the ligand are mixed in solution to form Au-ligand complexes that are subsequently treated with a reducing agent (normally $NaBH_4$). $Au_n(XR)_m$ clusters are formed by the aggregation

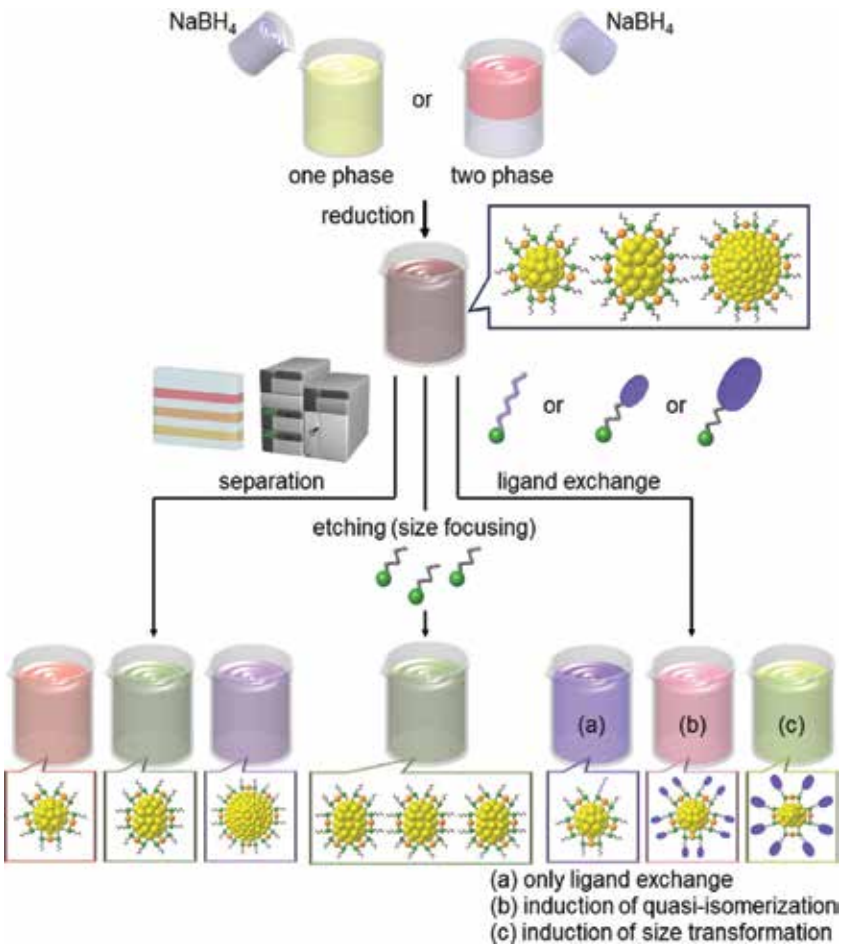

Figure 2. A typical procedure for the synthesis of $Au_n(SR)_m$ clusters having a well-defined chemical composition.

of the resulting gold atoms in conjunction with surface protection by the ligands [18]. In the first report published by Brust et al., dodecanethiolate was used as the ligand [17]. Because a gold salt and dodecanethiolate are soluble in different solvents, Brust transferred the gold salt from an aqueous phase to a ligand-containing toluene phase using a phase-transfer reagent (representing a two-phase system; **Figure 2**). In contrast, in more recent research, tetrahydrofuran (THF) has often been used as the solvent because it could dissolve both gold salt and ligand [68]. This removes the need for phase transfer of the gold salt and thereby simplifies the synthesis to a one-phase system (**Figure 2**). Similarly, when a hydrophilic thiol is used as the ligand, gold clusters can be synthesized in a one-phase system [69–71].

The product obtained from this technique is typically a mixture of $Au_n(XR)_m$ clusters having various numbers of constituent atoms. Because the physical and chemical properties of the clusters are greatly affected by the number of atoms, separation by size or conversion to stable clusters by exposure to severe conditions is required to obtain $Au_n(XR)_m$ clusters with well-defined physical properties and functions (**Figure 2**) [18, 72]. Polyacrylamide gel electrophoresis [69–72], high-performance liquid chromatography [72–77], and solvent extraction are the most frequently applied techniques for size separation. It is also common to use an etching reaction for size convergence [72, 78–82]. In addition to these techniques, the ligand exchange method, in which the ligands of a specific $Au_n(XR)_m$ cluster are replaced with other ligands, is an effective means of generating $Au_n(XR)_m$ clusters with a specific chemical composition (**Figure 2**) [83]. Recent results associated with such ligand exchange reactions are discussed in Section 6.

3. Geometrical structures of $Au_n(XR)_m$ clusters

Until 2007, it was believed that $Au_n(SR)_m$ clusters possess a geometrical structure in which an Au core is covered with thiolate ligands (**Figure 3(a)**) [84]. Since then, single-crystal X-ray

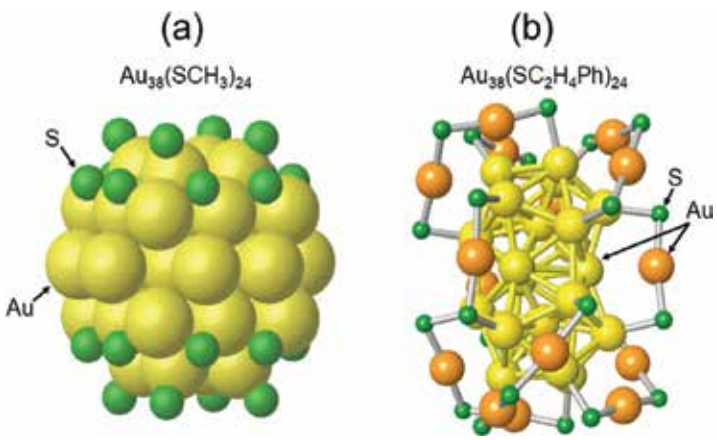

Figure 3. The geometrical structures of $Au_{38}(SR)_{24}$ (a) predicted by theoretical calculations in 1999 and (b) determined by single-crystal X-ray structural analysis in 2010. The R groups have been omitted for clarity (these figures were adapted from Refs. [30, 84]).

structural analysis has revealed that several $Au_n(SR)_m$ clusters consist of an Au core covered with multiple —S(R)[—Au—S(R)]$_x$— staples (**Figure 3(b)**) [30, 85–88]. Based on the geometrical structures determined for $Au_n(SR)_m$ clusters to date, it can be assumed that almost all small $Au_n(SR)_m$ clusters have this type of core-shell structure. Single-crystal X-ray structural analysis has also demonstrated that small $Au_n(SeR)_m$ clusters have core-shell structures similar to those of small $Au_n(SR)_m$ clusters (**Figure 1(c)**) [47, 48]. The geometrical structure of $Au_n(TeR)_m$ clusters has not yet been determined experimentally, although theoretical calculations [45, 89] have shown that these clusters are also likely to have a similar core-shell structure.

4. Electronic structures of $Au_n(XR)_m$ clusters

Unlike bulk gold, small $Au_n(SR)_m$ clusters have discrete electronic structures. As a result, multiple peak structures can be observed in the optical absorption spectra of these clusters. As an example, $Au_n(SC_{12}H_{25})_m$ clusters show multiple peak structures across the entire visible range in their optical absorption spectra up to the size of $Au_{144}(SC_{12}H_{25})_{60}$ (**Figure 4**) [75]. Such fine peak structures are not observed in the spectra of larger clusters, although peaks that can be attributed to surface plasmon resonance absorption have been identified at approximately

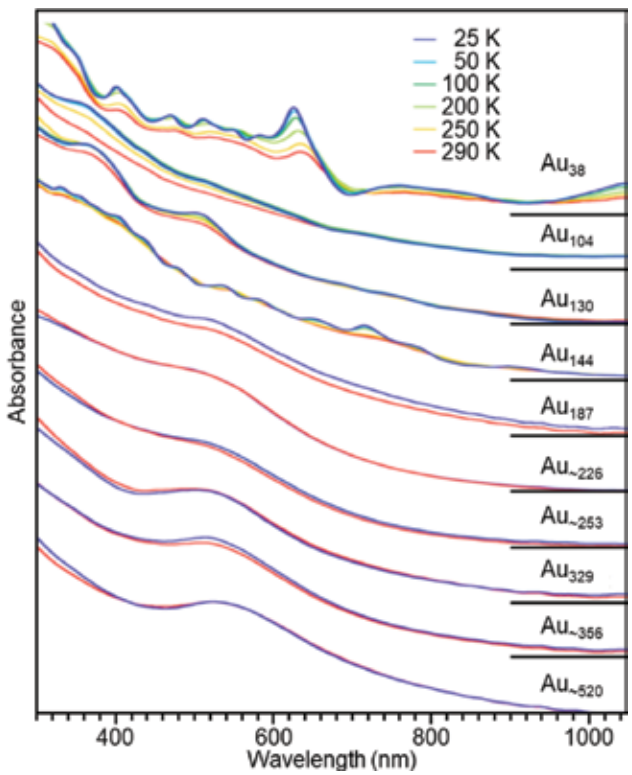

Figure 4. Optical absorption spectra of films composed of $Au_n(SC_{12}H_{25})_m$ clusters (n = 38–520) at various temperatures (25–290 K) (this figure was adapted from Ref. [75]).

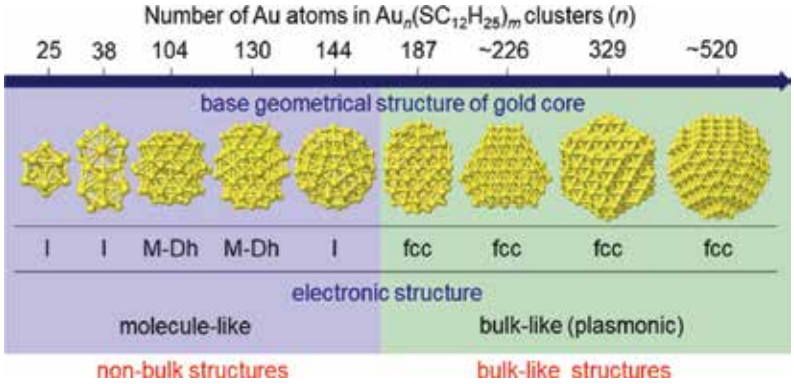

Figure 5. Structural changes in $Au_n(SC_{12}H_{25})_m$ clusters with varying numbers of gold atoms (this figure was adapted from Ref. [75]).

520 nm in their optical absorption spectra (**Figure 4**). Thus, the electronic structures of $Au_{187}(SC_{12}H_{25})_{68}$ and larger clusters tend to resemble that of bulk gold (**Figure 5**) [75].

At present, the relationship between cluster size and electronic structure is not well understood for $Au_n(SeR)_m$ and $Au_n(TeR)_m$ clusters, because only a small number of such compounds have been studied to date. However, the researches regarding $Au_{25}(SeR)_{18}$ and $Au_{38}(SeR)_{24}$ clusters have demonstrated that changing the ligands from SR to SeR reduces the HOMO-LUMO gap of the clusters [42, 43] and that this effect becomes more pronounced in the case of clusters containing TeR in the ligand shell [45].

5. Physical and chemical properties of $Au_n(XR)_m$ clusters

$Au_n(SR)_m$ clusters exhibit size-specific electronic structures, and their physical and chemical properties also vary with size. Herein, we first discuss typical physical and chemical characteristics of such $Au_n(SR)_m$ clusters.

5.1. Photoluminescence

Small $Au_n(SR)_m$ clusters have been shown to exhibit photoluminescence (**Figure 6(a)**) [18, 20, 23, 70, 71, 90]. As an example, $Au_{25}(SG)_{18}$ (SG = glutathionate) exhibits photoluminescence with an estimated quantum yield of ~1 $\times$ 10^{-3} [71], which can be used for sensing and imaging applications [91].

5.2. Redox behavior

$Au_n(SR)_m$ clusters also display redox behavior [20, 21]. **Figure 6(b)** shows a differential pulse voltammogram obtained from $Au_{25}(SC_2H_4Ph)_{18}$, in which the peaks at -1.9 and -0.3 V originate from $[Au_{25}(SC_2H_4Ph)_{18}]^{-/2-}$ and $[Au_{25}(SC_2H_4Ph)_{18}]^{0/-}$ redox couples, respectively. This

http://dx.doi.org/10.5772/intechopen.73441

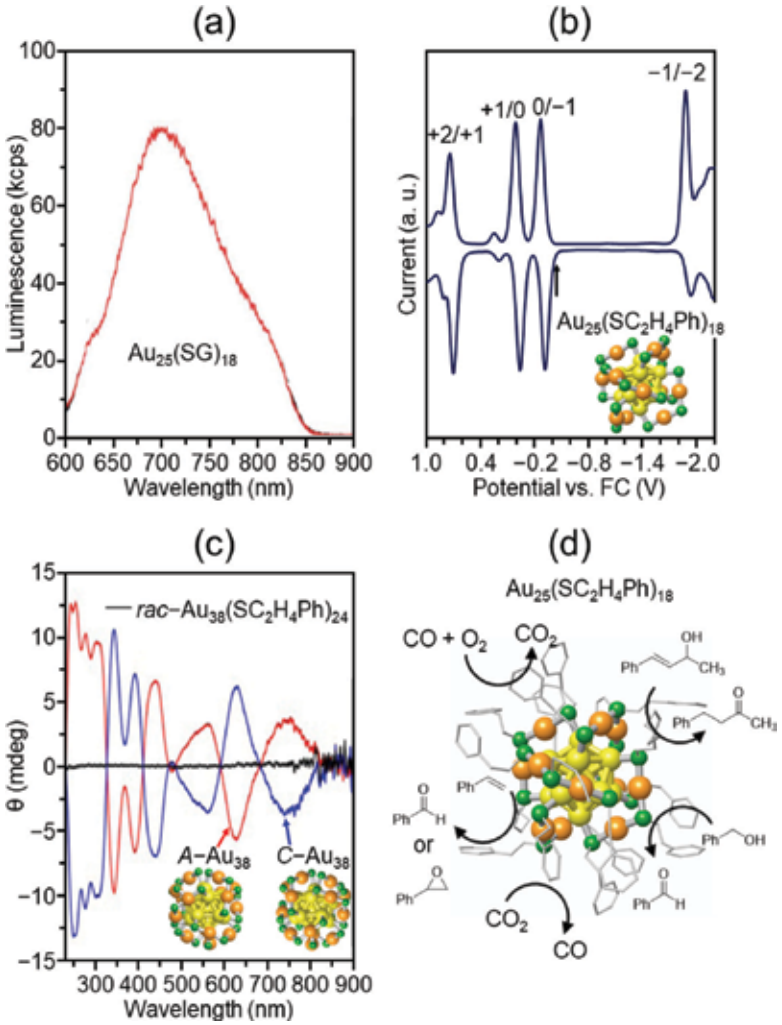

Figure 6. Size-specific physical and chemical properties of $Au_n(SR)_m$ clusters: (a) photoluminescence, (b) redox behavior, (c) optical activity, and (d) catalytic activity (these figures were adapted from Refs. [22, 90, 95]).

redox behavior is not confined to clusters with discrete electronic structures; $Au_n(SR)_m$ clusters larger than $Au_{144}(SR)_{60}$ also exhibit redox behavior as a result of quantized double-layer charging [21]. The redox properties of $Au_n(SR)_m$ clusters could be applied to single-electron transistors [92].

5.3. Optical activity

Several clusters, such as $Au_{38}(SR)_{24}$ and $Au_{40}(SR)_{24}$, have optical isomers with different —S(R)[—Au—S(R)]$_x$— staple (x = 1, 2) configurations [93–95] and thus are optically active [36]. **Figure 6(c)** presents the circular dichroism spectra of two optical isomers of $Au_{38}(SC_2H_4Ph)_{24}$

[95]. The anisotropy factor associated with the optical activity of this cluster increases with wavelength up to a maximum of 4×10^{-3}.

5.4. Catalytic activity

Catalytic activity is another typical size-specific property of $Au_n(SR)_m$ clusters (**Figure 6(d)**) [22, 72]. As an example, $Au_{25}(SR)_{18}$ catalyzes the oxidation of CO, styrene, benzyl alcohol, cyclohexane, and sulfides. The same cluster also exhibits catalytic activity for the hydrogenation of nitrophenol, aldehydes, and ketones and promotes C—C coupling reactions. As noted, several $Au_n(SR)_m$ clusters have optical isomers and therefore could potentially function as asymmetric catalysts [96].

5.5. Effect of changing ligands

Regarding $Au_n(SeR)_m$ and $Au_n(TeR)_m$ clusters, it has been reported that the incorporation of SeR or TeR ligands changes the nature of the bonding between the Au atoms and the ligands [97, 98]. In the case of $Au_n(SeC_{12}H_{25})_m$ clusters, this effect reduces the degree of charge transfer from the Au atoms to the ligands (**Figure 7(a)**) such that the Au—ligand bond becomes much more covalent than that in $Au_n(SC_{12}H_{25})_m$ clusters [41]. Owing to these changes in bonding characteristics, $Au_{25}(SeR)_{18}$ (R = $C_{12}H_{25}$ or C_8H_{17}) exhibits greater resistance to degradation in solution compared with $Au_{25}(SR)_{18}$ (R = $C_{12}H_{25}$ or C_8H_{17}) (**Figure 7(b)**) [42, 99]. In addition to such an improved stability, the use of SeR ligands is expected to improve conductivity between the gold core and the ligands [97, 100, 101], and future work is likely to demonstrate the conductivity of $Au_n(SeR)_m$ clusters. Furthermore, recent studies have found that $Au_{25}(SePh)_{18}$ exhibits catalytic activity for the reduction of 4-nitrophenol (**Figure 7(c)**) [48].

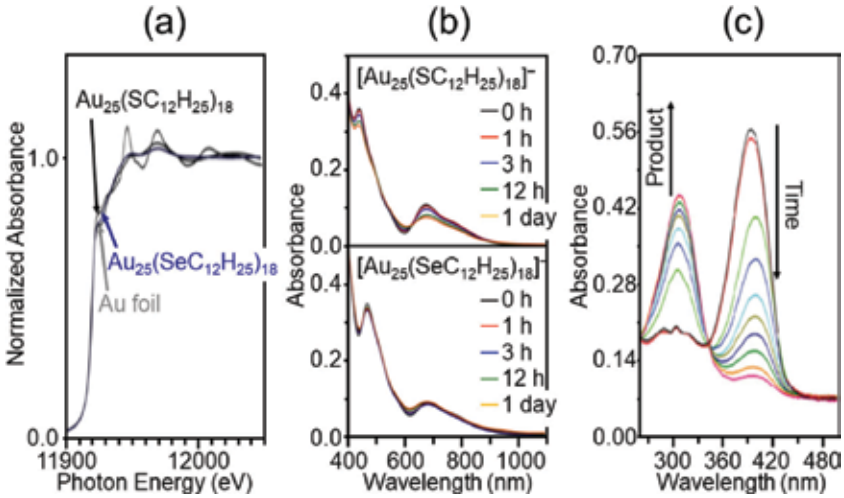

Figure 7. A comparison of (a) the Au L_3-edge X-ray absorption near-edge structure spectra of $Au_{25}(SeC_{12}H_{25})_{18}$ and $Au_{25}(SC_{12}H_{25})_{18}$ and (b) the stability of $Au_{25}(SeC_{12}H_{25})_{18}$ and $Au_{25}(SC_{12}H_{25})_{18}$ in solution under harsh conditions. (c) Representative UV-vis optical absorption spectra acquired during the reduction of 4-nitrophenol to 4-aminophenol over $Au_{25}(SePh)_{18}$ (these figures were adapted from Refs. [42, 43, 48]).

6. Ligand exchange reactions

As described above, $Au_n(SR)_m$ clusters tend to resist degradation. However, this type of metal cluster readily exchanges its ligands with other coexisting ligands in solution (**Figure 8(a)**). A complete understanding of the associated mechanism would allow these reactions to be controlled, thus permitting synthesis of novel metal clusters with specific functions. Recently, more details regarding exchange reactions between metal clusters and ligands have been reported, and these findings are discussed in this section.

6.1. Mechanism

Murray et al. reported the ligand exchange reactions of this type of cluster nearly 20 years ago [60–65]. However, their research was conducted using mixtures and did not use advanced techniques such as mass spectrometry and single-crystal X-ray structural analysis to characterize the products. Therefore, a thorough understanding of the details of these reactions was not obtained. More recent research has elucidated the associated mechanism. As an example, $Au_{25}(SR)_{18}$ has a geometry in which the Au_{13} core is covered by six —S(R)—[Au—S(R)]$_2$— staples (**Figure 9(a)**). As a result, there are two types of SR units in $Au_{25}(SR)_{18}$: those in contact with the Au_{13} core (core-site SR; **Figure 9(a)**) and those at the apex of each staple (apex-site SR; **Figure 9(a)**) [102, 103]. Ackerson et al. performed a single-crystal X-ray structural analysis of the product obtained from the reaction of $Au_{25}(SC_2H_4Ph)_{18}$ (SC_2H_4Ph = 2-phenyl ethanethiolate)

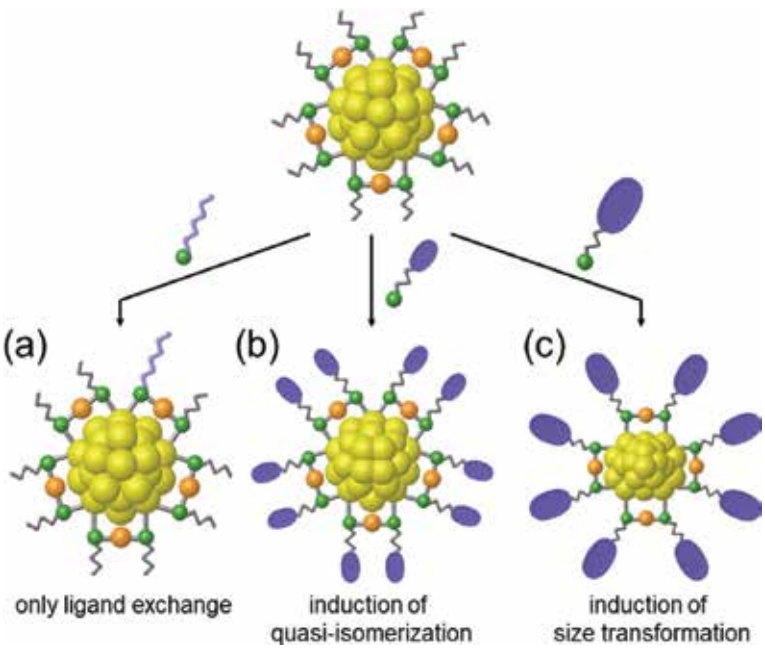

Figure 8. A schematic diagram of ligand exchange reactions including (a) only ligand exchange, (b) induction of quasi-isomerization, and (c) induction of size transformation.

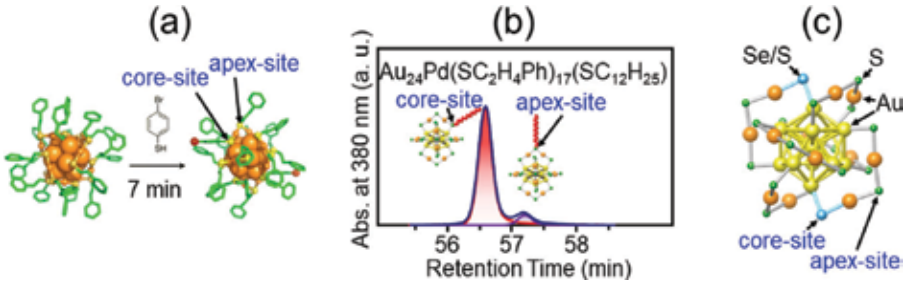

Figure 9. Preferential sites in ligand exchange reactions. (a) and (c) Geometrical structures of the products obtained from the reaction between $Au_{25}(SC_2H_4Ph)_{18}$ and *para*-bromobenzenethiol and benzeneselenol, respectively. (b) Chromatogram of the product obtained from the reaction between $Au_{24}Pd(SC_2H_4Ph)_{18}$ and dodecanethiol (these figures were adapted from Refs. [103, 104, 106]).

with *para*-bromobenzenethiol to ascertain which SR was more likely to be exchanged [103]. The results showed that $Au_{25}(SC_2H_4Ph)_{16}(p\text{-BBT})_2$ (*p*-BBT = *para*-bromobenzenethiolate), in which the substitution had occurred at the core-site SR ligands, was obtained (**Figure 9(a)**), suggesting that the ligand exchange occurred at the core-site SR locations. However, this prior work did not determine whether other structures may have been present in the reaction mixture or not. For this reason, Niihori et al. employed reversed-phase high-performance liquid chromatography to allow the high-resolution separation of the coordination isomers generated by a similar reaction and estimated the distribution of isomers in the product. It was confirmed that the product mixture mainly contained a coordination isomer in which the core-site SR ligands had been substituted (**Figure 9(b)**) [104]. Fernando and Aikens performed density functional theory (DFT) calculations at approximately the same time, and the results indicated that ligand exchange was likely to occur at core-site SR ligands in $Au_{25}(SR)_{18}$ [105]. These results demonstrated that ligand exchange preferentially proceeds at core-site SR ligands in $Au_{25}(SC_2H_4Ph)_{18}$. The research by Hossain et al. has revealed that preferential exchange at core-site SR ligands also occurs in the reaction between $[Au_{25}(SC_2H_4Ph)_{18}]^-$ and other chalcogenides (**Figure 9(c)**) [106].

6.2. Induction of quasi-isomerization

Studies have found that, in addition to ligand exchange, a change in geometry can also take place during reactions with thiol (RSH) (**Figure 8(b)**). This discovery originated from the prediction of the geometry of $Au_{24}(SR)_{20}$ clusters. Specifically, Jin et al. synthesized $Au_{24}(SC_2H_4Ph)_{20}$ in 2010 [107], after which Pei and coworkers predicted the geometry of these clusters via DFT calculations based on $Au_{24}(SCH_3)_{20}$ [108]. Thereafter, Jin et al. characterized $Au_{24}(SCH_2Ph\text{-}^tBu)_{20}$ ($SCH_2Ph\text{-}^tBu$ = 4-*tert*-butylphenylmethanethiolate) by single-crystal X-ray structural analysis but found that the resulting structure was different from that predicted by Pei's group [109]. This discrepancy prompted Jiang et al. to study the geometric structures of $Au_{24}(SR)_{20}$ clusters (R = CH_3, C_2H_4Ph, or $CH_2Ph\text{-}^tBu$) using DFT, leading to the conclusion that the most stable structure of a $Au_{24}(SR)_{20}$ cluster depends on the ligand [110]. At present, this theory has not been proven experimentally for $Au_{24}(SR)_{20}$. However, in 2016, Jin et al. reported that exchanging the ligands of $Au_{28}(SPh\text{-}^tBu)_{20}$ ($SPh\text{-}^tBu$ = 4-*tert*-butylbenzenethiolate) with cyclohexanethiolate (S-*c*-C_6H_{11}) altered the skeletal structure of the cluster (**Figure 10(a)**) [111].

http://dx.doi.org/10.5772/intechopen.73441

This same work also demonstrated that exchanging the ligands of $Au_{28}(S\text{-}c\text{-}C_6H_{11})_{20}$ with SPh-^{t}Bu regenerated the original geometry, meaning that the reaction was reversible (**Figure 10(a)**) [111]. Thus, it has recently been revealed that both ligand exchange and quasi-isomerization (as opposed to true isomerization because the ligand is different) can be induced for a particular $Au_n(SR)_m$ cluster.

6.3. Induction of size transformation

Researches have also shown that the introduction of a significant structural deformation via ligand exchange can result in the formation of $Au_n(SR)_m$ clusters with different chemical compositions (**Figure 8(c)**) [102]. An example is the reaction of $Au_{38}(SC_2H_4Ph)_{24}$ clusters (**Figure 3(b)**) with ^{t}Bu-PhSH in solution, from which $Au_{36}(SPh\text{-}^tBu)_{24}$ was generated as the main product (yield ~90%) (**Figure 10(b)**) [112]. This outcome indicates that exchange with a ligand containing a bulky functional group can affect the chemical composition of the cluster.

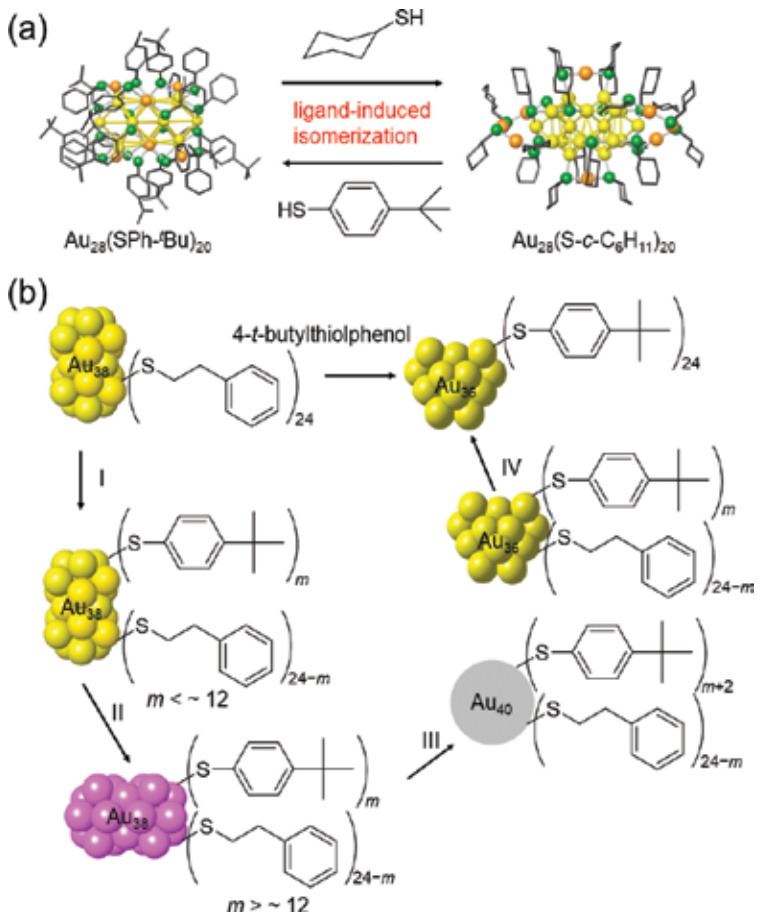

Figure 10. Examples of ligand exchange reactions, including (a) quasi-isomerization and (b) size transformation (these figures were adapted from Refs. [111, 112]).

Research regarding the mechanism of such reactions has also been conducted. Jin et al. found that the following four processes occur in the reaction between $Au_{38}(SC_2H_4Ph)_{24}$ and ^{t}Bu-PhSH: (I) ligand exchange, (II) structural distortion, (III) disproportionation, and (IV) size focusing conversion together with further ligand exchange (**Figure 10(b)**) [112]. In the first process, ligand exchange occurs without size or structural transformations, while the structural distortion of the resulting $Au_{38}(SC_2H_4Ph)_{24-m}(SPh\text{-}^tBu)_m$ (m > ~12) is initiated in the second process. During the third process, one $Au_{38}(SC_2H_4Ph)_{24-m}(SPh\text{-}^tBu)_m$ releases two gold atoms to form Au_{36} and another $Au_{38}(SC_2H_4Ph)_{24-m}(SPh\text{-}^tBu)_m$ captures these two atoms and two free ligands to form $Au_{40}(SC_2H_4Ph)_{24-m}(SPh\text{-}^tBu)_{m+2}$. In the final process, the $Au_{40}(SC_2H_4Ph)_{24-m}(SPh\text{-}^tBu)_{m+2}$ begins to convert to Au_{36}, such that pure $Au_{36}(SPh\text{-}^tBu)_{24}$ is eventually obtained (**Figure 1(b)**). $Au_n(SR)_m$ clusters such as $Au_{28}(SPh\text{-}^tBu)_{20}$, $Au_{36}(SPh\text{-}^tBu)_{24}$, and $Au_{36}(S\text{-}c\text{-}C_5H_9)_{24}$, none of which can be generated via direct synthesis at atomic precision, have also been synthesized in a size-selective manner by inducing this kind of structural deformation [102].

6.4. Relation between ligand structure and outcome

In this way, the outcomes are significantly affected by the bulkiness of the ligand in the ligand exchange reactions. Normally, ligand exchange with alkanethiol or PhC_2H_4SH does not result in structural transformation, but simply leads to ligand exchange. Conversely, a bulky ligand such as ^{t}Bu-PhSH often leads to structural transformation. At present, these are no clear rules for predicting the final state of the deformed cluster (whether quasi-isomerization or size transformation). The final state seems to be related to the magnitude of the structural transformation and the possibility of isomeric structures with similar stabilities.

7. Summary

This chapter summarized common methods of fabricating $Au_n(XR)_m$ clusters and surveyed the various geometric and electronic structures of these compounds, as well as their physical and chemical properties. Recent discoveries regarding ligand exchange reactions capable of enhancing the functionality of these clusters were also described. Although the precise synthesis of such clusters was first reported only 13 years ago at the time of writing, many studies regarding these clusters have been conducted in the interim, all of which have significantly improved our understanding of synthetic methods as well as the structures and functions of the clusters. It is expected that more information related to $Au_n(XR)_m$ clusters will be gained on the basis of continuing research, leading to the readily synthesis of metal clusters with desired functions in the near future.

Acknowledgements

This work was partly supported by the Japan Society for the Promotion of Science (JSPS) KAKENHI (grant numbers JP16H04099, 16 K17480, and 17 K19040) and by the Scientific

Research on Innovative Areas (Coordination Asymmetry) (grant number 17H05385). Funding from the Takahashi Industrial and Economic Research Foundation, Futaba Electronics Memorial Foundation, Iwatani Naoji Foundation, Murata Science Foundation, and Ube Industries Foundation is also gratefully acknowledged. We thank Michael D. Judge, MSc, from Edanz Group (www.edanzediting.com/ac) for editing a draft of this manuscript.

Conflict of interest

There are no conflicts to declare.

Author details

Sakiat Hossain[1], Lakshmi V. Nair[2], Junta Inoue[2], Yuki Koyama[2], Wataru Kurashige[2] and Yuichi Negishi[1,2]*

*Address all correspondence to: negishi@rs.kagu.tus.ac.jp

1 Photocatalysis International Research Center, Tokyo University of Science, Noda, Chiba, Japan

2 Department of Applied Chemistry, Faculty of Science, Tokyo University of Science, Tokyo, Japan

References

[1] Corain B, Schmid G, Toshima N, editors. Metal Nanoclusters in Catalysis and Materials Science: The Issue of Size Control. 1st ed. Amsterdam: Elsevier; 2007. 470 p

[2] McKenzie LC, Zaikova TO, Hutchison JE. Structurally similar triphenylphosphine-stabilized undecagolds, $Au_{11}(PPh_3)_7Cl_3$ and $[Au_{11}(PPh_3)_8Cl_2]Cl$, exhibit distinct ligand exchange pathways with glutathione. Journal of the American Chemical Society. 2014; **136**:13426-13435. DOI: 10.1021/ja5075689

[3] Vollenbroek FA, Bour J, Velden JWA. Gold-phosphine cluster compounds. The reactions of $[Au_9L_8]^{3+}$ (L = PPh_3) with L, SCN^- and Cl^- to $[Au_8L_8]^{2+}$ $(Au_{11}L_8(SCN)_2]^+$ and $[Au_{11}L_8Cl_2]^+$. Recueil des Travaux Chimiques des Pays-Bas. 1980;**99**:137-141. DOI: 10.1002/recl.19800990410

[4] Schulz-Dobrick M, Jansen M. Characterization of gold clusters by crystallization with polyoxometalates: The intercluster compounds $[Au_9(dpph)_4][Mo_8O_{26}]$, $[Au_9(dpph)_4][PW_{12}O_{40}]$ and $[Au_{11}(PPh_3)_8Cl_2]_2[W_6O_{19}]$. Zeitschrift für anorganische und allgemeine Chemie. 2007;**633**:2326-2331. DOI: 10.1002/zaac.200700210

[5] Woehrle GH, Warner MG, Hutchison JE. Ligand exchange reactions yield subnanometer, thiol-stabilized gold particles with defined optical transitions. The Journal of Physical Chemistry B. 2002;**106**:9979-9981. DOI: 10.1021/jp025943s

[6] Yang Y, Chen S. Surface manipulation of the electronic energy of subnanometer-sized gold clusters: An electrochemical and spectroscopic investigation. Nano Letters. 2003; **3**:75-79. DOI: 10.1021/nl025809j

[7] Shichibu Y, Negishi Y, Tsukuda T, Teranishi T. Large-scale synthesis of thiolated Au_{25} clusters via ligand exchange reactions of phosphine-stabilized Au_{11} clusters. Journal of the American Chemical Society. 2005;**127**:13464-13465. DOI: 10.1021/ja053915s

[8] Liu Y, Tsunoyama H, Akita T, Tsukuda T. Preparation of ~1 nm gold clusters confined within mesoporous silica and microwave-assisted catalytic application for alcohol oxidation. The Journal of Physical Chemistry C. 2009;**113**:13457-13461. DOI: 10.1021/jp904700p

[9] Walter M, Akola J, Lopez-Acevedo O, Jadzinsky PD, Calero G, Ackerson CJ, Whetten RL, Grönbeck H, Häkkinen H. A unified view of ligand-protected gold clusters as superatom complexes. Proceedings of the National Academy of Sciences of the United States of America. 2008;**105**:9157-9162. DOI: 10.1073/pnas.0801001105

[10] Briant CE, Theobald BRC, White JW, Bell LK, Mingos DMP, Welch AJ. Synthesis and X-ray structural characterization of the centred icosahedral gold cluster compound $[Au_{l3}(PMe_2Ph)_{10}Cl_2](PF_6)_3$; the realization of a theoretical prediction. Journal of the Chemical Society, Chemical Communications. 1981:201-202. DOI: 10.1039/C39810000201

[11] Teo B, Shi X, Zhang H. Pure gold cluster of 1:9:9:1:9:9:1 layered structure: A novel 39-metal-atom cluster $[(Ph_3P)_{14}Au_{39}Cl_6]Cl_2$ with an interstitial gold atom in a hexagonal antiprismatic cage. Journal of the American Chemical Society. 1992;**114**:2743-2745. DOI: 10.1021/ja00033a073

[12] Schmid G, Pfeil R, Boese R, Bandermann F, Meyer S, Calis GHM, Velden JWA. $Au_{55}[P(C_6H_5)_3]_{12}CI_6$ - a gold cluster of an exceptional size. Chemische Berichte-Recueil. 1981;**114**:3634-3642. DOI: 10.1002/cber.19811141116

[13] Schmid G. Large clusters and colloids. Metals in the embryonic state. Chemical Reviews. 1992;**92**:1709-1727. DOI: 10.1021/cr00016a002

[14] Boyen HG, Kästle G, Weigl F, Koslowski B, Dietrich C, Ziemann P, Spatz JP, Riethmüller S, Hartmann C, Möller M, Schmid G, Garnier MG, Oelhafen P. Oxidation-resistant gold-55 clusters. Science. 2002;**297**:1533-1536. DOI: 10.1126/science.1076248

[15] Inomata T, Konishi K. Gold nanocluster confined within a cage: Template-directed formation of a hexaporphyrin cage and its confinement capability. Chemical Communications. 2003:1282-1283. DOI: 10.1039/B302609D

[16] Balasubramanian R, Guo R, Mills AJ, Murray RW. Reaction of $Au_{55}(PPh_3)_{12}Cl_6$ with thiols yields thiolate monolayer protected Au_{75} clusters. Journal of the American Chemical Society. 2005;**127**:8126-8132. DOI: 10.1021/ja050793v

[17] Brust M, Walker M, Bethell D, Schiffrin DJ, Whyman R. Synthesis of thiol-derivatised gold nanoparticles in a two-phase liquid–liquid system. Journal of the Chemical Society, Chemical Communications. 1994:801-802. DOI: 10.1039/C39940000801

[18] Tsukuda T. Toward an atomic-level understanding of size-specific properties of protected and stabilized gold clusters. Bulletin of the Chemical Society of Japan. 2012;**85**: 151-168. DOI: 10.1246/bcsj.20110227

[19] Whetten RL, Shafigullin MN, Khoury JT, Schaaff TG, Vezmar I, Alvarez MM, Wilkinson A. Crystal structures of molecular gold nanocrystal arrays. Accounts of Chemical Research. 1999;**32**:397-406. DOI: 10.1021/ar970239t

[20] Parker JF, Fields-Zinna CA, Murray RW. The story of a monodisperse gold nanoparticle: $Au_{25}L_{18}$. Accounts of Chemical Research. 2010;**43**:1289-1296. DOI: 10.1021/ar100048c

[21] Murray RW. Nanoelectrochemistry: Metal nanoparticles, nanoelectrodes, and nanopores. Chemical Reviews. 2008;**108**:2688-2720. DOI: 10.1021/cr068077e

[22] Li G, Jin R. Atomically precise gold nanoclusters as new model catalysts. Accounts of Chemical Research. 2013;**46**:1749-1758. DOI: 10.1021/ar300213z

[23] Qian H, Zhu M, Wu Z, Jin R. Quantum sized gold nanoclusters with atomic precision. Accounts of Chemical Research. 2012;**45**:1470-1479. DOI: 10.1021/ar200331z

[24] Dass A. Nano-scaling law: Geometric foundation of thiolated gold nanomolecules. Nanoscale. 2012;**4**:2260-2263. DOI: 10.1039/c2nr11749e

[25] Negishi Y, Kurashige W, Niihori Y, Nobusada K. Toward the creation of stable, functionalized metal clusters. Physical Chemistry Chemical Physics. 2013;**15**:18736-18751. DOI: 10.1039/c3cp52837e

[26] Negishi Y. Toward the creation of functionalized metal nanoclusters and highly active photocatalytic materials using thiolate-protected magic gold clusters. Bulletin of the Chemical Society of Japan. 2014;**87**:375-389. DOI: 10.1246/bcsj.20130288

[27] Luo Z, Nachammai V, Zhang B, Yan N, Leong DT, Jiang DE, Xie J. Toward understanding the growth mechanism: Tracing all stable intermediate species from reduction of Au (I)–thiolate complexes to evolution of Au_{25} nanoclusters. Journal of the American Chemical Society. 2014;**136**:10577-10580. DOI: 10.1021/ja505429f

[28] Häkkinen H. The gold–sulfur interface at the nanoscale. Nature Chemistry. 2012;**4**: 443-455. DOI: 10.1038/nchem.1352

[29] Zhu M, Aikens CM, Hollander FJ, Schatz GC, Jin R. Correlating the crystal structure of a thiol-protected Au_{25} cluster and optical properties. Journal of the American Chemical Society. 2008;**130**:5883-5885. DOI: 10.1021/ja801173r

[30] Qian H, Eckenhoff WT, Zhu Y, Pintauer T, Jin R. Total structure determination of thiolate-protected Au_{38} nanoparticles. Journal of the American Chemical Society. 2010; **132**:8280-8281. DOI: 10.1021/ja103592z

[31] Pei Y, Zeng XC. Investigating the structural evolution of thiolate protected gold clusters from first-principles. Nanoscale. 2012;**4**:4054-4072. DOI: 10.1039/c2nr30685a

[32] Zhang P. X-ray spectroscopy of gold–thiolate nanoclusters. The Journal of Physical Chemistry C. 2014;**118**:25291-25299. DOI: 10.1021/jp507739u

[33] Jiang DE, Kühn M, Tang Q, Weigend F. Superatomic orbitals under spin–orbit coupling. The Journal of Physical Chemistry Letters. 2014;**5**:3286-3289. DOI: 10.1021/jz501745z

[34] Jadzinsky PD, Calero G, Ackerson CJ, Bushnell DA, Kornberg RD. Structure of a thiol monolayer-protected gold nanoparticle at 1.1 Å resolution. Science. 2007;**318**:430-433. DOI: 10.1126/science.1148624

[35] Knoppe S, Wong OA, Malola S, Häkkinen H, Bürgi T, Verbiest T, Ackerson CJ. Chiral phase transfer and enantioenrichment of thiolate-protected Au_{102} clusters. Journal of the American Chemical Society. 2014;**136**:4129-4132. DOI: 10.1021/ja500809p

[36] Dolamic I, Knoppe S, Dass A, Bürgi T. First enantioseparation and circular dichroism spectra of Au_{38} clusters protected by achiral ligands. Nature Communications. 2012;**3**: 798. DOI: 10.1038/ncomms1802

[37] Udayabhaskararao T, Pradeep T. New protocols for the synthesis of stable Ag and Au nanocluster molecules. The Journal of Physical Chemistry Letters. 2013;**4**:1553-1564. DOI: 10.1021/jz400332g

[38] Dainese T, Antonello S, Gascón JA, Pan F, Perera NV, Ruzzi M, Venzo A, Zoleo A, Rissanen K, Maran F. $Au_{25}(SEt)_{18}$, a nearly naked thiolate-protected Au_{25} cluster: Structural analysis by single crystal X-ray crystallography and electron nuclear double resonance. ACS Nano. 2014;**8**:3904-3912. DOI: 10.1021/nn500805n

[39] Li Y, Zaluzhna O, Tong YYJ. Critical role of water and the structure of inverse micelles in the Brust–Schiffrin synthesis of metal nanoparticles. Langmuir. 2011;**27**:7366-7370. DOI: 10.1021/la201158v

[40] Kwak K, Kumar SS, Pyo K, Lee D. Ionic liquid of a gold nanocluster: A versatile matrix for electrochemical biosensors. ACS Nano. 2014;**8**:671-679. DOI: 10.1021/nn4053217

[41] Negishi Y, Kurashige W, Kamimura U. Isolation and structural characterization of an octaneselenolate-protected Au_{25} cluster. Langmuir. 2011;**27**:12289-12292. DOI: 10.1021/la203301p

[42] Kurashige W, Yamaguchi M, Nobusada K, Negishi Y. Ligand-induced stability of gold nanoclusters: Thiolate versus selenolate. The Journal of Physical Chemistry Letters. 2012; **3**:2649-2652. DOI: 10.1021/jz301191t

[43] Kurashige W, Yamazoe S, Kanehira K, Tsukuda T, Negishi Y. Selenolate-protected Au_{38} nanoclusters: Isolation and structural characterization. The Journal of Physical Chemistry Letters. 2013;**4**:3181-3185. DOI: 10.1021/jz401770y

[44] Kurashige W, Munakata K, Nobusada K, Negishi Y. Synthesis of stable Cu_nAu_{25-n} nanoclusters (n = 1–9) using selenolate ligands. Chemical Communications. 2013;**49**: 5447-5449. DOI: 10.1039/c3cc41210e

[45] Kurashige W, Yamazoe S, Yamaguchi M, Nishido K, Nobusada K, Tsukuda T, Negishi Y. Au_{25} clusters containing unoxidized tellurolates in the ligand shell. The Journal of Physical Chemistry Letters. 2014;**5**:2072-2076. DOI: 10.1021/jz500901f

[46] Meng X, Xu Q, Wang S, Zhu M. Ligand-exchange synthesis of selenophenolate-capped Au_{25} nanoclusters. Nanoscale. 2012;**4**:4161-4165. DOI: 10.1039/c2nr30272a

[47] Song Y, Wang S, Zhang J, Kang X, Chen S, Li P, Sheng H, Zhu M. Crystal structure of selenolate-protected $Au_{24}(SeR)_{20}$ nanocluster. Journal of the American Chemical Society. 2014;**136**:2963-2965. DOI: 10.1021/ja4131142

[48] Song Y, Zhong J, Yang S, Wang S, Cao T, Zhang J, Li P, Hu D, Pei Y, Zhu M. Crystal structure of $Au_{25}(SePh)_{18}$ nanoclusters and insights into their electronic, optical and catalytic properties. Nanoscale. 2014;**6**:13977-13985. DOI: 10.1039/c4nr04631e

[49] Song Y, Abroshan H, Chai J, Kang X, Kim HJ, Zhu M, Jin R. Molecular-like transformation from PhSe-protected Au_{25} to Au_{23} nanocluster and its application. Chemistry of Materials. 2017;**29**:3055-3061. DOI: 10.1021/acs.chemmater.7b00058

[50] Song Y, Cao T, Deng H, Zhu X, Li P, Zhu M. Kinetically controlled, high-yield, direct synthesis of $[Au_{25}(SePh)_{18}]^-TOA^+$. Science China. 2014;**57**:1218-1224. DOI: 10.1007/s11426-014-5071-5

[51] Xu Q, Wang S, Liu Z, Xu G, Meng X, Zhu M. Synthesis of selenolate-protected $Au_{18}(SeC_6H_5)_{14}$ nanoclusters. Nanoscale. 2013;**5**:1176-1182. DOI: 10.1039/c2nr33466f

[52] Maity P, Takano S, Yamazoe S, Wakabayashi T, Tsukuda T. Binding motif of terminal alkynes on gold clusters. Journal of the American Chemical Society. 2013;**135**:9450-9457. DOI: 10.1021/ja401798z

[53] Wan XK, Tang Q, Yuan SF, Jiang DE, Wang QM. Au_{19} nanocluster featuring a V-shaped alkynyl−gold motif. Journal of the American Chemical Society. 2015;**137**:652-655. DOI: 10.1021/ja512133a

[54] Lei Z, Wan XK, Yuan SF, Wang JQ, Wang QM. Alkynyl-protected gold and gold–silver nanoclusters. Dalton Transactions. 2017;**46**:3427-3434. DOI: 10.1039/c6dt04763g

[55] Shichibu Y, Negishi Y, Watanabe T, Chaki NK, Kawaguchi H, Tsukuda T. Biicosahedral gold clusters $[Au_{25}(PPh_3)_{10}(SC_nH_{2n+1})_5Cl_2]^{2+}$ (n = 2−18): A stepping stone to cluster-assembled materials. The Journal of Physical Chemistry C. 2007;**111**:7845-7847. DOI: 10.1021/jp073101t

[56] Koshevoy IO, Chang YC, Chen YA, Karttunen AJ, Grachova EV, Tunik SP, Jänis J, Pakkanen TA, Chou PT. Luminescent gold(I) alkynyl clusters stabilized by flexible diphosphine ligands. Organometallics. 2014;**33**:2363-2371. DOI: 10.1021/om5002952

[57] Song Y, Jin S, Kang X, Xiang J, Deng H, Yu H, Zhu M. How a single electron affects the properties of the "non-superatom" Au_{25} nanoclusters. Chemistry of Materials. 2016; **28**:2609-2617. DOI: 10.1021/acs.chemmater.5b04655

[58] Kobayashi N, Kamei Y, Shichibu Y, Konishi K. Protonation-induced chromism of pyridylethynyl-appended [core+exo]-type Au_8 clusters. Resonance-coupled electronic perturbation through π-conjugated group. Journal of the American Chemical Society. 2013;**135**:16078-16081. DOI: 10.1021/ja4099092

[59] Kang X, Song Y, Deng H, Zhang J, Liu B, Pan C, Zhu M. Ligand-induced change of the crystal structure and enhanced stability of the Au_{11} nanocluster. RSC Advance. 2015; **5**:66879-66885. DOI: 10.1039/c5ra11674k

[60] Song Y, Huang T, Murray RW. Heterophase ligand exchange and metal transfer between monolayer protected clusters. Journal of the American Chemical Society. 2003;**125**:11694-11701. DOI: 10.1021/ja0355731

[61] Lee D, Donkers RL, Wang G, Harper AS, Murray RW. Electrochemistry and optical absorbance and luminescence of molecule-like Au_{38} nanoparticles. Journal of the American Chemical Society. 2004;**126**:6193-6199. DOI: 10.1021/ja049605b

[62] Guo R, Song Y, Wang G, Murray RW. Does core size matter in the kinetics of ligand exchanges of monolayer-protected Au clusters? Journal of the American Chemical Society. 2005;**127**:2752-2757. DOI: 10.1021/ja044638c

[63] Hostetler MJ, Templeton AC, Murray RW. Dynamics of place-exchange reactions on monolayer-protected gold cluster molecules. Langmuir. 1999;**15**:3782-3789. DOI: 10.1021/la981598f

[64] Tracy JB, Crowe MC, Parker JF, Hampe O, Fields-Zinna CA, Dass A, Murray RW. Electrospray ionization mass spectrometry of uniform and mixed monolayer nanoparticles: $Au_{25}[S(CH_2)_2Ph]_{18}$ and $Au_{25}[S(CH_2)_2Ph]_{18-x}(SR)_x$. Journal of the American Chemical Society. 2007;**129**:16209-16215. DOI: 10.1021/ja076621a

[65] Song Y, Murray RW. Dynamics and extent of ligand exchange depend on electronic charge of metal nanoparticles. Journal of the American Chemical Society. 2002;**124**:7096-7102. DOI: 10.1021/ja0174985

[66] Niihori Y, Hossain S, Kumar B, Nair LV, Kurashige W, Negishi Y. Perspective: Exchange reactions in thiolate-protected metal clusters. APL Materials. 2017;**5**:053201. DOI: 10.1063/1.4978373

[67] Niihori Y, Hossain S, Sharma S, Kumar B, Kurashige W, Negishi Y. Understanding and practical use of ligand and metal exchange reactions in thiolate-protected metal clusters to synthesize controlled metal clusters. The Chemical Record. 2017;**17**:473-484. DOI: 10.1002/tcr.201700002

[68] Wu Z, Suhan J, Jin R. One-pot synthesis of atomically monodisperse, thiol-functionalized Au_{25} nanoclusters. Journal of Materials Chemistry. 2009;**19**:622-626. DOI: 10.1039/b815983a

[69] Schaaff TG, Whetten RL. Giant gold–glutathione cluster compounds: Intense optical activity in metal-based transitions. The Journal of Physical Chemistry B. 2000;**104**:2630-2641. DOI: 10.1021/jp993691y

[70] Negishi Y, Takasugi Y, Sato S, Yao H, Kimura K, Tsukuda T. Magic-numbered Au_n clusters protected by glutathione monolayers (n = 18, 21, 25, 28, 32, 39): Isolation and spectroscopic characterization. Journal of the American Chemical Society. 2004;**126**:6518-6519. DOI: 10.1021/ja0483589

[71] Negishi Y, Nobusada K, Tsukuda T. Glutathione-protected gold clusters revisited: Bridging the gap between gold(I)−thiolate complexes and thiolate-protected gold nanocrystals. Journal of the American Chemical Society. 2005;**127**:5261-5270. DOI: 10.1021/ja042218h

[72] Tsukuda T, Häkkinen H, editors. Protected Metal Clusters: From Fundamentals to Applications. 1st ed. Amsterdam: Elsevier; 2015. 372 p

[73] Wolfe RL, Murray RW. Analytical evidence for the monolayer-protected cluster $Au_{225}[(S(CH_2)_5CH_3)]_{75}$. Analytical Chemistry. 2006;**78**:1167-1173. DOI: 10.1021/ac051533z

[74] Choi MMF, Douglas AD, Murray RW. Ion-pair chromatographic separation of water-soluble gold monolayer-protected clusters. Analytical Chemistry. 2006;**78**:2779-2785. DOI: 10.1021/ac052167m

[75] Negishi Y, Nakazaki T, Malola S, Takano S, Niihori Y, Kurashige W, Yamazoe S, Tsukuda T, Häkkinen H. A critical size for emergence of nonbulk electronic and geometric structures in dodecanethiolate-protected Au clusters. Journal of the American Chemical Society. 2015;**137**:1206-1212. DOI: 10.1021/ja5109968

[76] Niihori Y, Matsuzaki M, Uchida C, Negishi Y. Advanced use of high-performance liquid chromatography for synthesis of controlled metal clusters. Nanoscale. 2014;**6**:7889-7896. DOI: 10.1039/c4nr01144a

[77] Black DM, Bhattarai N, Bach SBH, Whetten RL. Selection and identification of molecular gold clusters at the nano(gram) scale: Reversed phase HPLC–ESI–MS of a mixture of Au-peth MPCs. The Journal of Physical Chemistry Letters. 2016;**7**:3199-3205. DOI: 10.1021/acs.jpclett.6b01403

[78] Negishi Y, Chaki NK, Shichibu Y, Whetten RL, Tsukuda T. Origin of magic stability of thiolated gold clusters: A case study on $Au_{25}(SC_6H_{13})_{18}$. Journal of the American Chemical Society. 2007;**129**:11322-11323. DOI: 10.1021/ja073580+

[79] Chaki NK, Negishi Y, Tsunoyama H, Shichibu Y, Tsukuda T. Ubiquitous 8 and 29 kDa gold: Alkanethiolate cluster compounds: Mass-spectrometric determination of molecular formulas and structural implications. Journal of the American Chemical Society. 2008;**130**:8608-8610. DOI: 10.1021/ja8005379

[80] Schaaff TG, Whetten RL. Controlled etching of Au:SR cluster compounds. The Journal of Physical Chemistry B. 1999;**103**:9394-9396. DOI: 10.1021/jp993229d

[81] Shichibu Y, Negishi Y, Tsunoyama H, Kanehara M, Teranishi T, Tsukuda T. Extremely high stability of glutathionate-protected Au_{25} clusters against core etching. Small. 2007; **3**:835-839. DOI: 10.1002/smll.200600611

[82] Jin R, Qian H, Wu Z, Zhu Y, Zhu M, Mohanty A, Garg N. Size focusing: A methodology for synthesizing atomically precise gold nanoclusters. The Journal of Physical Chemistry Letters. 2010;**1**:2903-2910. DOI: 10.1021/jz100944k

[83] Zeng C, Chen Y, Das A, Jin R. Transformation chemistry of gold nanoclusters: From one stable size to another. The Journal of Physical Chemistry Letters. 2015;**6**:2976-2986. DOI: 10.1021/acs.jpclett.5b01150

[84] Häkkinen H, Barnett RN, Landman U. Electronic structure of passivated $Au_{38}(SCH_3)_{24}$ nanocrystal. Physical Review Letters. 1999;**82**:3264-3267. DOI: 10.1103/PhysRevLett.82.3264

[85] Zeng C, Qian H, Li T, Li G, Rosi NL, Yoon B, Barnett RN, Whetten RL, Landman U, Jin R. Total structure and electronic properties of the gold nanocrystal $Au_{36}(SR)_{24}$. Angewandte Chemie International Edition. 2012;**51**:13114-13118. DOI: 10.1002/anie.201207098

[86] Dass A, Theivendran S, Nimmala PR, Kumara C, Jupally VR, Fortunelli A, Sementa L, Barcaro G, Zuo X, Noll BC. $Au_{133}(SPh\text{-}^tBu)_{52}$ nanomolecules: X-ray crystallography, optical, electrochemical, and theoretical analysis. Journal of the American Chemical Society. 2015;137:4610-4613. DOI: 10.1021/ja513152h

[87] Das A, Li T, Nobusada K, Zeng C, Rosi NL, Jin R. Nonsuperatomic $[Au_{23}(SC_6H_{11})_{16}]^-$ nanocluster featuring bipyramidal Au_{15} kernel and trimeric $Au_3(SR)_4$ motif. Journal of the American Chemical Society. 2013;**135**:18264-18267. DOI: 10.1021/ja409177s

[88] Heaven MW, Dass A, White PS, Holt KM, Murray RW. Crystal structure of the gold nanoparticle $[N(C_8H_{17})_4][Au_{25}(SCH_2CH_2Ph)_{18}]$. Journal of the American Chemical Society. 2008;**130**:3754-3755. DOI: 10.1021/ja800561b

[89] Pohjolainen E, Häkkinen H, Clayborne A. The role of the anchor atom in the ligand of the monolayer-protected $Au_{25}(XR)_{18}^-$ nanocluster. The Journal of Physical Chemistry C. 2015;**119**:9587-9594. DOI: 10.1021/acs.jpcc.5b01068

[90] Kumar S, Jin R. Water-soluble $Au_{25}(Capt)_{18}$ nanoclusters: Synthesis, thermal stability, and optical properties. Nanoscale. 2012;**4**:4222-4227. DOI: 10.1039/C2NR30833A

[91] Lin SY, Chen NT, Sum SP, Lo LW, Yang CS. Ligand exchanged photoluminescent gold quantum dots functionalized with leading peptides for nuclear targeting and intracellular imaging. Chemical Communications. 2008:4762-4764. DOI: 10.1039/b808207c

[92] Kano S, Azuma Y, Kanehara M, Teranishi T, Majima Y. Room-temperature coulomb blockade from chemically synthesized Au nanoparticles stabilized by acid–base interaction. Applied Physics Express. 2010;**3**:105003. DOI: 10.1143/APEX.3.105003

[93] Lopez-Acevedo O, Tsunoyama H, Tsukuda T, Häkkinen H, Aikens CM. Chirality and electronic structure of the thiolate-protected Au_{38} nanocluster. Journal of the American Chemical Society. 2010;**132**:8210-8218. DOI: 10.1021/ja102934q

[94] Malola S, Lehtovaara L, Knoppe S, Hu KJ, Palmer RE, Bürgi T, Häkkinen H. $Au_{40}(SR)_{24}$ cluster as a chiral dimer of 8-electron superatoms: Structure and optical properties. Journal of the American Chemical Society. 2012;**134**:19560-19563. DOI: 10.1021/ja309619n

[95] Knoppe S, Bürgi T. Chirality in thiolate-protected gold clusters. Accounts of Chemical Research. 2014;**47**:1318-1326. DOI: 10.1021/ar400295d

[96] Noyori R. Asymmetric catalysis: Science and opportunities (nobel lecture). Angewandte Chemie International Edition. 2002;**41**:2008-2022. DOI: 10.1002/1521-3773(20020617)41:12<2008::AID-ANIE2008>3.0.CO;2-4

[97] de la Llave E, Scherlis DA. Selenium-based self-assembled monolayers: The nature of adsorbate−surface interactions. Langmuir. 2010;**26**:173-178. DOI: 10.1021/la903660y

[98] Szelagowska-Kunstman K, Cyganik P, Schüpbach B, Terfort A. Relative stability of thiol and selenol based SAMs on Au(111)−exchange experiments. Physical Chemistry Chemical Physics. 2010;**12**:4400-4406. DOI: 10.1039/b923274p

[99] Kurashige W, Niihori Y, Sharma S, Negishi Y. Precise synthesis, functionalization and application of thiolate-protected gold clusters. Coordination Chemistry Reviews. 2016;**320-321**:238-250. DOI: 10.1016/j.ccr.2016.02.013

[100] Romashov LV, Ananikov VP. Self-assembled selenium monolayers: From nanotechnology to materials science and adaptive catalysis. Chemistry—A European Journal. 2013;**19**:17640-17660. DOI: 10.1002/chem.201302115

[101] Yokota K, Taniguchi M, Kawai T. Control of the electrode−molecule interface for molecular devices. Journal of the American Chemical Society. 2007;**129**:5818-5819. DOI: 10.1021/ja071365n

[102] Jin R, Zeng C, Zhou M, Chen Y. Atomically precise colloidal metal nanoclusters and nanoparticles: Fundamentals and opportunities. Chemical Reviews. 2016;**116**:10346-10413. DOI: 10.1021/acs.chemrev.5b00703

[103] Ni TW, Tofanelli MA, Phillips BD, Ackerson CJ. Structural basis for ligand exchange on $Au_{25}(SR)_{18}$. Inorganic Chemistry. 2014;**53**:6500-6502. DOI: 10.1021/ic5010819

[104] Niihori Y, Kikuchi Y, Kato A, Matsuzaki M, Negishi Y. Understanding ligand-exchange reactions on thiolate-protected gold clusters by probing isomer distributions using reversed-phase high-performance liquid chromatography. ACS Nano. 2015;**9**:9347-9356. DOI: 10.1021/acsnano.5b03435

[105] Fernando A, Aikens CM. Ligand exchange mechanism on thiolate monolayer protected $Au_{25}(SR)_{18}$ nanoclusters. The Journal of Physical Chemistry C. 2015;**119**:20179-20187. DOI: 10.1021/acs.jpcc.5b06833

[106] Hossain S, Kurashige W, Wakayama S, Kumar B, Nair LV, Niihori Y, Negishi Y. Ligand exchange reactions in thiolate-protected Au_{25} nanoclusters with selenolates or tellurolates: Preferential exchange sites and effects on electronic structure. The Journal of Physical Chemistry C. 2016;**120**:25861-25869. DOI: 10.1021/acs.jpcc.6b08636

[107] Zhu M, Qian H, Jin R. Thiolate-protected $Au_{24}(SC_2H_4Ph)_{20}$ nanoclusters: Superatoms or not? The Journal of Physical Chemistry Letters. 2010;**1**:1003-1007. DOI: 10.1021/jz100133n

[108] Pei Y, Pal R, Liu C, Gao Y, Zhang Z, Zeng XC. Interlocked catenane-like structure predicted in $Au_{24}(SR)_{20}$: Implication to structural evolution of thiolated gold clusters

from homoleptic gold(I) thiolates to core-stacked nanoparticles. Journal of the American Chemical Society. 2012;**134**:3015-3024. DOI: 10.1021/ja208559y

[109] Das A, Li T, Li G, Nobusada K, Zeng C, Rosi NL, Jin R. Crystal structure and electronic properties of a thiolate-protected Au_{24} nanocluster. Nanoscale. 2014;**6**:6458-6462. DOI: 10.1039/c4nr01350f

[110] Tang Q, Ouyang R, Tian Z, Jiang DE. The ligand effect on the isomer stability of $Au_{24}(SR)_{20}$ clusters. Nanoscale. 2015;**7**:2225-2229. DOI: 10.1039/c4nr05826g

[111] Chen Y, Liu C, Tang Q, Zeng C, Higaki T, Das A, Jiang DE, Rosi NL, Jin R. Isomerism in $Au_{28}(SR)_{20}$ nanocluster and stable structures. Journal of the American Chemical Society. 2016;**138**:1482-1485. DOI: 10.1021/jacs.5b12094

[112] Zeng C, Liu C, Pei Y, Jin R. Thiol ligand-induced transformation of $Au_{38}(SC_2H_4Ph)_{24}$ to $Au_{36}(SPh\text{-}t\text{-}Bu)_{24}$. ACS Nano. 2013;**7**:6138-6145. DOI: 10.1021/nn401971g

Section 2

Ligand in Biological Chemistry

Chapter 4

Neuropeptides as Ligands for GPCRs

Burcin Duan Sahbaz and Necla Birgul Iyison

Additional information is available at the end of the chapter

http://dx.doi.org/10.5772/intechopen.73504

Abstract

Neuropeptides constitute an important part of the nervous system, since the simple nerve nets (i.e. of *Hydra*). The assigned functions of these peptides vary enormously. For instance, besides inhibiting or stimulating the release of some hormones, they can be responsible for tentacle contraction of the *Hydra*, dropping the tail of the lizard, postnatal care of the beetles and also aggressiveness of humans. They perform these tasks via activating their cognate GPCRs, which are hypothesized to be coevolved with their ligand neuropeptides. In this chapter, we will introduce the concept of neuropeptide, its intracellular maturation process, characteristics of some typical neuropeptide families and the common properties of their cognate GPCRs. At last, we will try to give information about the widely used methods for studying GPCR-neuropeptide interactions.

Keywords: neuropeptide, GPCR, peptide hormone, interaction

1. Introduction

Neuropeptides are polypeptides expressed in and secreted from neurons. They are produced as propeptides, cleaved into smaller fragments and matured via posttranslational modifications, differing from classical neurotransmitters in size, concentration and secretion mechanisms. They are expressed everywhere in the nervous system, take role in synapsis and can have distal target organs, as do the hormones.

Neuropeptides constitute the most diverse class of molecules in the body. They have various roles in development, reproduction, physiology and behavior of the animals. There are at least 70 known genes coding for neuropeptide precursor proteins, called prepropeptides, in

mammals and 42 genes in *Drosophila*. Secreted forms are processed from these prepropeptides and can vary from 5 to 80 amino acids in length. They coexist with classical neurotransmitters; for instance, neurotensin is released with dopamine [1] or vasoactive intestinal peptide with acetylcholine [2]. They mostly act on G-protein coupled receptors (GPCRs) and transduce their signals via intracellular secondary messenger systems.

2. Evolution of neuropeptide signaling

Simple nerve nets have evolved since the earliest animals like cnidarians (such as *Hydra*, sea anemones and jellyfish). Even they have no real brain, their nervous system includes secretory vesicles and produces different types of neuropeptides [3]. Neuropeptides constitute an important part of their nervous system. Therefore, neuropeptide signaling should have been evolved before the divergence of cnidarians and bilaterians, which means more than 550 million years of evolution.

Secretory vesicles of cnidarian nervous system are accumulated at the synapses [4, 5]. This may help for directed-signal transmission such as tentacle contraction of *Hydra* [6]. However, in vertebrates, the peptide secretory vesicles are not localized only to the synapse but distributed also along the nerve body and soma. Because neuropeptides interact mostly with GPCRs, their action mechanism is slower than classical neurotransmitters. This fact should be disadvantageous for the peptidergic nervous system of the *Hydra*. However, it was found that they have evolved different receptor-binding mechanisms to overcome this problem. For instance, mammalian RFamide neuropeptides activate different GPCRs and this activation leads to a slow response. On the other hand, Hydra-RFamide I and II act through a so-called peptide-gated ionotropic receptor, which is a trimeric complex of ion channels [7]. This system results in an advantage like faster transmission than that of classical neuropeptide-GPCR system, in absence of classical neurotransmitters.

In evolution of neuropeptide signaling, echinoderms are the second most important because they constitute an intermediate step between Protostomia (which include fruit fly) and Deuterostomia (which include both the vertebrates and echinoderms). Echinoderm neuropeptides are suggested to be involved in unusual mechanisms such as autotomy (dropping the tail of the lizard) and regeneration, or control of stiffness of connective tissue [8].

The major assumptions behind the diversity of neuropeptide genes are tandem duplications and following substitutions. Neuropeptide sequences are conserved in most cases (such as oxytocin family). However, some neuropeptide sequences show variations, and these variations can lead to differences in half-life, receptor affinity or expression profiles. Finally, these changes can generate a pressure in the direction of neuropeptide-receptor coevolution. Additionally, the mature peptides that are processed from the same gene can have sequence variations. These variations cannot be explained by gene duplication. An example for this is 37 peptide products of metamorphosin A prepropeptide of sea anemone [9]. All of these peptides can show functional redundancy, which means that they can be coexpressed,

cosecreted and activating the same receptor. In a study on *Drosophila* genus, multiple copies of peptides from the same prepropeptide were analyzed [10], and it was found that they were highly conserved and under stabilizing selection. The numbers of peptide copies were the same within the genus (except FMRFamides). This conservation is important for receptor selectivity, affinity or the final response. Additionally, the researchers showed that the most conserved peptides were the most potent ligands for their receptors. Finally, these results on *Drosophila* neuropeptides supported the idea of evolutionary pressure of peptide-receptor coevolution on neuropeptide selection. This idea was proposed also for the vertebrate neuropeptides. Some regions of the vertebrate peptides are conserved, and these regions are thought to be the most important parts for functioning. For instance, the C-terminal residues of tachykinins are strictly conserved within vertebrates, and this region has roles in binding with tachykinin receptors. However, these similarities between neuropeptides of different species do not have to mean cross-reactivity with the receptors of different species [11, 12]. And this fact would be a support for the discussion of peptide-receptor coevolution.

3. Processing and trafficking of neuropeptides

Neuropeptides are the gene products that range from 5 to 80 amino acids in length. They born like prepropeptides, which contain an N-terminal signal sequence (between 15 and 40 residues in length). A typical signal sequence contains a positively charged region, a hydrophobic region and some polar but uncharged amino acids until the cleavage site, in the order [13]. This signal sequence is responsible for the anchorage of prepropeptide to the endoplasmic reticulum (ER) membrane via a complex called translocon, where folding and signal peptide cleavage occur. In some prepropeptides, the N-terminal region includes a signal anchor instead of a signal sequence. This signal anchor is responsible for the anchorage of precursor protein to the ER membrane but not cleaved. An example for this signal anchor can be given for the precursor of Allatostatin CC peptides of insects [14]. These signal anchors produce single-pass membrane proteins, which can act as juxtacrines in nervous system.

Cleaved propeptides are exported to the Golgi for further processing. Mainly, two types of "trypsin-like" endopeptidases are responsible for the cleavage of propeptides. These enzymes are called proprotein convertase 1 (PC1/3) and 2 (PC2). Seven PC types are expressed in mammals, but only three PCs in fruit fly (Amontillado, Dfurin1 and Dfurin2). PCs recognize and cleave the C-terminal site of dibasic residues such as KR or RR, especially of R-*X*-(R/K/*X*)-R motif on propeptides [15]. However, cleavage preferences differ within organisms. For instance, if valine or leucine is placed in place of X, the site will become resistant to cleavage by vertebrate PC (furin) but will be efficiently cleaved by insect PCs (Dfurin) [16]. In processing of neuropeptides, mammalian PC1 and PC2 and fly Amontillado are widely expressed in neurons, whereas furins have ubiquitous expression [17, 18].

Cleaved propeptide contains a basic C-terminus, which is further cleaved by carboxypeptidase E. In order to stabilize peptide structure against degradation, C-terminal glycine of most of

intermediate propeptides is amidated. This amidation is a multistep process of two enzymes in invertebrates, while vertebrates have a multifunctional enzyme to perform this task, called as peptidylglycine alpha-amidating monooxygenase (PAM).

Mature peptides are transported in large dense core vesicles (DCV), which are different from small vesicles delivering classical neurotransmitters. Furthermore, posttranslational modifications occur in DCVs. These modifications may include acetylation, sulfation, glycosylation, phosphorylation and cyclization. Some peptides can be processed even after secretion to the extracellular space. For instance, it was found that CPA6 of A/B family of carboxypeptidases is secreted to the extracellular matrix, cleaves hydrophobic C-terminal residues of neuropeptides and can lead to activation of Angiotensin I while degradation of some other peptides [19].

The engagement of DCVs to the nerve terminals is a very rare event. This is because DCVs respond to the changes in Ca^{+2} content and hundreds of spikes are needed to stimulate a DCV to release its content [20]. Even in these rare events, very large amounts of neuropeptides are released to the synaptic cleft where they are enzymatically cleaved and degraded. On the other hand, unlike neuropeptides, classical neurotransmitters are very rapidly transported to the membrane, easily released and recycled from the synaptic cleft.

Finally, one precursor protein can generate more than one neuropeptide and these peptides can be distinct or the same. Additionally, a precursor molecule can be alternatively spliced to yield different mature neuropeptides in different cells [21].

4. Types, cognate GPCRs and functions

As the simplest nervous system, cnidarians express at least 17 different neuropeptides, which can be grouped in three: FMRFamide-like peptides (FLPs), GLWamides and Hym-355 [3]. The neuropeptides expressed in worm *C. elegans* are also classified in three major groups, depending on their structural and functional similarities [21]. These groups are called as insulin-like peptides (ILPs), FLPs and neuropeptide-like peptides (NLPs). Vertebrate neuropeptides can be clustered in a wide range of families according to sequence similarities [22]. However, in human, neuropeptides expressed from 96 different genes were clustered in 22 distinct families together with the no-family peptides and deposited in neuropeptide databases [23].

In a study of metazoan (all animals) propeptides, neuropeptides of 10 phyla were taken and clustered in about 80 families according to their similarities within propeptide sequences [22]. Twenty-two of these families showed high similarity with each other. These included FMRFamides, LWamides, myoinhibitory peptide (MIP), neuropeptide FF and gonadotropin inhibitory hormone (GnIH).

In this chapter, we will introduce some of the neuropeptides that show conservation within species (as reviewed from the study of Jékely [22]) or that are specific examples for vertebrates and exclude the ligands interacting with non-GPCR targets. Summary of all mentioned neuropeptide families is given in **Table 1**.

Peptide family	Examples for active peptides	Expressed in	Structural similarity	Function(s)	Cognate GPCR
FMRFamide-like peptides	FMRFamide	Mollusks	Tetrapeptide FMRFamide	Cardioacceleration	*nd*
	FLP peptides	Nematodes	C-terminal FMRFamide	Control of feeding, reproduction, sensation	Various NPRs
	CCK/gastrin-type peptides		C-terminal QFamide	Control of feeding behavior, energy homeostasis	
	FMRFamide-like peptides	Arthropods and Cnidaria	C-terminal RFamide	Cardioacceleration	FMRFamide and sulfakinin receptors
	Gonadotropin-inhibitory hormone	Vertebrates		Inhibition of gonadotropin release	GPR147
	Neuropeptide FF			Nociception	NPFFR1, NPFFR2
	Pyroglutamylated RFamide peptide			Control of feeding	GPR103
	Prolactin-releasing peptide			Stimulation of prolactin release	PrRP receptors
	Kisspeptin			Reproductive development	Kisspeptin receptor
Tachykinins	Substance P-like tachykinins	Cnidaria, nematodes, arthropods	C-terminal FXGXRamide	Promotion of aggression, sexual activity and fecundity	NK-1
	Locustatachykinins	Invertebrates		Stimulation of muscle contractions	NKRs
	Eledoisin	*Eledone*	C-terminal F(Y/I)GLMamide	Vasodilation, hypotension	NK-1
	Sialokinin I and II	Arthropods		Vasodilation	NKRs
	Skin tachykinins	Amphibians	C-terminal FXGLMamide	Ion transport	
	Brain/gut tachykinins	Submammalian vertebrates		Vasodilation, smooth muscle contraction	
	Neurokinin A	Mammals		Regulation of inflammation and pain responses	NK-2
	Neurokinin B			Regulation of reproduction, secretion of gonadotropin-releasing hormone	NK-3
	Neuropeptide K			Regulation of sensation	NK-2
	Neuropeptide γ			Regulation of reproduction	NK-2
	Substance P				NK-1

http://dx.doi.org/10.5772/intechopen.73504

Peptide family	Examples for active peptides	Expressed in	Structural similarity		Function(s)	Cognate GPCR
					Regulation of inflammation and pain responses, promotion of aggression	
Vasopressin/ oxytocin	Conopressins	Invertebrates	Sequence similarity and disulfide bridge between the 1st and 6th residues		Regulation of reproduction	Conopressin receptor
	Diuretic hormones				Regulation of water balance	Diuretic hormone receptor
	Mesotocin	Submammalian vertebrates				Mesotocin receptor
	Vasopressin	Vertebrates			Antidiuretic activity	V1A, V1B and V2
	Oxytocin				Contraction of the uterus, lactation	OXTR
Myoinhibitory peptide/ GWamides	Sex peptide	From cnidarians through annelids	C-terminal W(X)8 W–amide		Increasing egg laying, reduction in the female's receptivity, stimulation of juvenile hormone synthesis	SPR
	Myoinhibitory/allatostatin-B peptide		C-terminal W(X)6 W–amide and disulfide bridge		Inhibition of contractions of hindgut and oviduct, ecdysteroid synthesis and juvenile hormone synthesis	MIPR
	Prothoracicostatic hormone				Regulation of reproduction, release of ecdysone hormone	Torso (not GPCR), also activates SPR
	APGWamides	Mollusks	Tetrapeptide		Sex organ growth, regulation of reproduction	*nd*
Orexin/ allatotropin	Allatotropin	Arthropods (except *Drosophila*), mollusks, annelids	N-terminal GFK residues	No structural similarity	Stimulation of juvenile hormone synthesis, cardioacceleration, myostimulation	AT receptor
	Orexin A	Mammals	Sequence similarity		Sleep and wakefulness	OX1 and OX2
	Orexin B					
GnRH/ corazonin/ AKH	Corazonin	Arthropods	N-terminal pyro-glutamate		cardioacceleration, melanization and developmental processes	Corazonin receptor
	Adipokinetic hormone	Arthropods		Phe in 8th position	Mobilization of carbohydrates, lipids and proteins from the fat body	AKH receptor
	GnRH-like peptides	Annelids and mollusks		Following HWS residues	Stimulation of testosterone and progesterone synthesis	GnRHR
	GnRH	Vertebrates			Stimulation of gonadotropin release	

Peptide family	Examples for active peptides	Expressed in	Structural similarity		Function(s)	Cognate GPCR
						GnRH1 and GnRH2 receptors
Neuropeptide Y	Neuropeptide Y	Vertebrates and invertebrates	C-terminal amidation and a pancreatic polypeptide fold structure		Regulation of blood pressure and feeding behavior	Y1,2,4,5 and y6
	Peptide tyrosine tyrosine	Vertebrates			Inhibition of gastric motility and electrolyte secretion	
	Pancreatic polypeptide	Vertebrates			Inhibition of pancreatic exocrine secretion	
Somatostatin/ allatostatin **C**	Allatostatin C	Arthropods	C-terminal PISCF and a disulfide bridge	No structural similarity	Inhibition of juvenile hormone synthesis	AlstR-C
	SST14	Vertebrates	Sequence similarity		Inhibition of growth hormone release	SSTR1, SSTR2A, SSTR2B, SSTR3, SSTR4 and SSTR5
	SST28					
Galanin/ allatostatin **A**	Allatostatin A	Arthropods	C-terminal FGLamide	No structural similarity	Inhibition of juvenile hormone synthesis, regulation of food intake	AST-A receptors
	Galanin	Vertebrates	N-terminal similarity and C-terminal amidation		Nociception, feeding and osmotic regulation	GalR1, GalR2 and GalR3
VIP/PACAP	α-Pigment dispersing factor	Invertebrates	C-terminal amidation	No structural similarity	Regulation of circadian clock	PDF receptor
	β-Pigment dispersing factor					
	VIP	Vertebrates	β-turns and α-helical structures			VPAC1 and VPAC2
	PHI					
	PHM					
	PHV					
	PACAP27					PAC1, VPAC1 and VPAC2
	PACAP38					

Table 1. Summary of the neuropeptide families and the similarities within these families.

4.1. FMRFamide-like peptides

Genome searches and mass spectrometry-based methods on nematode *C. elegans* yielded around 30 genes encoding for FLPs. These peptides share a common C-terminal motif like FMRF residues. RNAi studies on these genes showed that FLPs can have roles on different processes such as hyperactivity, timing of egg laying, number of laid eggs, fat metabolism and acetylcholine signaling [24–26]. In mollusk *Macrocallista nimbosa*, this neuropeptide takes role in cardioexcitatory activity [27]. FLPs are expressed in all of the animal species. However, the conserved C-terminal residues may become FMRFamide, QFamide or RFamide. In arthropods, sulfakinins, myosuppressins, RFamides and other extended FMRFamides have the common C-terminal amidated RF residues. Myosuppressins seem to be restricted to crustaceans and insects and have a role in inhibiting contractions of the hindgut, cardiac muscle and release of adipokinetic hormone [28, 29]. Extended FMRFamides of arthropods affect respiration, heart rate, gut motility and muscle contractions. *Drosophila* sulfakinin (drosulfakinin) was shown to regulate locomotor behavior [30], feeding behavior [31] and smooth muscle contraction [32]. FMRFamides act through two types of receptors. Most of them activate GPCRs. However, FMRFamides of snail *Helix aspersa* lead to an excitatory response in amiloride-sensitive Na^+ channels [33].

4.2. Tachykinins

Vertebrate tachykinins are one of the largest groups of neuropeptides expressed in both invertebrates and vertebrates. They contain conserved C-terminally amidated motifs such as FXGLM residues, while some of arthropod tachykinins show FXGXRamide conservation. These five residues are very conserved but not vital for receptor activation, instead phenylalanine at the fifth position and the C-terminal amidation are essential for their activity. They can be localized both to the brain and the gut of various organisms, as well as the skin of amphibians. They can be secreted from the enteroendocrine cells of mammals as paracrines or as true hormones.

Human tachykinin family includes neurokinin A (NKA), neurokinin B (NKB), neuropeptide K (NPK), neuropeptide γ (NPγ) and substance P (SP), which are expressed from two genes. These peptides activate three types of GPCRs: NK-1, NK-2 and NK-3. SP interacts with NK-1, while NKA with NK-2 and NKB with NK-3. Higher concentrations of SP in patients with personality disorders were correlated with aggressive behavior [34]. It was also shown that *Drosophila* tachykinins have aggression-promoting functions [35] and control systemic lipid homeostasis [36]. Tachykinin-like natalisin peptide regulates sexual activity and fecundity of arthropods [37]. Another tachykinin family peptide, eledoisin, was identified from the salivary glands of mollusk *Eledone* in 1962 [38]. And, eledoisin and kassinin were shown to be expressed and stimulated ion transport in the frog skin [39].

4.3. Vasopressin/oxytocin

Vasopressin (VP) and oxytocin (OXT) are members of the same family due to their sequence similarity. They are conserved from arthropods to mammals. Vertebrate VP/OXT peptides are

expressed from different genes. Processing of propeptides of vasopressin gene produces three peptides called VP, neurophysin II and copeptin, while processing of oxytocin gene produces only OXT and neurophysin I peptides. OXT and VP bind with their corresponding neurophysins, OXT with neurophysin I and VP with neurophysin II. These neurophysins are responsible for the storage of VP and OXT inside DCVs. In physiological pH, VP and OXT do not bind with neurophysins and circulate freely in the plasma. Both mature VP and OXT are nine amino acids in length, eight of which are identical and contain a disulfide bridge between the first and sixth residues [40], while neurophysins have seven bridges. The first cysteine and the following tyrosine residues play the major role in neurophysin binding [41]. Although VP and OXT show sequence similarity, their functions differ from each other. VP has antidiuretic activity and released as a response to increased blood plasma osmolarity, while OXT has roles in contraction of the uterus and in lactation and is stimulated with suckling movement of the newborn. VP and OXT receptors constitute a big family of GPCRs. There are three types of vasopressin receptors: V1A, V1B and V2. However, only one type of oxytocin receptor was identified: OXTR [42].

Invertebrate homologous peptides also contain the disulfide bridge at the same position and five or six amino acids of the peptides are well conserved. The invertebrate homologs of vertebrate VP/OXT peptides are conopressins and diuretic hormones (DH) [43].

4.4. Myoinhibitory peptide/GWamides

These peptides are expressed from *Cnidaria* to Annelids but not present in vertebrates. This family of peptides shares a common motif like $W(X)_6W$ and includes various similar peptides such as myoinhibitory/allatostatin-B peptide (MIP/AST-B), sex peptide (SP), prothoracicostatic hormone (PTTH) and GWamides (of mollusks).

The first AST-B peptide is identified in *Locusta migratoria* as an MIP. It inhibits contractions of hindgut and oviduct, as well as ecdysteroid synthesis. It has a $W(X)_6$Wamide motif on its C-terminus and is widely expressed in the central nervous system. Similar peptides are identified in *Gryllus bimaculatus* and found that they inhibited juvenile hormone synthesis in *corpora allata*. Therefore, they are called as allatostatins.

SP is found in *Drosophila* male accessory glands and regulates mating behaviors of the females. During mating, SP is released from male's ejaculatory duct and acts on the corresponding receptor on the female reproductive duct, increases egg laying and reduces the female's receptivity. This peptide is 36 amino acids in length. N-terminal eight residues are responsible for sperm binding and stimulation of juvenile hormone synthesis. Following 12 amino acids have roles in innate immune responses against bacteria. And the C-terminal 16 amino acids have role in postmating responses. A disulfide bridge is localized to the C-terminal part of the peptide. In addition, there is an internal $W(X)_8W$ motif instead of $W(X)_6$Wamide of the others. Therefore, the tryptophan residues on both peptides seem to be important for receptor binding [44]. Sex peptide receptor (SPR) of *Drosophila* is CG16752, and this receptor is expressed in female reproductive organs and in the central nervous system of both genders. It is proposed to be $G\alpha_i$-coupled. MIP and SP both activate SPR, but MIP has lower affinity for this receptor [45].

APGWamide is a mollusk tetrapeptide. It is mostly correlated with sex organ growth and reproduction of the animal.

PTTH is a homodimer of two identical peptide chains that are hold together by disulfide bridges [46]. It regulates the reproduction and release of ecdysone hormone. The target receptor of PTTH is Torso, which is a kind of receptor tyrosine kinase [47]. However, it can also activate SPR [48].

4.5. Orexin/allatotropin

Allatotropin (AT) was first identified in *Manduca sexta*, stimulating juvenile hormone synthesis [49]. These peptides show conservation on their N- and C-termini. They include glycine, phenylalanine and a following basic residue in the order in their N-termini (for instance, GFK residues). This N-terminus is important for biological activity of the peptide. On their C-termini, aromatic amino acids are conserved, followed by an amide group (such as R-amide or Y-amide). These peptides are not identified in *Drosophila*, *Apis mellifera* and *Nasonia vitripennis*. However, *Drosophila* expresses sex peptide for the same function. Therefore, it seems that different peptides may work for the same function in different species. Additionally, AT has other roles such as cardioacceleration, stimulation of muscle contractions and myostimulation in the gut [50–52].

Orexin receptors (or hypocretin receptors) are found to be orthologs of AT receptors, via similarity on their C-terminus [22]. However, their peptide ligands are not structurally or functionally related. Orexin peptides are about 28–33 amino acids in length. They are hypothalamic neuropeptides and have roles mainly in sleep and wakefulness [53].

4.6. GnRH/corazonin/AKH

Gonadotropin releasing hormone (GnRH) is the peptide-stimulating gonadotropin release in vertebrates. However, invertebrates, such as annelids and mollusks, also express GnRH-like peptides. Octopus GnRH induces synthesis of testosterone and progesterone in the ovary and testis, respectively. From tunicates to mammals, GnRH sequence shows a high conservation. It is a decapeptide that has an N-terminal pyroglutamine and following HWS residues and C-terminal PGamide residues [54].

Insects express corazonin and adipokinetic hormone (AKH), instead. Corazonin is 11 amino acids in length and has a cardioacceleratory effect in cockroaches. However, other actions are defined in other insects, such as melanization in locusts and developmental pathways in other insects such as *M. sexta* and *Bombyx mori.* AKH is generally 8–10 amino acids in length. It has an N-terminal pyroglutamate, C-terminal amidation and at least two aromatic residues in between. These aromatic residues (at positions 4 and 8) are important for receptor binding. Its structure exhibits a β-turn between these positions. It regulates mobilization of carbohydrates, lipids and proteins from the fat body. Additionally, it has roles in cardioacceleration as corazonin.

Vertebrate GnRH receptors and insect AKH receptors are closely related. *Drosophila* corazonin receptor is clustered in the same family of AKH and VP receptors. However, corazonin receptor is highly selective for corazonin peptide [55].

4.7. Neuropeptide Y

Neuropeptide Y (NPY) family of vertebrate neuropeptides includes NPY, peptide tyrosine tyrosine (PYY) and pancreatic polypeptide (PP). These peptides are C-terminally amidated and show a hairpin-like structure called pancreatic polypeptide fold (PP-fold). This fold was composed of one polyproline helix and one α-helix running antiparallel to each other [56]. Five types of Y receptors (for NPY family) are expressed in mammals ($Y_{1,2,4,5}$ and y_6). It is proposed that hydrophobic surface of the PP-fold is responsible for receptor binding. NPY is localized to the brain, while PP and PYY are localized to the gastrointestinal tract. NPY is a highly conserved peptide from frog to human. Circulating NPY acts on regulation of blood pressure and eating behavior [57].

A mollusk NPY was identified in *Lymnaea stagnalis* via activation assays on its corresponding NPY receptor homolog [58]. This peptide was 39 amino acids in length and very similar to the vertebrate NPYs. Invertebrate NPY prepropeptides lead to two peptides, one is NPY and the other one is C-terminal peptide of NPY (CPON). The important residues that are responsible for the PP-fold of vertebrate NPYs are conserved in mollusk NPYs, but only some of them are conserved in *Drosophila* NPYs. Additionally, C-terminal four residues and amidation, which are essential for the activity of the peptide [59], are conserved between vertebrate and invertebrate NPYs. *Lymnaea* NPY has role in regulation of energy consumption processes, while the other invertebrate NPYs mostly affect food intake of the animal [60].

4.8. Somatostatin/allatostatin C

Allatostatin C (AST-C) is the arthropod homolog of vertebrate somatostatin (SST). SST is found as the inhibitor of growth hormone release from the pituitary gland. And AST-C is the inhibitor of juvenile hormone synthesis in *corpora allata*. From the same SST propeptide, one peptide with 14 amino acids and another with 28 amino acids are released, which are secreted from and acting on different tissues such as central and peripheral nervous system, as well as gastrointestinal tract. Both SST and AST-C peptides exhibit a disulfide bridge, which is important for receptor affinity [11]. The pharmacophore of SST is defined with FWKT residues. And it functions for the inhibition of pituitary hormones such as growth hormone, thyroid stimulating hormone and adrenocorticotropic hormone. SST acts on six different subtypes of SST receptors (SSTRs), SSTR1, SSTR2A, SSTR2B, SSTR3, SSTR4 and SSTR5.

On the other hand, AST-C has highly conserved C-terminal PISCF amino acids. In addition to juvenile hormone inhibition, it inhibits heart muscle contraction in *Drosophila*.

4.9. Galanin/allatostatin A

Galanin peptide is first identified in porcine intestine. Human galanin propeptide produces two peptides, galanin (30 amino acids) and galanin-message associated peptide (GMAP), after cleavage. N-terminal residues and a C-terminal amidation (except in human) of galanin are highly conserved. These peptides are expressed in both central and peripheral nervous systems and have roles in nociception, feeding and osmotic regulation, via acting on three GPCRs; GalR1, GalR2 and GalR3.

Allatostatin A (AST-A) exhibits a conserved C-terminal FGLamide group, which is not similar to galanin peptide. However, these two peptides activate ortholog receptors of vertebrates and arthropods. AST-A peptides are mainly expressed in brain and gut and serve for the inhibition of juvenile hormone synthesis and regulation of food intake, as similar to other AST types.

4.10. Vasoactive intestinal peptide/pituitary adenylate cyclase activating peptide

Expression of vasoactive intestinal peptide (VIP) and pituitary adenylate cyclase activating peptide (PACAP) is restricted to vertebrates. They belong to the glucagon/secretin superfamily that also includes glucagon, secretin, growth hormone releasing hormone (GHRH) and gastric inhibitory peptide (GIH). VIP and PACAP show structural similarity on their N-terminal 27 amino acids. VIP is expressed in both central and peripheral nervous system, while PACAP in hypothalamus, central nervous system, respiratory and gastrointestinal tract. Mature VIP peptide is very well conserved in both mammals and nonmammalian vertebrates. Short PACAP (27 amino acids in length) is restricted to mammals, but the longer form (38 amino acids in length) can be found also in nonmammalian vertebrates [61]. It exhibits an α-helical structure on binding to the receptor but can fold into different secondary structures in different solutions. PACAP is responsible for the release of growth hormone, luteinizing hormone, adrenocorticotropic hormone, follicle-stimulating hormone and prolactin from the pituitary gland, acts on testis and ovary and stimulates insulin and glucagon release [62]. VIP was discovered due to its vasodilatory effects [63]. It can act as both a paracrine or a hormone. However, its half-life is very short when compared to classical hormones [64]. VIP gene produces other forms of peptides such as peptide histidine isoleucine (PHI), peptide histidine methionine (PHM) and peptide histidine valine (PHV), in different organisms. However, the information about the functions of these peptides is limited.

High similarity between PACAP and VIP peptides make them to activate the same receptors, but with different affinities. Three different PACAP receptors are identified (PAC1, VPAC1 and VPAC2). And two types of PACAP selectivity were detected in tissues. In one type, PAC1 receptor has high affinity for PACAP peptides (PACAP27 and PACAP38) and expressed in anterior pituitary and hypothalamus. For the second selectivity, VPAC1 and VPAC2 receptors showed affinity for both PACAP and VIP peptides, and this was detected in peripheral organs. All of these receptors are known to activate adenylate cyclase, leading to cAMP stimulation. In other circumstances, they can stimulate Ca^{+2} levels and phospholipase D.

Pigment dispersing factor (PDF) receptors are homologs of VPAC2 in invertebrates. They regulate circadian clock. In nematodes, they regulate locomotion, but in crustaceans, they regulate pigment movements in the retina.

There are other additional neuropeptide families that interact with GPCRs, such as proopiomelanocortin (POMC) family, which is typical for its precursor complexity and others. However, we will not go into details of other families in this chapter.

http://dx.doi.org/10.5772/intechopen.73504

5. Common features of neuropeptide GPCRs

Neuropeptides activate various receptors most of which are GPCRs. Some neuropeptides as given in Section 4.4 can bind to membrane receptors that couple with receptor tyrosine kinases (i.e. insulin receptors and Torso for PTTH). Some small neuropeptides do not have defined receptors but are ligands for other peptides or enzymes (i.e. 7B2 binding to PC enzymes and neurophysins binding to VP or OXT). Most of the others interact with their cognate GPCRs from the extracellular region and activate a downstream signal transduction pathway. Peptide GPCRs belong to either Class A (rhodopsin-like) or Class B1 (secretin-like) receptor.

Class A GPCRs exhibit two types of ligand-binding pockets. In one type, the hydrophobic ligand interacts with the transmembrane (TM) region, and the N-terminal region together with the second extracellular loop (ECL2) forms a closed lid-like structure (i.e. rhodopsin and S1P receptors that have highly hydrophobic ligands). However, in the second type, ECL2 folds over the extracellular region of the receptor and forms a pocket-like vacancy, which is exposed to the soluble environment. Peptide GPCRs show the characteristics of this latter binding pocket. Here, ECL2 comprises sheets, instead of β-hairpin loops of rhodopsin or helices of adrenergic receptors. Another feature of Class A GPCRs is the presence of a disulfide bridge between transmembrane domain 3 (TM3) and ECL2. This bridge is important for the stability of the receptor and serves as a barrier against conformational changes in this region, which is important for the ligand affinity. In a review on the defined 3D structures of Class A GPCRs, the depths of bound ligands were compared with regard to positioning of TM4 [65]. Within the Class A GPCRs that exhibit open binding pockets, amines (i.e. doxepine) were interacting deeply, while peptides and nucleoside ligands were closer to the extracellular environment. Three TM regions (TM3, TM6 and TM7) of Class A GPCRs were proposed to have consensus binding residues. These consensus amino acid positions are 3.32, 3.33, 3.36, 6.48, 6.51 and 7.39 (Ballesteros-Weinstein numbering). However, peptide receptors such as neurotensin receptor (NTSR) and allatostatin C receptor (AlstR-C) were shown to have different interactions within the TM regions. For instance, neurotensin forms salt bridges and hydrogen bonds with the Y3.29, R6.54, R6.55, F6.58 and Y7.35 residues of NTSR1 [66]. Additionally, AST-C was binding with proposed AlstR-C model from the extracellular site, except for the two amino acids of TM6 (I6.59 and F6.60 residues) [67]. In addition to these consensus residues, Venkatakrishnan et al. proposed that the positions 6.48 and 6.51, which were conserved within Class A GPCRs, might be responsible for the structural folding of the binding pocket, forming a scaffold consensus [65]. However, the evidences for these consensus residues of binding pockets and scaffold interfaces of peptide GPCRs are limited.

Secretin-like neuropeptide GPCRs include the receptors for VIP/PACAP, PDF (in invertebrates), calcitonin, insect DHs, corticotropin releasing factor (CRF), GHRH and parathyroid hormone (PTH) peptides. There is less information about the structures of secretin-like neuropeptide receptors than that of rhodopsin-like receptors. Within the receptors mentioned above, the only solved full-length structures come from CRF1 receptor (PDB entry: 4Z9G) and calcitonin receptor (PDB entry: 5UZ7). Additionally, there are ligand-bound structures of glucagon

receptors of which the ligand is not a neuropeptide. Because glucagon receptor has the most well-known structure and secretin receptor is the most studied in this class, we will use them as examples to understand ligand binding of secretin-like neuropeptide GPCRs, even though they are not neuropeptides. Additional information comes from the N-terminal region of ligand-bound structures of PAC1 (PDB ID: 2JOD) and PTH receptor (PDB ID: 3C4M), together with the free forms of V2 receptor (PDB ID: 2X57) and GHRH receptor (PDB ID: 2XDG).

In order to understand ligand-binding features of this class, we need to look at their ligands. Neuropeptide ligands that couple with secretin-like GPCRs have a common secondary structure of at least one α-helix. As that of glucagon peptide, PACAP and CRF exhibit two α-helices. VIP, PTH and calcitonin peptides have only one helical structure. On the other hand, the common feature of these family receptors is that they have a long and complex N-terminus that may include three disulfide bridges forming an α-β-β-α fold [68]. This N-terminal region of the receptors is shown to be important in ligand binding. Provided by the experimental structure of human glucagon receptor, another region on the N-terminus was identified as "stalk" at the top of TM1. And mutagenesis studies on this stalk region proved that it was important for ligand binding, by providing a defined conformation of N-terminal loop with regard to TM1 [69, 70]. As another hypothesis, Dong et al. proposed an endogenous agonism for the N-terminal region of secretin receptor [71]. Here, binding of C-terminus of the ligand to the N-terminus of the receptor results in a conformational change that results in movement of a hidden tripeptide region and becomes an endogenous agonist for the receptor itself. This tripeptide region consists of WDN residues (inside one of the N-terminal helices) on secretin receptor, which are also conserved for calcitonin and VPAC1 neuropeptide receptors.

According to FRET study by Harikumar et al., C-terminal part of secretin peptide was in proximity to the groove above the β-hairpin of receptor N-terminus, while N-terminal part of it was in proximity to ECL3 and TM6 [72]. This model of secretin binding is proposed as a general mechanism for all secretin-like GPCRs. N-terminus of the peptide ligands was shown to be important for receptor activation (i.e. for CRF, calcitonin, glucagon and VIP) [73–76]. Deletion of this region revealed antagonism for the receptor. And C-terminus of the peptide was shown to be involved in ligand binding to the receptor (i.e. VIP, PTH and CRF) [77–79]. This binding includes hydrophobic residues of the helical structures on receptor N-terminus, as well as hydrogen bonds or salt bridges formed between the ligand and polar receptor residues. In this model, the ligand adopts an α-helical structure upon binding to the receptor. This is supported by the soluble structures of glucagon, PTH or PACAP in aqueous solution and their helical structures in organic solvents. Only calcitonin did not change in either media, due to stabilization by disulfide bridges. The salt bridges between the ligand and the receptor are thought to be responsible for the helix formation. After forming a binding helix, this structure is covered by two β-sheets of the receptor N-terminus. Exceptionally, in case of PACAP binding, the peptide wraps around the helical structures of receptor N-terminus [80].

All the details proposed for ligand binding to secretin-like GPCRs add up to a common model of "two-domain" binding. The C-terminus of the peptide is responsible for receptor binding, mostly to the N-terminus of the receptor, producing a conformational change here. And N-terminus of the peptide enters to the TM region and produces a second conformational change that will lead to signal transduction.

http://dx.doi.org/10.5772/intechopen.73504

6. Methods to study neuropeptide-GPCR interactions

Studying the ligand interaction properties of GPCRs is an essential concept in pharmacology. Neuropeptide GPCRs contribute to the majority of drug targets in central nervous system disorders. Also, insect neuropeptide GPCRs are valuable targets for pesticide designs. Finding the binding sites, discovering agonists, antagonist and even allosteric modulators, understanding the binding affinities and thermodynamic properties and measuring retention times produce a need for case-specific types of GPCR-ligand interaction studies. These may require direct, indirect or *in silico* methods, or a combination of these.

Direct methods for studying GPCR-ligand interactions involve nuclear magnetic resonance (NMR) spectroscopy, X-ray diffraction and surface plasmon resonance (SPR) techniques. The information coming from these studies are deposited in Protein Data Bank (PDB) and increasing every day. However, the increase in deposition of GPCR structures is not as fast as that of soluble protein structures. For instance, most of the data coming from NMR studies include only partial GPCR structures bound with their ligands. Obtaining pure crystals of GPCRs is a challenge in X-ray analysis. And studying with hydrophobic ligands is difficult in SPR method. Therefore, we will not go in detail of these direct methods in this chapter, due to their challenges in working with membrane-bound proteins.

Indirect methods for studying GPCR-ligand interactions include fluorescent-based methods, radioligand binding, photoaffinity labeling, luminescence-based methods, force spectroscopy and activity-based assays.

In silico approaches do not yield direct or indirect evidence for GPCR-ligand interactions, but they reduce the problem space, facilitate the following assays and qualitative comparisons between molecules and can mimic the assay conditions, so that they are highly valuable tools for drug design studies.

In this chapter, we will only focus on the indirect methods that are widely used for GPCR-ligand interaction.

6.1. Radioligand-binding assays

In principle of radioligand-binding assays, the ligand is previously radiolabeled and added onto the receptor, and its binding is measured quantitatively. The first study of radioligands on GPCRs is that of Lefkowitz and his collaborators where they used I^{125}-labeled adrenocorticotropic hormone (ACTH) against ACTH receptor [81]. Since then, modifications on the method made use of membrane patches and also whole cells [82]. With the help of radioligand saturation binding, indirect binding or kinetic-binding assays can be performed and result in calculation of EC_{50}, K_d values together with the retention time of the ligand on the receptor. Also, they show if the ligand binding is reversible or not. The major challenges of this method are the cost and half-lives of radioligands and the health issues in regard to exposure to them. Agonists cannot be distinguished from antagonists with these assays. Additionally, optimizations should be performed to minimize nonspecific binding (i.e. to the cell, to the plastic ware).

6.2. Photoaffinity labeling

In the study of GPCR-ligand interactions, photoaffinity labeling (PAL) is one of the oldest methods. Here, the ligand is bound with a photoreactive group (PRG). Upon binding with the receptor, PRG is activated by UV light and forms an irreversible covalent bond with the closest residues on the receptor. This approach can be combined with immunoprecipitation and mass spectrometry to sequence the amino acids that are in proximity to the ligand-binding pocket. An example can be given as the study of Ceraudo et al. for the interaction between VIP and VPAC1 receptor. They first labeled the C-terminus of VIP with a photoreactive p-benzoyl-p-phenylalanine (Bpa) group. Then they followed by cleavage and Edman sequencing. Finally, they found that the C-terminus of VIP was interacting with the N-terminus of VPAC1 [83].

In another study, Grunbect et al. have performed site-directed mutagenesis on some proposed residues of CXCR4. These mutant residues were producing amber stop codons, which can be engineered to incorporate photocrosslinkers (i.e. BzF and azF). They have transfected HEK cells with these mutant constructs and treated the cells with the ligand. After UV activation, lysis and immunopurification of the receptor-ligand complexes, they saw that 189F residue of the receptor was in close proximity to the ligand during binding [84].

6.3. Fluorescence-based methods

The use of fluorescently labeled ligands has many advantages when compared to radioactively labeled ligands. For instance, detection efficiency is higher in fluorescent ligands, and health safety issues are easier to handle for the methods utilizing fluorescent ligands. Additionally, fluorescence-based methods can generate quantitative data as given by radioligand assays (i.e. EC50, etc.). For instance, microscopy and flow cytometry can be used in real-time experiments; they can measure the amount of fluorescence that is interacting with or within the cells [85]. Dissociation rate constants (K_d) of fluorescently labeled ligands can be calculated in various approaches. First, physical separation of bound ligand from free ligand in different fractions can be measured by means of concentrations. Second, the emission intensity of the ligand changes upon binding with the receptor and this change can be measured. Third, diffusion rates of bound and free ligands differ. In an approach called fluorescence correlation spectroscopy (FCS), diffusion rate of labeled ligand can be measured on a highly sensitive confocal microscope. Another approach depends on anisotropy, which means that polarization of the molecule changes between bound and free ligands. As a fifth approach, flow cytometry can be used to detect presence of labeled ligands on receptor carrying cells or beads. At last, the most frequently used sensitive approach is called as fluorescence resonance energy transfer (FRET).

There are other methods such as fluorescence recovery after photobleaching (FRAP) that is similar to FCS in principle. However, this method is used only for GPCR oligomerization or G-protein coupling until now [86, 87], but no study was performed on GPCR-ligand interactions yet. Another complex approach combines two-photon excitation microscopy with FCS and quantum dot technology (TPE-XCS), which seems very promising for the following days [88]. In this chapter, we will give some more detail on FRET experiments performed on GCPR-ligand studies that are widely preferred by the researchers.

FRET is based on the energy transfer between two different fluorophores when they come close to a defined distance (typically between 10 and 100 Å). In principle, emission of first fluorophore (donor) should excite the second fluorophore (acceptor). In case of GPCR-ligand interactions, different approaches can be used. First, the ligand and an extracellular domain of the receptor can be expressed in fusion with different fluorescent proteins. When the ligand is in proximity to the receptor, two fluorophores also come close to yield an energy transfer. The difference between the FRET signals of interacting and noninteracting GPCR-ligand couples gives an information about the presence of interaction. FRET can also be time-resolved so that information on kinetics of ligand binding can be achieved. This method was used for various types of receptors such as M1 muscarinic acetylcholine receptor, PTH receptors, neurokinin NK2 receptor, cholecystokinin receptor and secretin receptor [89–93]. In another approach, mapping of the ligand-binding region is possible. Here, cysteine residues can be added to different locations of the proposed binding pocket of GPCR via site-directed mutagenesis. These cysteine residues can bind with small fluorophores which would not interfere ligand binding. Additionally, the environment of the ligand-binding pocket can be assessed, via accessibility of aqueous solution and changes in quenching and polarity upon ligand binding. In a technique by Hoffman et al., tetracysteine residues were added to ICL3 and C-terminus of the GPCR. These residues can bind with FlAsH reagent, which is a small fluorophore. When used in combination with cyan fluorescent protein (CFP), conformational changes upon binding of the ligand were made possible to detect [93].

6.4. Bioluminescence resonance energy transfer (BRET)

In principle, BRET is similar to FRET by using a bioluminescent donor on one molecule and a fluorescent acceptor on the target molecule. Generally, a luciferase (i.e. Rluc8) is used as the donor. It can be performed real time, giving quantitative information about ligand binding. It is advantageous over FRET, because it does not require an initial illumination of the donor molecule. As an example, Stoddart et al. performed BRET on beta adrenergic receptor 2 (β_2AR) with an antagonist in live cells. They generated the N-terminus of the receptor with luminescent donor and used a fluorescently labeled ligand [94].

6.5. Atomic force microscopy (AFM)

AFM is based on the principle of single-molecule force spectroscopy, in which binding force of two single molecules is measured as a difference in laser deflection. One molecule is bound on the tip of a cantilever and the other molecule stays on a rigid surface (or on cell surface). If interaction occurs, the laser deflection from the cantilever tip differs from the state of no-interaction events. Here, the receptors can be in lipid bilayers, as performed by Pfreundschuh et al. [95] and Alsteens et al. [96], and binding the ligand to the cantilever tip. Also, the method can utilize the receptors on live cells directly as performed by our group for AlstR-C receptor [67].

In AFM, direct measurements can be obtained from single molecules, and the controls can be designed to exclude nonspecific-binding events. There is no need for fluorescent, luminescent or radiolabeling of the molecules, which may interfere with the binding sites. In most of the cases, peptide ligands are much smaller than fluorescent proteins. However, in AFM, the peptides can

be utilized in their native forms, or they can be functionalized from defined terminal sites. The method in our study also provides the native environment of the receptor as in FRET experiments. And this makes it more advantageous than the methods analyzing purified receptors. AFM setup is suitable for working on adherent cancer cells for long hours, so that the performer can take hundreds of data points from the same cell. And ectopic expression produces enough saturation of the receptor on the surface to detect at each approaching step. Therefore, AFM seems a promising and easy way to study GPCR-ligand interactions on live cells.

6.6. Activity-based assays

Activity-based assays depend on the previously known downstream effects of the GPCR in cells. The advantage of these assays is that they allow discrimination of agonists from antagonists and also partial agonists. Quantification of EC50 values is possible, so that they can also be used in high-throughput pharmacological studies. Examples can be given as GTPγS (guanosine 5'-O-[gamma-thio]triphosphate) binding assays, cAMP (cyclic adenosine monophosphate) assays, IP_3 (inositol triphosphate) and Ca^{+2} assays, TGF-α (transforming growth factor alpha) shedding assay, β-arrestin recruitment and internalization assay, dimerization assays and voltage-clamp experiments. These assays can be coupled with fluorescent techniques or site-directed mutagenesis of the receptor when required.

7. Conclusion

There are at least 80 genes encoding for neuropeptide precursors in human. These precursors give rise to at least 150 mature neuropeptides. And until now, at least 109 of these peptides were shown to signal via GPCRs. All these peptides and their cognate GPCRs are still being studied against the neurological disorders, which range from the simplest stress and pain relief cases to the complex schizophrenia and Alzheimer's disease. Therefore, understanding the kinetics, interactions and transduction pathways of GPCR-neuropeptide signaling systems will remain crucial for the human wealth.

Author details

Burcin Duan Sahbaz* and Necla Birgul Iyison

*Address all correspondence to: burcin.duan1@boun.edu.tr

Molecular Biology and Genetics Department, Bogazici University, Istanbul, Turkey

References

[1] Ruggeri M, Ungerstedt U, Agnati LF, Mutt V, Harfstrand A, Fuxe K. Effects of cholecystokinin peptides and neurotensin on dopamine release and metabolism in the rostral and

caudal part of the nucleus accumbens using intracerebral dialysis in the anaesthetized rat. Neurochemistry International. 1987;**10**(4):509-520

[2] Dori I, Parnavelas JG. The cholinergic innervation of the rat cerebral cortex shows two distinct phases in development. Experimental Brain Research. 1989;**76**(2):417-423

[3] Takahashi T, Takeda N. Insight into the molecular and functional diversity of cnidarian neuropeptides. International Journal of Molecular Sciences. 2015;**16**:2610-2625. DOI: 10.3390/ijms16022610

[4] Westfall JA, Grimmelikhuijzen CJP. Antho-RFamide immunoreactivity in neuronal synaptic and nonsynaptic vesicles of sea anemones. The Biological Bulletin. 1993;**185**(1):109-114

[5] Westfall JA, Sayyar KL, Elliott CF, Grimmelikhuijzen CJP. Ultrastructural localization of antho-RWamides I and II at neuromuscular synapses in the gastrodermis and oral sphincter muscle of the sea anemone *Calliactis parasitica*. The Biological Bulletin. 1995;**189**(3):280-287

[6] Rushforth NB, Hofman F. Behavioral and electrophysiological studies of hydra. III. Components of feeding behavior. The Biological Bulletin. 1972;**142**(1):110-131

[7] Dürrnagel S, Kuhn A, Tsiairis CD, Williamson M, Kalbacher H. Three homologous subunits form a high affinity peptide-gated ion channel in hydra. The Journal of Biological Chemistry. 2010;**285**(16):11958-11965

[8] Elphick MR. The protein precursors of peptides that affect the mechanics of connective tissue and/or muscle in the echinoderm *Apostichopus japonicus*. PLoS One. 2012;**7**(8): e44492. DOI: 10.1371/journal.pone.0044492

[9] Leviev I, Grimmelikhuijzen CJ. Molecular cloning of a preprohormone from sea anemones containing numerous copies of a metamorphosis-inducing neuropeptide: A likely role for dipeptidyl aminopeptidase in neuropeptide precursor processing. Proceedings of the National Academy of Sciences of the United States of America. 1995;**92**(25):11647-11651

[10] Wegener C, Gorbashov A. Molecular evolution of neuropeptides in the genus Drosophila. Genome Biology. 2008;**9**(8):R131. DOI: 10.1186/gb-2008-9-8-r131

[11] Kreienkamp HJ, Larusson HJ, Witte I, Roeder T, Bigul N, Hönck HH, et al. Functional annotation of two orphan G-protein coupled receptors, Drostar1 and 2, from *Drosophila melanogaster* and their ligands by reverse pharmacology. Journal of Biological Chemistry. 2002;**277**(42):39937-39943

[12] Belmont M, Cazzamali G, Williamson M, Hauser F, Grimmelikhuijzen CJP. Identification of four evolutionarily related G protein-coupled receptors from the malaria mosquito *Anopheles gambiae*. Biochemical and Biophysical Research Communications. 2006;**344**:160-165

[13] Nielsen H, Krogh A. Prediction of signal peptides and signal anchors by a hidden Markov model. Intelligent Systems for Molecular Biology. 1998;**6**:122-130. DOI: 10.1.1.47.4026

[14] Veenstra JA. Allatostatin C and its paralog allatostatin double C: The arthropod somatostatins. Insect Biochemistry and Molecular Biology. 2009;**39**(3):161-170. DOI: 10.1016/j.ibmb.2008.10.014

[15] Remacle A, Shiryaev S, Oh E, Cieplak P, Srinivasan A, Wei G, et al. Substrate cleavage analysis of furin and related proprotein convertases: A comparative study. Journal of Biological Chemistry. 2008;**203**(30):20897-20906

[16] Cano-Monreal GL, Williams JC, Heidner HW. An arthropod enzyme, Dfurin 1, and a vertebrate furin homolog display distinct cleavage site sequence preferences for a shared viral proprotein substrate. Journal of Insect Science. 2010;**10**(29). Available online: insectscience.org/10.29

[17] Seidah NG, Prat A. The biology and therapeutic targeting of the proprotein convertases. Nature Reviews Drug Discovery. 2012;**11**:367-383. DOI: 10.1038/nrd3699

[18] Siekhaus DE, Fuller RS. A role for amontillado, the Drosophila homolog of the neuropeptide precursor processing protease PC2, in triggering hatching behavior. Journal of Neuroscience. 1999;**19**(16):6942-6954

[19] Lyons PJ, Callaway MB, Fricker LD. Characterization of carboxypeptidase A6, an extracellular-matrix peptidase. Journal of Biological Chemistry. 2008;**283**(11):7054-7063

[20] Leng G, Ludwig M. Neurotransmitters and peptides: Whispered secrets and public announcements. The Journal of Physiology. 2008;**586**:5625-5632. DOI: 10.1113/jphysiol.2008.159103

[21] Li C, Kim K. Neuropeptides. In: WormBook. ed. The C. elegans Research Community, WormBook. 2008. pp. 1-36. DOI: 10.1895/wormbook.1.142.1

[22] Jékely G. Global view of the evolution and diversity of metazoan neuropeptide signaling. Proceedings of the National Academy of Sciences of the United States of America. 2013; **110**(21):8702-8707

[23] Neuropeptides [Internet]. Available from: www.neuropeptides.nl [Accessed: October 8, 2017]

[24] Nelson LS, Rosoff ML, Li C. Disruption of a neuropeptide gene, flp-1, causes multiple behavioral defects in *Caenorhabditis elegans*. Science. 1998;**281**:1686-1690. DOI: 10.1126/science.281.5383.1686

[25] Ringstad N, Horvitz HR. FMRFamide neuropeptides and acetylcholine synergistically inhibit egg-laying by *C. elegans*. Nature Neuroscience. 2008;**11**:1168-1176. DOI: 10.1038/nn.2186

[26] Cohen M, Reale V, Olofsson B, Knights A, Evans P, de Bono M. Coordinated regulation of foraging and metabolism in *C. elegans* by RFamide neuropeptide signaling. Cell Metabolism. 2009;**9**:375-385. DOI: 10.1016/j.cmet.2009.02.003

[27] Price DA, Greenberg MJ. Structure of a molluscan cardioexcitatory neuropeptide. Science. 1977;**197**(4304):670-671

[28] Stevens JS, Cashman CR, Smith CM, Beale KM, Towle DW, Christie AE, et al. The peptide hormone pQDLDHVFLRFamide (crustacean myosuppressin) modulates the *Homarus americanus* cardiac neuromuscular system at multiple sites. The Journal of Experimental Biology. 2009;**212**:3961-3976. DOI: 10.1242/jeb.035741

[29] Nichols R. Signaling pathways and physiological functions of *Drosophila melanogaster* FMRFamide-related peptides. Annual Review of Entomology. 2003;**48**:485-503

[30] Kiss B, Szlanka T, Zvara A, Zurovec M, Sery M, Kakaš S, et al. Selective elimination/RNAi silencing of FMRF-related peptides and their receptors decreases the locomotor activity in *Drosophila melanogaster*. General and Comparative Endocrinology. 2013;**191**:137-145

[31] Williams MJ, Goergen P, Rajendran J, Zheleznyakova G, Hägglund MG, Perland E, et al. Obesity-linked homologues TfAP-2 and Twz establish meal frequency in *Drosophila melanogaster*. PLoS Genetics. 2014;**10**(9):e1004499. DOI: 10.1371/journal.pgen.1004499

[32] Palmer GC, Tran T, Duttlinger A, Nichols R. The drosulfakinin 0 (DSK 0) peptide encoded in the conserved Dsk gene affects adult *Drosophila melanogaster* crop contractions. Journal of Insect Physiology. 2007;**53**(11):1125-1133

[33] López-Vera E, Aguilar MB, Heimer de la Cotera EP. FMRFamide and related peptides in the phylum mollusca. Peptides. 2008;**29**(2):310-317. DOI: 10.1016/j.peptides.2007.09.025

[34] Coccaro EF, Lee R, Owens MJ, Kinkead B, Nemeroff CB. Cerebrospinal fluid substance P-like immunoreactivity correlates with aggression in personality disordered subjects. Biological Psychiatry. 2012;**72**:238-243

[35] Asahina K, Watanabe K, Duistermars BJ, Hoopfer E, González CR, Eyjólfsdóttir EA, et al. Tachykinin-expressing neurons control male-specific aggressive arousal in Drosophila. Cell. 2014;**156**(1):221-235

[36] Song W, Veenstra JA, Perrimon N. Control of lipid metabolism by tachykinin in Drosophila. Cell Reports. 2014;**9**(1):40-47. DOI: 10.1016/j.celrep.2014.08.060

[37] Jiang H, Lkhagva A, Daubnerová I, Chae HS, Šimo L, Jung SH, et al. Natalisin, a tachykinin-like signaling system, regulates sexual activity and fecundity in insects. Proceedings of the National Academy of Sciences of the United States of America. 2013; **110**(37):E3526-E3534. DOI: 10.1073/pnas.1310676110

[38] Erspamer V, Anastasi A. Structure and pharmacological actions of eledoisin, the active endecapeptide of the posterior salivary glands of Eledone. Experientia. 1962;**18**:58-59

[39] Lippe C, Bellantuono V, Ardizzone C, Cassano G. Eledoisin and Kassinin, but not Enterokassinin, stimulate ion transport in frog skin. Peptides. 2004;**25**(11):1971-1975

[40] Koehbacha J, O'Brienb M, Muttenthalerc M, Miazzoa M, Akcand M, Elliottd AG, et al. Oxytocic plant cyclotides as templates for peptide G protein-coupled ligand design. Proceedings of the National Academy of Sciences of the United States of America. 2013; **110**(52):21183-21188

[41] Wu CK, Hu B, Rose JP, Liu ZJ, Nguyen TL, Zheng C, et al. Structures of an unliganded neurophysin and its vasopressin complex: Implications for binding and allosteric mechanisms. Protein Science. 2001;**10**:1869-1880

[42] Kimura T, Tanizawa O, Mori K, Brownstein MJ, Okayama H. Structure and expression of a human oxytocin receptor. Nature. 1992;**356**:526-529. DOI: 10.1038/356526a0

[43] Cruz LJ, de Santos V, Zafaralla GC, Ramilo CA, Zeikus R, Gray WR. Invertebrate vasopressin/oxytocin homologs. Characterization of peptides from *Conus geographus* and *Conus striatus* venoms. The Journal of Biological Chemistry. 1987;**262**(33):15821-15824

[44] Conzelmanna M, Williamsa EA, Tunarub S, Randela N, Shahidia R, Asadulina A. Conserved MIP receptor–ligand pair regulates Platynereis larval settlement. Proceedings of the National Academy of Sciences of the United States of America. 2013;**110**(20): 8224-8229

[45] Kima YJ, Bartalskaa K, Audsleyc N, Yamanakad N, Yapicia N, Lee JY, et al. MIPs are ancestral ligands for the sex peptide receptor. Proceedings of the National Academy of Sciences of the United States of America. 2010;**107**(14):6520-6525

[46] Ishizaki H, Suzuki A. The brain secretory peptides that control moulting and metamorphosis of the silkmoth, *Bombyx mori*. The International Journal of Developmental Biology. 1994;**38**(2):301-310

[47] Rewitz KF, Yamanaka N, Gilbert LI, O'Connor MB. The insect neuropeptide PTTH activates receptor tyrosine kinase torso to initiate metamorphosis. Science. 2009;**326**(5958): 1403-1405. DOI: 10.1126/science.1176450

[48] Yamanaka N, Hua YJ, Roller L, Spalovská-Valachová I, Mizoguchi A, Kataoka H, et al. Bombyx prothoracicostatic peptides activate the sex peptide receptor to regulate ecdysteroid biosynthesis. Proceedings of the National Academy of Sciences of the United States of America. 2010;**107**(5):2060-2065. DOI: 10.1073/pnas.0907471107

[49] Kataoka H, Toschi A, Li JP, Carney RL, Schooley DA, Kramer SJ. Identification of an allatotropin from adult *Manduca sexta*. Science. 1989;**243**(4897):1481-1483

[50] Duve H, East PD, Thorpe A. Regulation of lepidopteran foregut movement by allatostatins and allatotropin from the frontal ganglion. The Journal of Comparative Neurology. 1999; **412**(2):405-416

[51] Sterkel M, Riccillo FL, Ronderos JR. Cardioacceleratory and myostimulatory activity of allatotropin in *Triatoma infestans*. Comparative Biochemistry and Physiology. 2010;**155**(3): 371-377. DOI: 10.1016/j.cbpa.2009.12.002

[52] Alzugaray ME, Adami ML, Diambra LA, Hernandez-Martinez S, Damborenea C, Noriega FG, et al. Allatotropin: An ancestral myotropic neuropeptide involved in feeding. PLoS One. 2013;**8**(10):e77520. DOI: 10.1371/journal.pone.0077520

[53] Ebrahim IO, Howard RS, Kopelman MD, Sharief MK, Williams AJ. The hypocretin/orexin system. Journal of the Royal Society of Medicine. 2002;**95**(5):227-230

[54] Tsai PS. Gonadotropin-releasing hormone in invertebrates: Structure, function, and evolution. General and Comparative Endocrinology. 2006;**148**(1):48-53

[55] Kim YJ, Spalovská-Valachová I, Cho KH, Zitnanova I, Park Y, Adams ME. Corazonin receptor signaling in ecdysis initiation. Proceedings of the National Academy of Sciences of the United States of America. 2004;**101**(17):6704-6709

[56] Blundell TL, Pitts JE, Tickle IJ, Wood SP, Wu CW. X-ray analysis (1. 4-Å resolution) of avian pancreatic polypeptide: Small globular protein hormone. Proceedings of the National Academy of Sciences of the United States of America. 1981;**78**(7):4175-4179

[57] Kokot F, Ficek R. Effects of neuropeptide Y on appetite. Mineral and Electrolyte Metabolism. 1999;**25**(4–6):303-305

[58] Tensen CP, Cox KJA, Burke JF, Leurs R, van der Schors RC, Geraerts WPM, et al. Molecular cloning and characterization of an invertebrate homologue of a neuropeptide Y receptor. European Journal of Neuroscience. 1998;**10**:3409-3416

[59] Lundberg JM, Franco-Cereceda A, Hemsen A, Lacroix JS, Pernow J. Pharmacology of noradrenaline and neuropeptide tyrosine (NPY)-mediated sympathetic cotransmission. Fundamental and Clinical Pharmacology. 1990;**4**:373-391

[60] Jong-Brinka M, Maata A, Tensenb CP. NPY in invertebrates: Molecular answers to altered functions during evolution. Peptides. 2001;**22**:309-315

[61] Holmgren S, Jensen J. Evolution of vertebrate neuropeptides. Brain Research Bulletin. 2001;**55**(6):723-735

[62] Kastin A, editor. Handbook of Biologically Active Peptides. 2nd ed. San Diego, CA: Elsevier/Academic Press; 2013. p. 2032

[63] Said SI, Mutt V. Potent periphery and splanchnic vasodilator peptide from normal gut. Nature. 1970;**225**:863-864

[64] Henning RJ, Sawmiller DR. Vasoactive intestinal peptide: Cardiovascular effects. Cardiovascular Research. 2001;**49**(1):27-37

[65] Venkatakrishnan AJ, Deupi X, Lebon G, Tate CG, Schertler GF, Babu MM. Molecular signatures of G-protein-coupled receptors. Nature. 2013;**494**:185-194

[66] White JF, Noinaj N, Shibata Y, Love J, Kloss B, Xu F, et al. Structure of the agonist-bound neurotensin receptor. Nature. 2012;**490**(7421):508-513

[67] Duan Sahbaz B, Sezerman OU, Torun H, Birgul Iyison N. Ligand binding pocket of a novel allatostatin receptor type C of stick insect, *Carausius morosus*. Scientific Reports. 2017;**7**:41266. DOI: 10.1038/srep41266

[68] Furness SGB, Wootten D, Christopoulos A, Sexton PM. Consequences of splice variation on secretin family G protein-coupled receptor function. British Journal of Pharmacology. 2012;**166**(1):98-109. DOI: 10.1111/j.1476-5381.2011.01571.x

[69] Siu FY, He M, Graaf C, Han GW, Yang D, Zhang Z, et al. Structure of the class B human glucagon G protein coupled receptor. Nature. 2013;**499**(7459):444-449. DOI: 10.1038/nature12393

[70] Zhang H, Qiao A, Yang D, Yang L, Dai A, Graaf C, et al. Structure of the full-length glucagon class B G-protein-coupled receptor. Nature. 2017;**546**:259-264

[71] Dong M, Pinon DI, Asmann YW, Miller LJ. Possible endogenous agonist mechanism for the activation of secretin family G protein-coupled receptors. Molecular Pharmacology. 2006;**70**(1):206-213. DOI: 10.1124/mol.105.021840

[72] Harikumar KG, Lam PCH, Dong M, Sexton PM, Abagyan R, Miller LJ. Fluorescence resonance energy transfer analysis of secretin docking to its receptor. The Journal of Biological Chemistry. 2007;**282**:32834-32843. DOI: 10.1074/jbc.M704563200

[73] Rivier J, Rivier C, Vale W. Synthetic competitive antagonists of corticotropin-releasing factor: Effect on ACTH secretion in the rat. Science. 1984;**224**:889-891

[74] Feyen JH, Cardinaux F, Gamse R, Bruns C, Azria M, Trechsel U. N-terminal truncation of salmon calcitonin leads to calcitonin antagonists. Structure activity relationship of N-terminally truncated salmon calcitonin fragments in vitro and in vivo. Biochemical and Biophysical Research Communications. 1992;**187**(1):8-13

[75] Unson CG, Andreu D, Gurzenda EM, Merrifield RB. Synthetic peptide antagonists of glucagon. Proceedings of the National Academy of Sciences of the United States of America. 1987;**84**:4083-4087

[76] Turner JT, Jones SB, Bylund DB. A fragment of vasoactive intestinal peptide, VIP(10-28), is an antagonist of VIP in the colon carcinoma cell line, HT29. Peptides. 1986;**7**(5):849-854

[77] Wulffa B, Knudsenb SM, Adelhorstc K, Fahrenkrugb J. The C-terminal part of VIP is important for receptor binding and activation, as evidenced by chimeric constructs of VIP/secretin. FEBS Letters. 1997;**413**(3):405-408

[78] Pioszak AA, Xu HE. Molecular recognition of parathyroid hormone by its G protein-coupled receptor. Proceedings of the National Academy of Sciences of the United States of America. 2008;**105**(13):5034-5039

[79] Pioszak AA, Parker NR, Suino-Powell K, Xu HE. Molecular recognition of corticotropin-releasing factor by its G-protein-coupled receptor CRFR1. Journal of Biological Chemistry. 2008;**283**(47):32900-32912. DOI: 10.1074/jbc.M805749200

[80] Parthier C, Reedtz-Runge S, Rudolph R, Stubbs MT. Passing the baton in class B GPCRs: Peptide hormone activation via helix induction? Cell. 2009;**34**(6):303-310. DOI: 10.1016/j.tibs.2009.02.004

[81] Lefkowitz RJ, Roth J, Pricer W, Pastan I. ACTH receptors in the adrenal: Specific binding of ACTH-125I and its relation to adenyl cyclase. Proceedings of the National Academy of Sciences of the United States of America. 1970;**65**(3):745-752

[82] Flanagan CA. GPCR-radioligand binding assays. Methods in Cell Biology. 2016;**132**:191-215. DOI: 10.1016/bs.mcb.2015.11.004

[83] Ceraudo E, Tan Y, Nicole P, Couvineau A, Laburthe M. The N-terminal parts of VIP and antagonist PG97–269 physically interact with different regions of the human VPAC1 receptor. Journal of Molecular Neuroscience. 2008;**36**(1–3):245-248

[84] Grunbeck A, Huber T, Sachdev P, Sakmar TP. Mapping the ligand-binding site on a GPCR using genetically-encoded photocrosslinkers. Biochemistry. 2011;**50**(17):3411-3413. DOI: 10.1021/bi200214r

[85] Sridharana R, Zubera J, Connellya SM, Mathewa E, Mark E. Fluorescent approaches for understanding interactions of ligands with G protein coupled receptors. Biochimica et Biophysica Acta. 2014;**1838**(100):15-33. DOI: 10.1016/j.bbamem.2013.09.005

[86] Guo H, An S, Ward R, Yang Y, Liu Y, Guo X, et al. Methods used to study the oligomeric structure of G-protein-coupled receptors. Bioscience Reports. 2017;**37**(2). DOI: 10.1042/BSR20160547

[87] Aguila B, Simaan M, Laporte SA. Study of G protein-coupled receptor/β-arrestin interactions within endosomes using FRAP. Methods in Molecular Biology. 2011;**756**:371-380. DOI: 10.1007/978-1-61779-160-4_23

[88] Swift JL, Heuff R, Cramb DT. A two-photon excitation fluorescence cross-correlation assay for a model ligand-receptor binding system using quantum dots. Biophysical Journal. 2006;**90**(4):1396-1410

[89] Markovic D, Holdich J, Al-Sabah S, Mistry R, Krasel C, Mahaut-Smith MP, et al. FRET-based detection of M1 muscarinic acetylcholine receptor activation by orthosteric and allosteric agonists. PLoS One. 2012;**7**(1):e29946. DOI: 10.1371/journal.pone.0029946

[90] Castro M, Nikolaev VO, Palm D, Lohse MJ, Vilardaga JP. Turn-on switch in parathyroid hormone receptor by a two-step parathyroid hormone binding mechanism. Proceedings of the National Academy of Sciences of the United States of America. 2005;**102**:16084-16089

[91] Lecat S, Bucher B, Mely Y, Galzi JL. Mutations in the extracellular amino-terminal domain of the NK2 neurokinin receptor abolish cAMP signaling but preserve intracellular calcium responses. The Journal of Biological Chemistry. 2002;**277**:42034-42048

[92] Harikumar KG, Miller LJ. Fluorescence resonance energy transfer analysis of the antagonist- and partial agonist-occupied states of the cholecystokinin receptor. The Journal of Biological Chemistry. 2005;**2800**:18631-18635

[93] Hoffmann C, Gaietta G, Bünemann M, Adams SR, Oberdorff-Maass S, et al. A FlAsH-based FRET approach to determine G protein–coupled receptor activation in living cells. Nature Methods. 2005;**2**(3):171-176

[94] Stoddart LA, Johnstone EKM, Wheal AJ, Goulding J, Robers MB, Wood KV, et al. Application of BRET to monitor ligand binding to GPCR. Nature Methods. 2015;**12**:661-663. DOI: 10.1038/nmeth.3398

[95] Pfreundschuh M, Alsteens D, Wieneke R, Zhang C, Coughlin SR, Tampé R, et al. Identifying and quantifying two ligand-binding sites while imaging native human membrane receptors by AFM. Nature Communications. 2015;**6**:8857. DOI: 10.1038/ncomms9857

[96] Alsteens D, Pfreundschuh M, Zhang C, Spoerri PM, Coughlin SR, Kobilka BK, et al. Imaging G protein-coupled receptors while quantifying their ligand-binding free-energy landscape. Nature Methods. 2015;**12**(9):845-851. DOI: 10.1038/nmeth.3479

Chapter 5

Role of Soluble Fas Ligand in Severity of Dengue Disease

Nurfadly Zain

Additional information is available at the end of the chapter

http://dx.doi.org/10.5772/intechopen.74617

Abstract

Dengue disease, which is caused by dengue virus infection, is a major public health in the tropical and subtropical countries in the world. It has a wide spectrum of clinical manifestations ranging from an undifferentiated fever in a mild clinical form (dengue fever [DF]) to the severe clinical and potentially fatal dengue hemorrhagic fever and shock syndrome (DHF/DSS). Recently, a study has suggested that excessive inflammation and apoptosis contribute to the pathogenesis of severe dengue disease. Soluble FasL is a type II membrane protein belonging to the tumor necrosis factor (TNF) family, which induces apoptosis in Fas-bearing cells and neutrophil chemotactic functions. The apoptosis of microvascular endothelial cells may explain the plasma leakage mechanism in DHF and there was a significant increase in soluble Fas-ligand level in DHF patients compared to DF patients. It can be concluded that the soluble Fas ligand is related to the pathogenesis of dengue infection.

Keywords: soluble Fas ligand, dengue fever, dengue hemorrhagic fever, apoptosis, immune response

1. Introduction

Dengue is a public health problem in much of the tropical and subtropical countries in the world. Two-thirds of the world's population is at risk of dengue infection; an estimated 50 million cases occur annually, and around 2.5% of those affected die [1]. Dengue has a wide spectrum of clinical presentations and often has unpredictable clinical outcomes, may be asymptomatic, or may cause undifferentiated febrile illness (viral syndrome), dengue fever (DF), or dengue hemorrhagic fever (DHF) including dengue shock syndrome (DSS), and this

can cause death [2]. Despite much research, pathogenesis which can explain the severity of dengue remains unclear [3, 4]. Severe dengue is characterized by plasma leakage and abnormal bleeding that can lead to shock and death [1, 2, 5]. Pathogenesis of severe dengue diseases (DHF/DSS) has been suggested to be caused by the amplified production of cytokines that ultimately targets the vascular endothelium and leads to an increase in vascular permeability [4, 6, 7]. There is currently no specific treatment for severe dengue due to gaps in understanding the underlying mechanisms.

Soluble FasL is a type II membrane protein belonging to the tumor necrosis factor (TNF) family, which induces apoptosis in Fas-bearing cells [8] and neutrophil chemotactic functions [9]. A recent study showed that in addition to the immune response, apoptosis also contributes to the pathogenesis of DHF. An autopsy examination showed that dengue cases show apoptosis in liver cells, brain, intestine, and lungs. The apoptosis of microvascular endothelial cells may explain the plasma leakage mechanism in DHF [10].

2. Role of soluble Fas ligand in the severity of dengue disease

2.1. Dengue infection

Dengue fever (DF) and its severe forms, dengue hemorrhagic fever (DHF) and dengue shock syndrome (DSS), have become a major international public health problem, especially in the tropical and subtropical regions around the world. An estimated 50 million infections per year occur across approximately 100 countries, with potential for further spread [1, 2]. The disease is caused by a virus belonging to the family Flaviviridae that is spread by Aedes mosquitoes. There are four distinct serotypes of dengue virus (DENV 1–4). All dengue serotypes are capable of causing diseases with a wide spectrum of clinical manifestations, ranging from an undifferentiated fever in a mild clinical form (DF) to the severe clinical and potentially fatal DHF/DSS. Infection with one serotype confers protective immunity against that serotype but not against other serotypes [11]. Dengue fever (DF) is an acute and self-limited illness manifested by fever, headache, myalgia, and arthralgia, and on physical examination there occurs rash. Laboratory tests reveal leukopenia and thrombocytopenia. The more severe dengue DHF is complicated by plasma leakage that occurs around 3–5 days after the disease. A sudden and extensive plasma leakage may result in shock or death, a phenomenon called DSS. Then, patients undergo a defervescence phase marked by an abrupt drop in body temperature, at which point the illness may either wane to recovery or proceed to serious complications [1, 5].

DENV infection in humans starts with a DENV-infected mosquito bite. DENV can replicate in a wide spectrum of cells, including liver, spleen, lymph node, kidney, and other organs, but monocytes, macrophages, and dendritic cells (DC) have been shown to be the major targets for DENV [12]. Monocytes and T lymphocytes, which are infected by DENV, produce several pro-inflammatory mediators which become sources of intense cytokine production [13].

Abnormal hemostasis and plasma leakage are the main pathophysiological hallmarks in DHF. There is no vasculitis and hence no injury to the vessel walls, and plasma leakage results from the cytokine-mediated increase in vascular permeability [14]. During inflammation, increased vascular permeability occurs primarily via changes in the integrity of inter-endothelial cell junctions. The increase vascular permeability is affected by a number of soluble factors on the endothelium and among them are thrombin, bradykinin, histamine, oxygen free radicals, vascular endothelial growth factor (VEGF), and tumor necrosis factor-α (TNFα) [15]. Some neutrophil products like arachidonic acid (AA) or leukotriene (LT) A4 are further processed by endothelial enzymes through transcellular metabolism before the resulting products thromboxane A2, LTB4, or LTC4 can activate their cognate receptors. Neutrophils also generate reactive oxygen species that induce vascular leakage [16].

2.2. Fas ligand

Fas ligand is a 40-kDa type II membrane protein belonging to the tumor necrosis factor (TNF) family of proteins which induce defined cellular responses upon binding to their respective receptors (Fas receptors). The interaction of Fas ligand with its receptor induced programmed cell death (apoptosis) [8].

FasL is expressed by many cell types; it is primarily recognized as associated with activated T lymphocytes and natural killer (NK) cells [17]. Fas ligand is expressed in three distinct forms:

1. a membranous form on the cell surface;
2. a membranous form stored in intracellular microvesicles which are excreted into the intercellular milieu in response to various physiologic stimuli; and
3. the soluble form generated from the cleavage of the membranous molecule by matrix metalloproteinases within minutes of cell surface expression [9].

   Membrane Fas ligand can be cleaved by metalloproteinases to release soluble protein segments. The soluble and membranous forms of the Fas ligand have different functions in apoptosis. Membranous Fas ligand is the primary mediator of apoptosis through formation of trimers and higher-order structures on the cell surface, while soluble Fas ligand can have proapoptotic, antiapoptotic, and neutrophil chemotactic functions, depending on the nature of other contextual mediators in the microenvironment. Soluble Fas ligand exists as a homotrimer, which is ineffective in co-aggregating Fas receptors. Soluble Fas ligand can induce apoptosis following aggregation with fibronectin of extracellular matrix proteins to form tetramers and higher-order structures. Besides its role in apoptosis, the soluble Fas ligand is a potent inflammatory agent; it induces B cell proliferation and IgE synthesis in conjunction with IL-4, and soluble B cell activating factor (BAFF) co-stimulates B cells.

   Expression of soluble Fas ligand in several cell types has been shown to induce an effusive neutrophil-mediated inflammatory response, as documented in vivo by either tissue transplant infiltration or neutrophil extravasation to the peritoneal cavity [18].

Soluble Fas ligand-binding cells express Fas receptors and lead to apoptosis whereas there are some cells that have a default death pathway that can be blocked by a survival factor such as a hormone or growth factor [19].

The binding of the Fas ligand to the Fas receptor results in the binding of the adapter protein Fas-associated death domain (FADD). FADD then associates with procaspase-8 via dimerization of the death effector domain forming a death-inducing signaling complex (DISC). Once caspase-8 is activated, the execution phase of apoptosis is triggered. Caspases are widely expressed in an inactive proenzyme form in most cells and once activated can often activate other procaspases, allowing initiation of a protease cascade. One caspase activates other caspases and causes the apoptotic signaling pathway to be activated. Caspases have proteolytic activity and are able to cleave proteins at aspartic acid residues. Once caspases are initially activated, it leads an irreversible commitment towards cell death. There are 10 major caspases that have been identified and categorized into initiators (caspase-2,-8,-9,-10), effectors or executioners (caspase-3,-6,-7), and inflammatory caspases (caspase-1,-4,-5) [20].

There are morphological changes that occur during apoptosis. At the early process of apoptosis, cell shrinkage and pyknosis occur. At the cell shrinkage stage, the cells are smaller in size, the cytoplasm is dense, and the organelles are more tightly packed. Pyknosis is the result of chromatin condensation. Furthermore, plasma membrane blebbing occurs followed by karyorrhexis and separation of cell fragments into apoptotic bodies. The organelle integrity is still maintained and all of this is enclosed within an intact plasma membrane. Then, apoptotic bodies are subsequently phagocytosed by macrophages degraded within phagolysosomes. There is essentially no inflammatory reaction associated with the process of apoptosis [21].

The recent studies show that soluble Fas ligand also induces cellular activation signals. Soluble Fas ligand induced monocyte responses to secrete pro-inflammatory cytokines and chemotactic factors [22, 23]. Soluble Fas ligand-induced monocyte cytokine responses were associated with rapid expression of pro-inflammatory cytokine genes, suggesting at least partial regulation at the transcriptional level and involving nuclear factor-kappa beta (NF-kB) activation. There are important maturation-dependent differences in the soluble Fas ligand that depend on the signaling pathway whether inducing apoptosis or the silent disappearance of inflammatory cells. Soluble Fas ligand may serve to activate circulating monocytes and recruited macrophages to produce pro-inflammatory mediators that can initiate acute inflammation. This is may play an important role in the regulation of innate immune responses and may contribute to the pathogenesis of a variety of clinically important inflammatory diseases [24].

2.3. Role of soluble Fas ligand in pathogenesis in dengue

Soluble Fas ligand can induce apoptosis and inflammatory responses. Recently the study has suggested that excessive inflammation and apoptosis contribute to the pathogenesis of severe dengue disease. Although elevated-level cytokines occur in DF patients, the higher level was found in severe dengue disease (DHF/DSS) [25]. The evidence has suggested that there is

significantly an increase in the number of human tissues that undergo apoptosis in dengue disease [26]. Apoptosis in white blood cells, brain cells, intestine, and pulmonary endothelial cells form microvasculature in DENV cases. The apoptosis of microvascular endothelial cells may be associated with plasma leakage and hemorrhage during DHF/DSS [27].

The interaction between DENV and humans leads to the activation of transcription factors, cytokines, and enzymatic factors. These interactions may induce not only inflammatory responses but also apoptotic responses that influence the severity and progression of the disease. The human monocytes infected in vitro by DENV have upregulated Fas expression concomitant with the viral peak, indicating that DENV apoptosis is induced by extrinsic apoptotic pathway [13].

The dengue patients during acute infection found that TNF-α is the first cytokine detected in patients in the peripheral blood mononuclear cell (PBMC) cultures [28]. These findings showed that TNF-α and its family members are important apoptosis mediators during DENV infection. Among the TNF-α family, the Fas ligand is related to the pathogenesis of dengue infection [29–31]. The apoptotic event is an important event in life and is involved in pathogenesis of dengue infection, and these events occur in response to the variety of signals and stimuli, both internal and external. Mitochondria play a central role in mediating intrinsic apoptotic signals. Changes in the external membrane mitochondria lead to the production of reactive oxygen species related to initial apoptotic events. The extrinsic signal that usually induced apoptosis is by a death receptor such as Fas receptor binding to Fas ligand. After signaling, an enzymatic cascade leads to the activation of a series of cysteinyl aspartate proteases known as caspases and then to cell degradation [29]. DENV can induce apoptosis in DENV-infected cells and disseminate its viral progenies to the neighbor cells. The induction of apoptosis may be an attempt by the host immune system to limit the extent of the infection [13].

Apoptotic signaling may first be triggered by the interaction of the DENV envelope protein with the endosomal membrane during the fusion process while newly synthesized viral proteins may enhance apoptosis. There was indicate the involvement of NF-kB in mediating apoptosis. DENV triggers an apoptotic pathway through phospholipase A2 (PLA2) activation to superoxide anion generation and subsequently to NF-kB activation.

This apoptotic effect can be either directly derived from the action of arachidonic acid (AA) and superoxide anion on the mitochondria or indirectly derived from the products of apoptosis-related genes activated by NF-kB [32].

The recent study showed that soluble Fas ligand can be used as a potential marker of severity of dengue infection because the study showed that there was a significant increase in the soluble Fas ligand level in DHF patients compared to DF patients [33].

3. Conclusions

Soluble Fas ligand contributes to the pathogenesis of the severe dengue disease. The interactions between DENV and humans induce not only inflammatory responses but also apoptotic

responses that influence the severity and progression of the disease. Soluble Fas ligand can induce apoptosis and is a potent inflammatory agent.

Acknowledgements

I greatly appreciate Professor Suhartono Taat Putra (University of Airlangga) for stimulating discussions which contributed to this chapter. This work was supported by University of Muhammadiyah Sumatera Utara, Indonesia.

Conflict of interest

The authors declare that they have no conflicts of interests with commercial or other affiliations.

Author details

Nurfadly Zain

Address all correspondence to: drnurfadly@gmail.com

Department of Tropical Medicine, University of Muhammadiyah Sumatera Utara, Indonesia

References

[1] World Health Organization. Dengue: Guidelines for Diagnosis, Treatment, Prevention and Control. Geneva, Switzerland: World Health Organization; 2009

[2] World Health Organization. Comprehensive Guidelines for Prevention and Control of Dengue and Dengue Haemorrhagic Fever. Regional offoce for South-East Asia; 2011

[3] Martina BE, Koraka P, Osterhaus AD. Dengue virus pathogenesis: An integrated view. Clinical Microbiology Reviews. 2011;**22**(4):564-581

[4] Chaturvedi UC, Agarwal R, Elbishbishi EA, Mustafa AS. Cytokine cascade in dengue hemorrhagic fever: Implications for pathogenesis. FEMS Immunology and Medical Microbiology. 2000;**28**:183-188

[5] World Health Organization. Handbook for Clinical Management of Dengue. Geneva, Switzerland: World Health Organization; 2011

[6] Costa VV, Fagundes CT, Sauza DG, Teixeira MM. Inflammatory and innate immune responses in dengue infection. The American Journal of Pathology. 2013;**186**(2): 1950-1960. DOI: 10.1016/j.ajpath.2013.02.027

[7] Mangione J, Huy NT, Lan NTP, Mbanefo EC, Ngoc Ha TT, Bao LQ, Phi Nga CT, et al. The association of cytokines with severe dengue in children. Tropical Medicine and Health. 2013;**42**(4):137-144. DOI: 10.2149/tmh.2014-09

[8] Nagata S. Cell. 1997;**88**:355-365

[9] Tanaka M, Itai T, Adachi M, Nagata S. Downregulation of Fas ligand by shedding. Nature Medicine. 1998;**4**:31-36

[10] Limonta D, Capó V, Torres G, Guzmán MG, López LX, Pérez AB, González D, et al. New evidence of the contribution of apoptosis to dengue hemorrhagic fever pathophysiology. Biotecnologia Aplicada. 2010;**27**(1)

[11] Azeredo EL, Monteiro RQ, Pinto LO. Thrombocytopenia in dengue: Interrelationship between virus and the imbalance between coagulation and fibrinolysis and inflammatory. Mediators of Inflammation. 2015. DOI : 10.1155/2015/313842

[12] Neves-Souza PC, Azeredo EL, Zagne SM, Valls-de-Souza R, Reis SR, Cerqueira DI, Nogueira RM, Kubelka CF. Inducible nitric oxide synthase (iNOS) expression in monocytes during acute dengue fever in patients and during in vitro infection. BMC Infectious Diseases. 2005;**5**:64

[13] Carvalho AT, Azeredo EL, Reis SRI, Miranda AS, Gandini M, Barbosa LS, Kubelka CF. Dengue-2 infection and the induction of apoptosis in human primary monocytes. Memórias do Instituto Oswaldo Cruz, Rio de Janeiro. 2009;**104**(8):1091-1099

[14] Sellahewa KH. Pathogenesis of dengue haemorrhagic fever and its impact on case management. ISRN Infectious Diseases. 2013. DOI: 10.5402/2013/571646

[15] Mehta D, Malik AB. Signaling mechanisms regulating endothelial permeability. Physiological Reviews. 2006;**86**(1):279-367

[16] DiStasi MR, Ley K. Opening the flood-gates: How neutrophil-endothelial interactions regulate permeability. Trends in Immunology. 2009;**30**(11):547-556. DOI: 10.1016/j.it.2009.07.012

[17] Brunner T, Wasem C, Torgler R, Cima I, Jakob S, Corazza N. Fas (CD95/Apo-1) ligand regulation in T cell homeostasis, cell-mediated cytotoxicity and immune pathology. Seminars in Immunology. 2003;**15**:167-176. DOI: 10.1016/ S1044-5323(03)00035-6

[18] Hohlbaum AM, Moe S, Marshak-Rothstein A. Opposing effects of transmembrane and soluble Fas ligand expression on inflammation and tumor cell survival. The Journal of Experimental Medicine. 2000;**191**:1209-1220

[19] Zeiss CJ. The apoptosis-necrosis continuum: Insights from genetically altered mice. Veterinary Pathology. 2003;**40**:481-495

[20] Elmore S. Apoptosis: A review of programmed cell death. Toxicologic Pathology. 2007;**35**(4):495-516

[21] Savill J, Fadok V. Corpse clearance defines the meaning of cell death. Nature. 2000;**407**:784-788

[22] Ahn J-H, Park S-M, Cho H-S, Lee M-S, Yoon J-B, Vilcek J, Lee TH. Non-apoptotic signaling pathways activated by soluble Fas ligand in serum-starved human fibroblasts: Mitogen- activated protein kinases and NF B-dependent gene expression. The Journal of Biological Chemistry. 2001;**276** 47100

[23] Daigle I, Ruckert B, Schnetzler G, Simon HU. Induction of the IL-10 gene via the fas receptor in monocytes—An anti-inflammatory mechanism in the absence of apoptosis. European Journal of Immunology. 2000;**30**:2991

[24] Park DR, Thomsen AR, Frevert CW, Pham U, Skerrett SJ, Kiener PA, Conrad Liles W. Fas (CD95) induces proinflammatory cytokine responses by human monocytes and monocyte-derived macrophages.. Journal of Immunology 2013; 170:6209-6216. DOI: 10.4049/jimmunol.170.12.6209

[25] Srikiatkhachorn A. Plasma leakage in dengue haemorrhagic fever. Thrombosis and Haemostasis. 2009;**102**:1042-1049

[26] Huerre MR, Lan NT, Marianneau P, Hue NB, Khun H, Hung NT, et al. Liver histopathology and biological correlates in five cases of fatal dengue fever in Vietnamese children. Virchows Archiv. 2001;**438**:107-115

[27] Limonta D, Capó V, Torres G, Guzmán MG, López LX, Pérez AB, González D, Álvarez M, Rosario D, Rodríguez R, Díaz J Pelegrino JL. New evidence of the contribution ofapoptosis to dengue hemorrhagic fever pathophysiology. Biotecnología Aplicada. 2010; 271

[28] Reis SR, Sampaio AL, Henriques MG, Gandini M, Azeredo EL, Kubelka CF. An in vitro model for dengue virus infection that exhibits human monocyte infection, multiple cytokine production and dexamethasone immunomodulation. Memórias do Instituto Oswaldo Cruz. 2007;**102**:983-990

[29] Limjindaporn T, Netsawang J, Noisakran S, Thiemmeca S, Wongwiwat W, Sudsaward S, Avirutnan P, et al. Sensitization to Fas-mediated apoptosis by dengue virus capsid protein. Biochemical and Biophysical Research Communications. 2007;**362**:334-339

[30] Cardier JE, Marino E, Romano E, Taylor P, Liprandi F, Bosch N, Rothman AL. Proinflammatory factors present in sera from patients with acute dengue infection induce activation and apoptosis of human microvascular endothelial cells: Possible role of TNF-alpha in endothelial cell damage in dengue. Cytokine. 2005;**30**:359-365

[31] Lemasters JJ. Dying a thousand deaths: Redundant pathways from different organelles to apoptosis and necrosis. Gastroenterology. 2005;**129**:351-360

[32] Jan JT, Chen BH, Ma SH, Liu C, Tsai HP, Wu HC, Jiang SY, et al. Potential dengue virus-triggered apoptotic pathway in human neuroblastoma cells: Arachidonic acid, superoxide anion, and NF-kB are sequentially involved. Journal of Virology. 2000:8680-8691

[33] Zain N, Putra ST, Zein U, Hariman H. Soluble Fas ligand as potential marker of severity of dengue infection. Malaysian Journal of Medical Science. 2017i;**24**(2):28-32. DOI: 10.21315/mjms2017.24.1.4

Edited by Chandraleka Saravanan and Bhaskar Biswas

The book *Ligand* describes the diversity and versatility of ligands, covering structural features, donor-acceptor properties and secondary functions like molecular recognition. Moreover, this book also provides a comprehensive account on the applicability like catalysis, sensors, supramolecular assembly, photochemical property, bioinorganic chemistry, and so on. The advancement of fundamentals in ligand design and the control of physicochemical properties of coordination compounds has largely increased emphasis on understanding the structural and electronic features toward different perspectives in materials science. In this regard, this book has a special appeal to chemists, biologists and others. This book will be beneficial for the graduate students, teachers, researchers and other professionals who are interested to fortify and expand their knowledge in chemistry, biology, microbiology, biotechnology, materials science, environmental science and so on.

Published in London, UK

IntechOpen

ISBN 978-1-83881-319-2